UNIVERSITY OF CALIFORNIA, SAN DIEGO

X-ray Crystallographic and Biochemical Studies on the Bone Morphogenetic Protein Family

A Dissertation submitted in partial satisfaction of the

Requirements for the degree Doctor of Philosophy

in

Chemistry

by

George P. Allendorph IV

Committee in charge:

Professor Senyon Choe, Chair
Professor Partho Gosh, Co-Chair
Professor Ethan Bier
Professor Elizabeth A. Komives
Professor Xuong Nguyen-huu
Professor Jerry Yang

2007

The dissertation of George P. Allendorph, IV is approved, and it is acceptable in quality and form for publication on microfilm:

_____

_____

_____

_____

_____
Co-Chair

_____
Chair

University of California, San Diego

2007

In dedication to my friends and family who have offered their continued support in all my endeavors.

EPIGRAPH

I begin to be almost sorry I was born so soon, since I cannot have the happiness of knowing what will be known a hundred years hence.

Benjamin Franklin

It is the pervading law of all things organic and inorganic,
Of all things physical and metaphysical,
Of all things human and all things super-human,
Of all true manifestations of the head,
Of the heart, of the soul,
That the life is recognizable in its expression,
That form ever follows function. This is the law.

Louis Henri Sullivan

TABLE OF CONTENTS

LIST OF SYMBOLS AND ABBREVIATIONS

α	alpha
Å	Ångstrøm; 10^{-10} m
$Å^2$	squared Ångstrøm
ActRI	Acitivin Receptor Type I
ActRII	Activin Receptor Type II
Ala	alanine
Alk	activin like receptor kinase
ALS	Advanced Light Source
Arg	Arginine
Asn	Asparagine
Asp	Aspartic acid
β	beta
BAMBI	BMP and Activin Membrane Bound Inhibitor
BMP	Bone Morphogenetic Protein
BMPRI	Bone Morphogenetic Protein Receptor I
BMPRII	Bone Morphogenetic Protein Receptor II
°C	degree Celsius
CHAPS	3-[(3-Cholamidopropyl)dimethylammonio]-1-propanesulfonate
CH_3CN	acetonitrile
CHO	Chinese Hamster Ovary

Cys	cysteine
Cl	chlorine, chloride
cm^{-1}	inverse centimeter
°	degree
DAN	Differential screening-selected gene Aberrative in Neuroblastoma
DMEM	Dulbecco's minimum essential medium
DTT	Dithiothreitol
E. coli	Escherichia coli
ECD	Extra-Cellular Domain
EDTA	ethylenediaminetetraacetic acid
ε	molar extinction coefficient; M^{-1} cm^{-1}
FBS	Fetal Bovine Serum
γ	gamma
GDF	Growth and Differentiation Factor
Glu	Glutamic acid
HCl	Hydrogen chloride
HEPES	4-(2-hydroxyethyl)-1-piperazineethanesulfonic acid
HSTC	High salt Tris CHAPS buffer
His	Histidine
h	hour
hMSC	human Mesenchymal Stem Cells
H_2O	water, hydrate

Hz	hertz
kD	kilo Dalton
K	Kelvin
K_{off}	Dissociation rate
K_{on}	Association rate
K_D	Dissociation constant
λ	wavelength, lambda
Leu	Leucine
Lys	Lysine
µL	microliter
µM	micromolar
M	molar; mol L^{-1}
Met	Methionine
mg	milligram
min	minute
mL	mililiter
mM	milimolar
mmol	milimol
MH	Mad Homology
MIS	Mullerian Inhibiting Substance
MISR	Mullerian Inhibiting Substance Receptor
MPD	2-methyl-2,4-pentanediol

MS	mass spectrometry
MW	molecular weight
NaCl	Sodium Chloride
NCS	Non-crystallographic symmetry
nm	nanometer; 10^{-9} m
nM	nanomolar
%	Percent
P. pastoris	Pichia Pastoris
PAGE	Polyacrylamide gel electrophoresis
PBS	Phosphate Buffered Saline
PC	Propeptide Convertase
Phe	Phenylalanine
Pro	Proline
π	Pi; ratio of the circumference of a circle to its diameter
RMS_{dev}	Root Mean Square deviation
RU	Response Unit
s	second
Ser	Serine
SDS	Sodium dodecyl sulfate
Smad	mothers against decapentaplegic
SSRL	Stanford Synchrotron Radiation Laboratory
TGF-β	Transforming Growth Factor beta

TGF-βR	Transforming Growth Factor beta Receptor
TLS	Translation, Libration, and Screw
Tris	trishydroxymethylaminomethane
Trp	Tryptophan
Tyr	Tyrosine
ν	wave number, cm^{-1}
Val	Valine

LIST OF FIGURES

LIST OF TABLES

ACKNOWLEDGEMENTS

I must first start by thanking my entire family for the support they have shown for me throughout my education. In particular, I thank my parents Jane and George Allendorph, III, my grandparents Margaret and Edward Fucik, and my grandmother Carol Allendorph. Further, a brief remembrance is in order for my grandfather George Allendorph, Jr. If he is watching, I hope that this makes him proud.

Further, I would like to thank Senyon Choe for taking a chance on an unknown kid many years ago. He has shown nothing but support and unbridled enthusiasm for all my projects. I also thank all members of the Structural Biology Laboratory (SBL) for their help and guidance. In particular, Jason Greenwald and Kent Baker provided advice and tutelage over my graduate career. Also, without the patient help of Witek Kwiatowski I might never have been able to understand and use Linux operating systems.

I cannot forget the Chapman Foundation which has generously provided support for my time at the Salk Institute. Without their support, I might still be working towards my degree.

The text, tables, and figures from Chapter 2 are in part reprints of published material as it appears: George P. Allendorph, Wylie Vale, Senyon Choe, "Structure of the ternary signaling complex of a TGF-β superfamily member" Proc Natl Acad Sci. 2006, May 16;103(20):7643-8. The dissertation author was the primary investigator and author of this paper.

The text, tables, and figures from Chapter 3 are, in part, reprints of published materials as it appears: Jason Greenwald, Mark E Vega, George P Allendorph, Wolfgang H Fischer, Wylie Vale and Senyon Choe, "A flexible activin explains the membrane-dependent cooperative assembly of TGF-beta family receptors" *Mol Cell*. 2004 Aug 13;15(3):485-9. While not the author of the paper, the dissertation author was the primary investigator for the work presented.

The text, tables, and figures from Chapter 4 have, in part, been submitted for publication and may appear as: George P. Allendorph, Michael J. Isaacs, Yasuhiko Kawakami, Juan Carlos Izpisua Belmonte, and Senyon Choe, "BMP-3 and BMP-6 Structures Illuminate the Nature of Binding Specificity with Receptors" *Biochemistry* 2007. The dissertation author was the primary investigator and author of this paper.

VITA

Education

May 2001 Bachelor of Science in Chemistry and Bachelor of Arts in Economics, University of Virginia

June 2003 Master of Science in Chemistry, University of California, San Diego

September 2007 Doctor of Philosophy in Chemistry, University of California, San Diego

Research Fellowships and Experiences

March 2000 – May 2001 Blood Platelet Function: Role of chemokines and small molecules in platelet aggregation. Under the supervision of Dr. Adrian R.L. Gear

March 2002 – Sept. 2007 TGF-β Superfamily: Structural determinants of receptor affinity and binding. Supported by the Chapman Foundation Fellowship under the supervision of Dr. Senyon Choe.

Presentations

March 2007 West Coast Protein Crystallography Workshop (WCPCW) Pacific Grove, CA. "A Structural Insight into the TGF-β Superfamily".

Publications

1) Jason Greenwald, Mark E. Vega, **George P. Allendorph**, Wolfgang H. Fischer, Wylie W. Vale, and Senyon Choe, "A Flexible Activin Explains the Membrane-Dependent Cooperative Assembly of TGF-β Family Receptors" *Mol Cell.* 2004 Aug 13;15(3):485-9.

2) **George P. Allendorph,** Wylie Vale, and Senyon Choe "Structure of the ternary signaling complex of a TGF-beta superfamily member" *Proc Natl Acad Sci*. 2006 May 16;103(20):7643-8.

3) **George P. Allendorph**, Michael J. Isaacs, Yasuhiko Kawakami, Juan Carlos Izpisua Belmonte, and Senyon Choe, "BMP-3 and BMP-6 Structures Illuminate the Nature of Binding Specificity with Receptors" *Pending acceptance*.

ABSTRACT OF THE DISSERTATION

X-ray Crystallographic and Biochemical Studies on the Bone Morphogenetic Protein Family

by

George Pitcher Allendorph IV

Doctor of Philosophy in Chemistry

University of California, San Diego, 2007

Professor Senyon Choe, Chair
Professor Partho Ghosh, Co-Chair

Bone Morphogenetic Proteins (BMPs) are extracellular messenger ligands involved in controlling a wide array of developmental and intercellular signaling processes. To initiate their specific intracellular signaling pathways, the ligands recognize and bind two structurally related serine/threonine kinase receptors, termed type I and type II, on the cell surface. To address the structural arrangement of the receptors when bound to the ligand, the structure of BMP-2, ligand, bound to its type I receptor BMPRIa-ECD and type II receptor ActRII-ECD was determined. The structural arrangement this complete, signaling competent complex confirms that the two receptor types do not directly contact each other. Further, comparison of

previously solved high affinity type II receptor/ligand interfaces with the lower affinity interface of BMP-2/ActRII-ECD allowed for identification of ligand residues important for determining receptor affinity.

A known feature of BMP complex assembly is the cooperative nature of receptor binding. When bound to its high affinity receptor, the ligand's affinity for the lower affinity receptor is increased. However, the lack of conformational changes to either the receptors or ligand in the ternary complex leaves the mechanism unclear. Using the natural homo/hetero-dimer system of activin/Inihibin, the nature of this cooperativity was probed. Activin's receptor affinity was shown to vary depending on the surface concentration of the receptor, whereas Inhibin's receptor affinity remained constant. This finding suggests cooperative receptor binding is a result of increased local concentration and loss of rotational freedom of the ligand upon binding to a high affinity receptor.

Finally, structural and biochemical studies were undertaken for two new BMP ligands, BMP-3 and BMP-6. Interestingly, while BMP-6 exhibited many similarities to BMP-7, BMP-3 displayed a previously unseen 30-fold specificity difference between ActRIIb-ECD and ActRII-ECD. Comparison of the predicted interfaces of these receptors with BMP-3 yielded a single residue interaction which regulates this receptor preference. The combination of these related studies illustrates how single amino acid differences between ligands can effect receptor binding and, ultimately, impact BMP signaling and function.

Chapter 1. Introduction

1.1. Introduction

The Transforming Growth Factor Beta (TGF-β) superfamily consists of a large number of structurally conserved polypeptide extracellular messenger ligands. Approximately 40 members of the superfamily have been identified in the human genome and can be broken down into several distinct functional subfamilies including TGF-β, Bone Morphogenetic Protein (BMP), Growth and Differentiation Factor (GDF), Nodal, activin and inhibin, and Mullerian Inhibiting Substance (MIS). TGF-β superfamily members are expressed in a wide range of cell and tissue types and have been shown to be prominent mediators in many cellular signaling processes. GDF-5 has been shown to be critical for bone and joint formation, while BMP-2 and BMP-4 are involved in dorsal/ventral patterning and numerous other TGF-β and BMP ligands govern cell proliferation and differentiation (1-4). Misregulation of TGF-β ligands and their corresponding downstream signaling responses are linked to numerous diseases. TGF-βI has been linked to breast cancer metastasis and GDF-8 is closely related to muscle abnormalities (5-7). More recently, BMP-4, activin, Inhibin, TGF-βI, Noggin, and Nodal have been shown to have significant impact and influence on the maintenance and guidance of stem cell differentiation as well as play important roles in wound repair and tissue regeneration (8-10).

TGF-β ligands are synthesized as large precursor molecules containing an N-terminal pro-domain and a C-terminal mature domain separated by a protease cleavage site (Figure 1-2). The N-terminal pro-domain is larger than the mature domain, roughly 30-50 kDs compared to ~15 kDs for the mature domain, and its true function

remains uncertain. Certain TGF-β pro-domains, such as the pro-domains of activin and TGF-βI, have been shown to exhibit a chaperone like effect where the pro-domain helps the mature domain to properly fold following translation (*11*). A second role for TGF-β pro-domains might be to function as regulatory molecules. The pro-domain of BMP-4, while still fused to the mature domain, has been shown to inhibit mature ligand activity (*12, 13*) whereas for other ligands, such as MIS or GDF-8, following cleavage from the mature domain the pro-domain is seen to non-covalently associate with the mature domain and prevent receptor binding and ligand induced signaling (*14, 15*). A third, less characterized function of TGF-β pro-domains may be to target the mature domain to specific regions of the extracellular matrix. The pro-domain of BMP-7 has been shown to bind fibrillin-1 and this interaction may localize and concentrate BMP-7 on the cell surface (*16*).

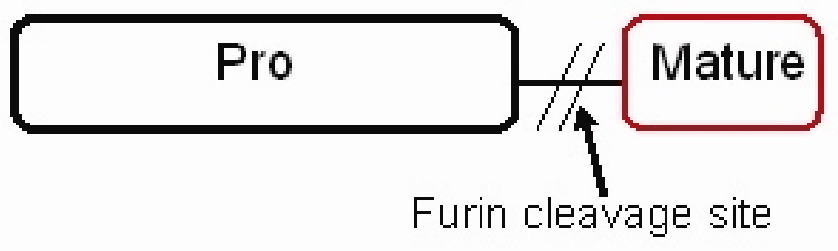

Figure 1-1. Diagram of TGF-β ligand. The ~30-50 kD pro-domain (black) is linked to the ~15 kD mature domain (red) by a protease linker region.

The protease cleavage site separating the two domains is a basic sequence recognized by specific propetide convertases (PCs). For the majority of TGF-β ligands this cleavage site shares the R-X-X-R motif recognized by the PC furin (*12,*

17). Once cleaved from the pro-domain, the mature domain is free to recruit and bind its appropriate receptor targets and initiate an intracellular signaling cascade. The hallmark feature of the mature domains of TGF-β ligands are their conserved structural architecture throughout the superfamily. In general, each mature TGF-β ligand contains seven structurally conserved cysteines, six of which form three intra-subunit disulfide bonds arranged into the 'cystine knot' motif (*18*). Using BMP-2 numbering, the knot is formed by disulfide bonds of Cys-14 to Cys 79, Cys-47 to Cys-113, and Cys-43 to Cys-111 (Figure 1-2, inset). The seventh cysteine, Cys-78, forms an inter-subunit disulfide bond with equivalent residue of a second mature ligand, creating a covalently linked dimer. This dimer has been shown to be the biologically active unit for the TGF-β superfamily (*19*). In addition to the cystine knot, all TGF-β ligand monomers possess four beta strands, forming two fingers, which extend outward from the cystine knot. Connecting these two fingers is the conserved single α-helix H3 (Figure 1-2). This characteristic TGF-β monomer fold gives the dimer the overall appearance of a butterfly with the fingers as wings stretching away from the cystine knot or body (Figure 1-2). Some TGF-β ligands, such as BMP-15 and GDF-9, lack the cysteine required to form the inter-subunit disulfide bond, yet still are able to form stable, non-covalent dimers (*20*). Further, in GDF-5 Cys-84, the equivalent of Cys-78 in BMP-2, was removed and GDF-5 was still shown to be active and believed to form a non-covalent dimer (*21*). The majority of TGF-β ligands have been found to be homodimers but heterodimers have also been found to exist *in vivo* and these heterodimers may have important biological functions (*22, 23*).

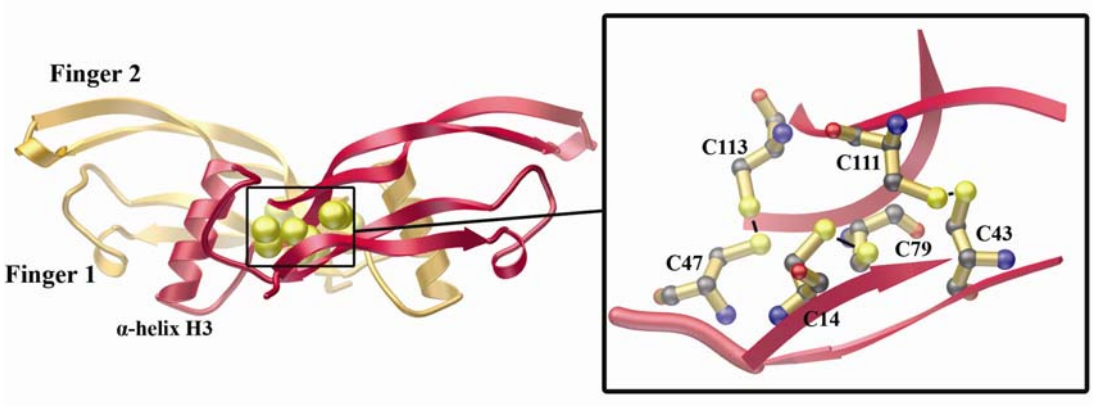

Figure 1-2. General overview of TGF-β Architecture. The inset shows a close-up of the cysteine knot. Monomer A is shown in red and monomer B is shown in yellow. Sulfur atoms are shown as yellow spheres.

To initiate a specific intracellular signaling pathway, a TGF-β ligand dimer must first bind to two sets of structurally related serine/threonine kinase receptors, termed type I and type II. These receptors range between 50-75 kD in size and are divided into three functional domains. At the N-terminus, there is a small extracellular domain (ECD) of approximately 15 kD which has been shown to adopt the three finger toxin fold for both type I and type II receptors (*24, 25*). A single transmembrane helix connects the ECD to the large intracellular kinase domain of around 50 kD. The kinase domain of the type II receptors is an autophosphorylated and constitutively active serine/threonine kinase which preferentially phosphorylates serine residues *in vivo* but also has the ability to phosphorylate threonine residues *in vitro (26-28)*. The type I receptor shares a similar serine/threonine kinase domain but, in addition, possesses a highly conserved SGSGSGLP sequence or GS domain immediately upstream of the kinase domain. This GS domain is only present in type I

receptors and interacts with intra-cellular signaling molecules of the TGF-β pathway (*29*). Compared to the over 40 TGF-β ligands, only 12 TGF-β receptors have been identified in the human genome (*30*). The receptors are divided almost evenly into the two receptor types: 7 type I and 5 type II. The type I receptors are universally named activin-like kinase (Alk) 1-7 but most have a secondary name associated with them to more accurately describe the ligands with which they interact. Alk-3 and Alk-6 are also named BMPRIa and BMPRIb, Alk-2 and Alk-4 can be called ActRIa and ActRIb, and Alk-5 goes by TGF-βRI. Alk-7 was originally designated an orphan receptor but has now been shown to bind any Nodal like ligand (*31*), while Alk-1 has been shown to bind both TGF-βI (*32*) and BMP-9 (*33*). The type II receptors lack the Alk designations and go by ActRII, ActRIIb, TGF-βRII, BMPRII, and MISRII (Figure 1-3).

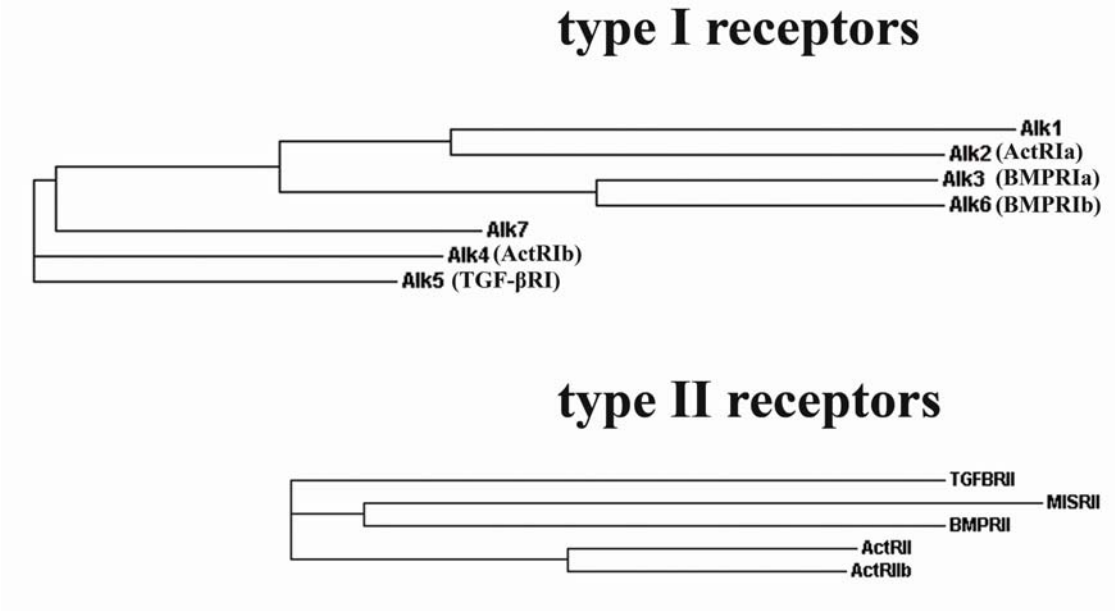

Figure 1-3. Phylogenic tree of TGF-β receptors**.** The receptors are broken into their respective types, either type I or type II.

The TGF-β ligands have been shown to interact with their receptors in a stepwise fashion by first binding two of their high affinity receptors followed by the binding of two of their lower affinity receptors. For both TGF-β and activin, the high affinity receptors have been shown to be the type II receptors. Indeed, binding of the type I receptors has not been seen in the absence of type II receptors (*29, 34*). Interestingly, in the BMP family, this trend of higher affinity for the type II receptors does not appear to be strictly followed. BMP-5,-6,-7, and -8 all bind type II receptors with high affinity, yet BMP-2 and -4 bind type I receptors with higher affinity (*35*). Further, in contrast to TGF-β and activin, BMP family members have been shown to be able to weakly bind their lower affinity receptors in the absence of the high affinity receptors. Once both high affinity receptors are bound, the TGF-β dimers can bind

two of their lower affinity receptors, forming a 6-member ternary complex consisting of a ligand dimer bound to two type I and two type II receptors. Binding of the lower affinity receptors is enhanced upon the presence of the high affinity receptors (*36*). The structural basis for this cooperative receptor binding remains unclear. One proposed model is the lower affinity interface is not formed until after the binding of the high affinity receptors (*37*). There is evidence that only when all four receptors are bound can downstream, intracellular signaling then occur (*38*). The exact nature of the sequential receptor binding and its impact on intracellular signaling remains unclear.

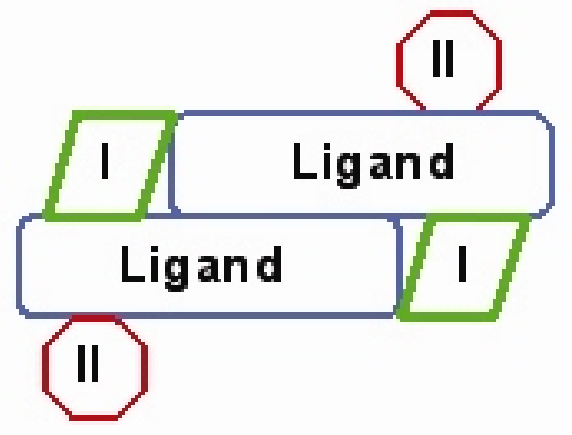

Figure 1-4. Schematic of TGF-β signaling complex. The type I receptors (green) bind at the interface of the ligand monomers (blue). The type II receptors (red) bind on the outside of each monomer.

Once bound to the TGF-β ligand, the close proximity of the kinase domains of both the type II and type I receptors allows the constitutively active type II receptors to phosphorylate the GS domain of the type I receptors. Following phosphorylation, the

type I receptors in turn are able to bind and phosphorylate intracellular receptor regulated signaling molecules called Smads (*39*). These receptor Smads, or R-Smads, consist of two Mad homology (MH) domains connected by a non-conserved linker region. The R-Smads are phosphorylated at two serine residues located at the extreme C-terminus of the molecule found in the highly conserved S-X-S motif (*40*). Currently, there are five known R-Smads, Smads-1, -2, -3, -5, and -8, and they can be broken down into two groups depending on which type I receptors they interact with. Smads-1/5/8 interact with type I receptors Alk-1, BMPRIa (Alk-3), BMPRIb (Alk-6), and ActRIa (Alk-2), while Smads 2/3 bind to type I receptors ActRIb (Alk-4), TGF-βRI (Alk-5), and Alk-7 (*40, 41*). Upon phosphorylation, the R-Smads dissociate from the type I receptors and form new complexes with a common Smad (Co-Smad), Smad-4. This R-Smad:Co-Smad complex is able to translocate to the nucleus where it binds a consensus DNA sequence on transcription factors, co-activators, or co-repressors (Figure 1-5) (*42, 43*).

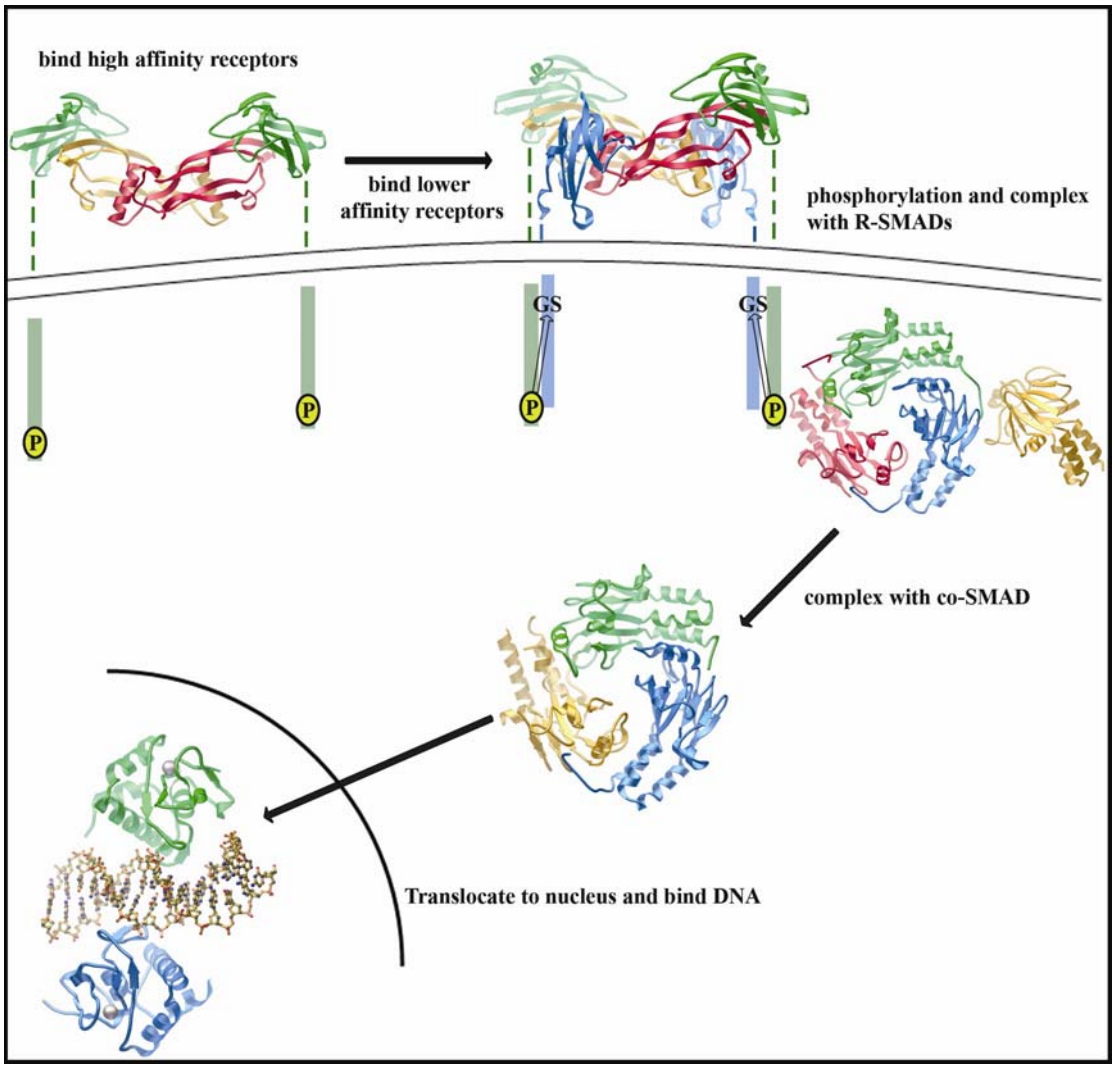

Figure 1-5. Overview of TGF-β Signal Transduction. The TGF-β ligand first binds it receptors, followed by phosphorylation of the GS domain and eventual interaction with intracellular Smad molecules.

As TGF-β ligands are in involved in numerous signaling pathways in a wide array of cell types, their functions must be tightly regulated. At the individual cell level, the mechanism of regulation can be divided into three distinct functional classes. The first form of TGF-β ligand regulation occurs in the extracellular milieu and this regulation is accomplished through the presence of extracellular antagonists. Similar

to the TGF-β superfamily, these antagonists can be divided into many different sub-families including Noggin, follistatin, the DAN family, and inhibin (*44*). These molecules have been found to function in two distinct ways. For molecules similar to Noggin and follistatin, these antagonists directly bind to TGF-β ligands, thereby preventing the ligands from interacting with the type I or type II receptors (Figure 1-6) (*45, 46*). Inhibin regulates TGF-β signaling in a slightly different manner by interacting not with the TGF-β ligands but with the receptors. Inhibin binds type II receptors ActRII or ActRIIb and sequesters them in a non-signaling complex. By binding all the type II receptors on the cell surface, none are left to bind to and signal with other TGF-β ligands (*47*). The second class of TGF-β antagonists can be found on the cell membrane where regulation is controlled by the actions of pseudo-receptors. These molecules, such as BMP and activin membrane bound inhibitor (BAMBI), contain an ECD and transmembrane domain but lack the intracellular kinase domain found in type I and type II receptors. When BAMBI is incorporated into a TGF-β ligand-receptor complex, the absence of the kinase domain prevents intracellular signaling from occurring (Figure 1-7) (*44*). The third class of TGF-β antagonists exists in the cytoplasm of the cell where intracellular regulation is controlled by inhibitory Smads or I-Smads. Smad -6 and -7 fall into this class of regulatory molecules and function by binding to the intracellular kinase domains of type I receptors, blocking the R-Smads from binding, effectively halting the remainder of the signaling cascade (Figure 1-8) (*48*).

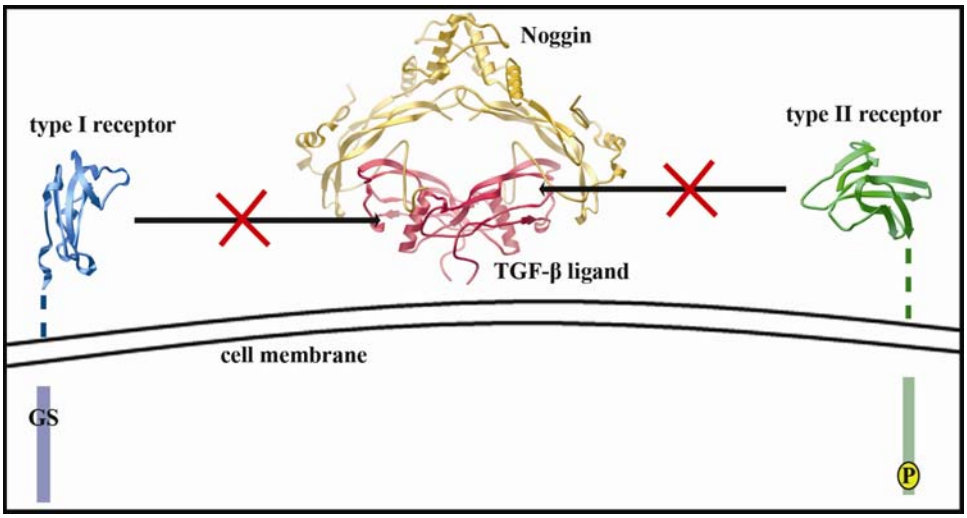

Figure 1-6. Extracellular regulation of TGF-β signaling. Noggin is positioned such that it blocks both receptor binding sites on the TGF-β ligand.

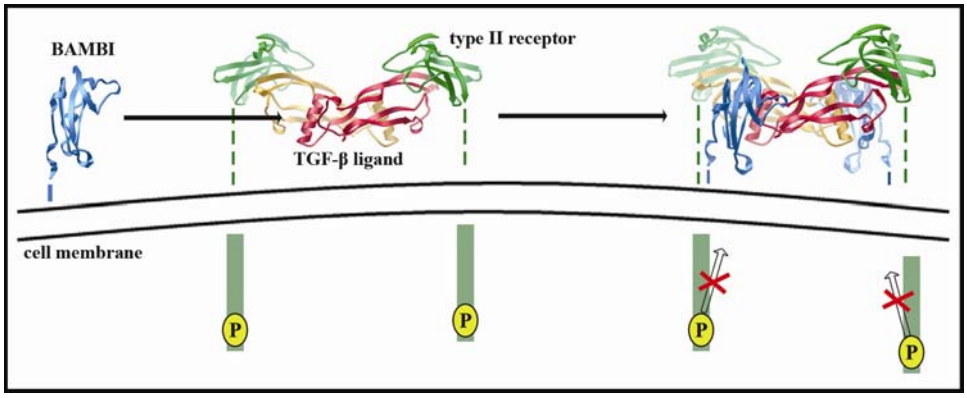

Figure 1-7. Intramembrane regulation of TGF-β signaling. BAMBI is incorporated into the ligand-receptor complex, but the complex cannot signal since BAMBI lacks an intracellular domain.

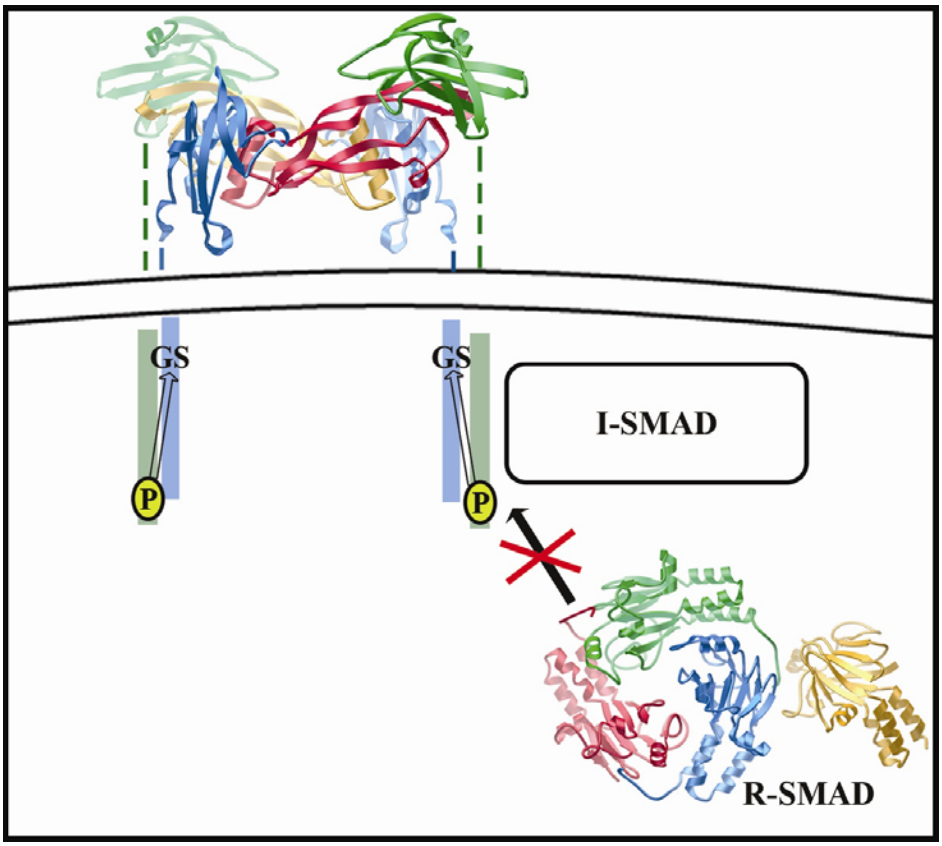

Figure 1-8. Intracellular regulation of TGF-β signaling. The I-Smads bind to the intracellular domains of type I receptors and block their interactions with R-Smads.

While tightly regulated at the individual cell level, TGF-β ligand function is also closely regulated on a larger, multi-cell or tissue level. One way in which this large scale regulation is controlled is through the formation of concentration gradients. To establish this type of regulation, a high concentration of TGF-β ligands is initially expressed in one particular region of cells. As the secreted TGF-β ligands proceed to diffuse outward from these starting cells, a morphogen gradient is created across over many cell diameters (*49*). The cells at the edge of the diffusion gradient experience a lower concentration of TGF-β ligands than the cells at the center of the diffusion

gradient and a variety of cells have been shown to respond differently to the specific level of TGF-β ligands experienced (*49, 50*). In *Xenopus* embryos dorsal/ventral patterning has been shown to be regulated by such a gradient of BMP-4 (*51*). Further, cells in animal caps switch from epidermal to mesodermal cell fates in response to changes in activin concentrations (*52*).

To better address the exact mechanisms of TGF-β signaling, the initial event of ligand-receptor binding at the cell surface has been closely examined on a structural level. A limited number of x-ray crystal structures with a TGF-β ligand dimer bound one receptor type, either type I or type II, have been solved. The crystal structure of TGF-βIII bound to TGF-βRII-ECD shows a mode of receptor binding in which one TGF-βRII-ECD molecule binds to one TGF-βIII monomer at the tip region of the ligand fingers (Figure 1-9a). Surprisingly, in this complex one monomer of the TGF-βIII dimer undergoes a large rotational unfolding ~100° out of plane (*37*). This dimer unfolding combined with the receptors binding to the tips of the ligand fingers gives the overall complex an elongated form. A second structure, of BMP-7 bound to ActRII-ECD, shows the ligand dimer in a different position compared to the TGF-βIII/TGF-βRII-ECD structure. In the BMP-7/ActRII-ECD complex, the BMP-7 dimer does not display the unfolding seen in TGF-βIII but rather is seen in its predicted active conformation (Figure 1-9b). Further, the position of the ActRII-ECD molecules interacting with the BMP-7 monomers differs from the location of the TGF-βRII molecules bound to TGF-βIII. One ActRII-ECD molecule is positioned on the outside

or concave face of the fingers rather than at the tips of the fingers on each ligand monomer as seen for TGF-βRII-ECDs (Figure 1-9).

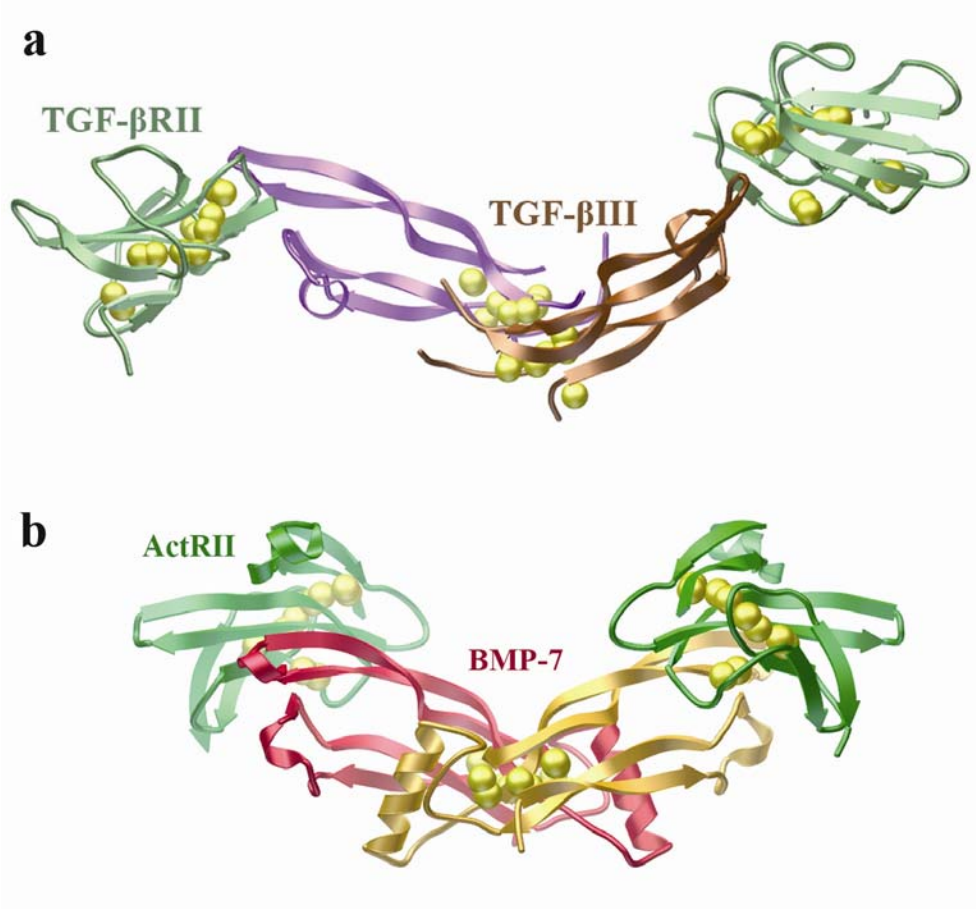

Figure 1-9. Comparison of type II receptor-ligand complexes. Panel (a) shows TGF-βIII bound to TGF-βRII, while panel (b) shows BMP-7 bound to ActRII.

To generate a complete, signaling competent ligand-receptor model, the TGF-βIII/TGF-βRII-ECD and BMP-7/ActRII-ECD structures were combined with the previously solved type I receptor complex of BMP-2/BMPRIa-ECD (*25*). Two differing modes of receptor complex formation were generated based on these

predicted ternary models. To form the homology model of TGF-βIII/TGF-βRII-ECD/BMPRIa-ECD, the ligand dimer must first be refolded back into its predicted active fold. This refolding allows for the formation of the α-helix H3 known to be directly involved in type I binding (*25*) which had become unstructured during the unfolding of the TGF-βIII monomer. The placement of the BMPRIa-ECD molecules in this model has one BMPRIa-ECD making contact with both monomers of TGF-βIII in a manner similar to that seen in the BMP-2/BMPRIa-ECD structure. In addition to the contacts made with the TGF-βIII monomers, one BMPRIa-ECD is also predicted to form contacts with one TGF-βRII-ECD molecule (Figure 1-10a). If accurate, this model helps explain why certain TGF-β ligands are unable bind type I receptor in the absence of type II receptors since the type I binding site would not completely formed until the type II receptors are bound. Focusing on the BMP-7/ActRII-ECD/BMPRIa-ECD homology model, a slightly different receptor binding arrangement is predicted. When modeled, the BMPRIa-ECD molecules are shown to only make contact with the monomers of BMP-7 and not with the ActRII-ECD molecules (Figure 1-10b). This difference in receptor complex assembly is a direct result of the placement of the ActRII-ECD molecules on BMP-7 compared to the position of the TGF-βRII-ECD molecules bound to TGF-βIII. By binding to the outside of the BMP-7 fingers, the ActRII-ECD molecules are shifted away from the type I binding site and are no longer in position to contact the type I receptors. If supported by additional structural data, the lack of contacts between receptor types in the BMP-7 ternary complex would confirm a unique mode of receptor complex formation. However, this model does not

fully explain the basis for the sequential and cooperative nature of receptor binding since the BMP-7 dimer does not appear to undergo conformational changes, unlike TGF-βIII.

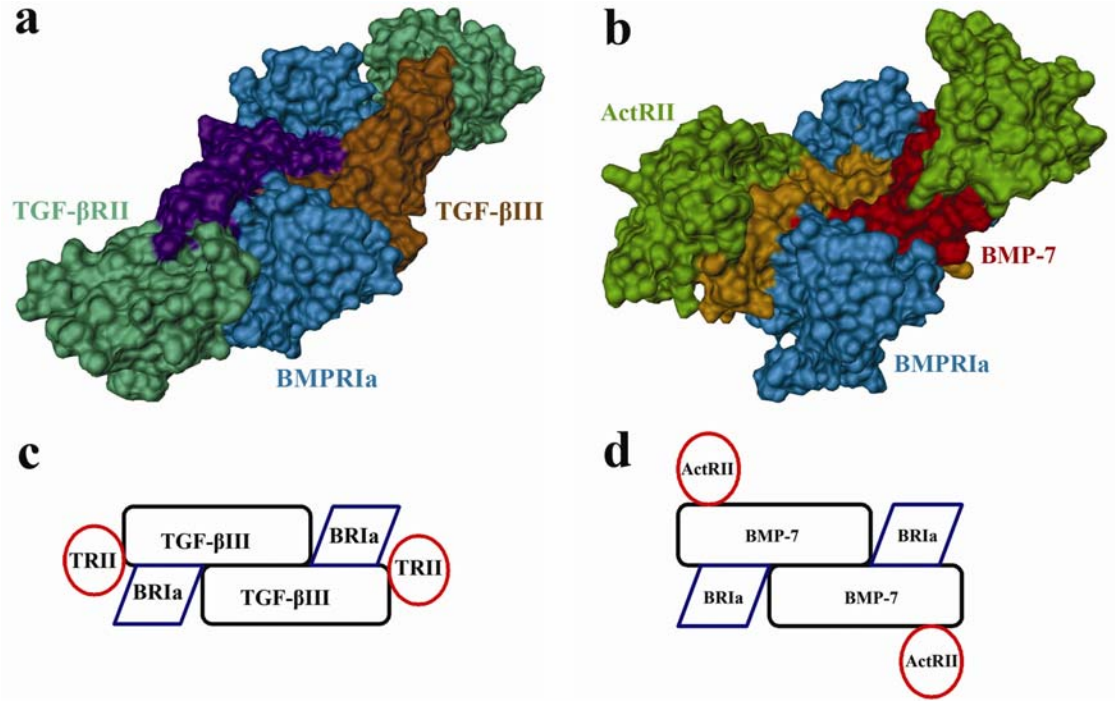

Figure 1-10. Representation of the ternary complexes. Panel (a) depicts the TGF-βIII/TGF-βRII/BMPRIa model, while (b) shows the BMP-7/ActRII/BMPRIa model. Panels (c) and (d) show a schematic of (a) and (b).

In addition to dissecting TGF-β ligand-receptor complex formation, determining how ligands regulate receptor affinity and specificity is also of importance. The disparity in the large number of ligands compared to the relatively few number of receptors necessitates that each receptor must be able to interact with multiple ligands. For instance, activin has been shown to bind ActRIb (Alk-4), ActRII, and ActRIIb, while BMPs have been shown to bind BMPRIa (Alk-3), BMPRIb (Alk-

6), and BMPRII in addition to ActRIa (Alk-2), ActrII, and ActRIIb (*53*). Not only do the receptors bind multiple ligands, they do so with varying affinity. ActRII was seen to bind activin with ~0.1 nM affinity, but can also bind BMP-7 with 1 nM and BMP-2 with ~50 nM affinity (*36*). While, the conserved structural architecture of the TGF-β superfamily must provide the underlying basis for this overlapping receptor specificity, specific interface residues must be responsible for the reported differing affinities. Only with additional TGF-β ligand-receptor structures can the determinants governing ligand-receptor binding be clearly identified.

To more accurately determine the true nature of ligand-receptor complex formation, the ternary structure of a TGF-β ligand bound to both sets of receptors (type I and type II) was needed. To that point, the complex of BMP-2 bound to two BMPRIa-ECD (type I) and two ActRII-ECD (type II) molecules was crystallized and solved to a resolution of 2.15 Å. The structure of a complete TGF-β signaling complex allows for numerous questions about the structural arrangement of receptors, the presence of any receptor-receptor contacts, and ligand conformational changes upon complex formation to be structrually addressed. Additionally, the BMP-2:ActRII-ECD interface is the first interface of a TGF-β ligand bound to a lower affinity receptor. Comparison of this interface with previously solved high affinity type II interfaces should yield insight into the structural determinants of receptor binding affinity. Though sharing a conserved core region, major differences between the type II interfaces were seen in the peripheral contact residues. Based on these differences, three residues were identified which, when inserted into BMP-2,

displayed a modest 2-fold increase in affinity to ActRII-ECD, while a fourth mutation exhibited a 5 to 10-fold increase.

To better understand the basis of co-operative receptor binding, the natural homo/hetero dimer system of activin/Inhibin was utilized. Using surface plasmon resonance (BIAcore), activin displayed a change in affinity to ActRIIb depending on the receptor density on the chip surface. Interestingly, inhibin which has only one ActRIIb binding site, did not share this density dependent affinity. This result suggests that complex formation is facilitated by the ligand's loss of rotational freedom upon high receptor affinity binding and is not solely dependent on conformational changes to the ligand. The immobilization of the ligand reduces the entropy of binding for the lower affinity receptor, thereby increasing its relative affinity.

To further explore if the presence of single or unique residues at receptor interfaces is a conserved mechanism for the modulation of TGF-β ligand-receptor binding affinity and specificity throughout the TGF-β superfamily, the structures of two less well characterized ligands, BMP-3 and BMP-6, were crystallized and solved to a resolution of 2.2 Å and 2.49 Å, respectively. BIAcore studies revealed the affinity of BMP-3 to ActRIIb was 30-fold higher than to ActRII. Using previously solved TGF-β ligand-receptor structures and the BMP-2 ternary structure, homology models of BMP-3 bound to ActRII or ActRIIb were generated. Analysis of these interfaces revealed a single residue swap between the receptors as the major difference. ActRIIb contains a glutamic acid in residue position 76, while in ActRII the equivalent residue

is a lysine. When the E76K mutation was inserted into ActRIIb, the receptor specificity of BMP-3 for ActRIIb was abolished.

The novel crystal structure of BMP-2/ActRII-ECD/BMPRIa-ECD combined with the structures of unbound BMP-3 and BMP-6 allow for new structural insights into TGF-β superfamily. Through structural analysis and mutagenesis studies, a conserved mechanism for determining receptor affinity and specificity was identified and a model proposed for the co-operative nature of receptor binding. Continued studies into modulating ligand-receptor interactions may yield promising results for therapeutic purposes.

1.2. References

1. Hogan, B. L. M. (1994) Developmental Signaling: Sorting out the signals, *Current Biology 4*, 1122-1124.

2. Massagué, J., and Chen, Y.-G. (2000) Controlling TGF-beta signaling, *Genes Dev. 14*, 627-644.

3. de Caestecker, M. (2004) The transforming growth factor-β superfamily of receptors, *Cytokine & Growth Factor Reviews 15*, 1-11.

4. Whitman, M., and Mercola, M. (2001) TGF-β Superfamily Signaling and Left-Right Asymmetry, *Sci. STKE 2001*, re1-.

5. Buck, M. B., and Knabbe, C. (2006) TGF-Beta Signaling in Breast Cancer, *Ann. N. Y. Acad. Sci. 1089*, 119-126.

6. Jakowlew, S. B. (2006) Transforming growth factor-β in cancer and metastasis, *Cancer Metastasis Rev. 25*, 23.

7. Massagué, J., Blain, S. W., and Lo, R. S. (2000) TGFβ Signaling in Growth Control, Cancer, and Heritable Disorders, *Cell 103*, 295-309.

8. Zhang, J., and Li, L. (2005) BMP signaling and stem cell regulation, *Developmental Biology 284*, 1-11.

9. Mishra, L., Shetty, K., Tang, Y., Stuart, A., and Byers, S. W. (2005) The role of TGF-β and Wnt signaling in gastrointestinal stem cells and cancer, *Oncogene 24*, 5775-5789.

10. Franceschi, R. T. (2005) Biological Approaches to Bone Regeneration by Gene Therapy, *J. Dent. Res. 84*, 1093-1103.

11. Gray, A. M., and Mason, A. J. (1990) Requirement for activin A and transforming growth factor--beta 1 pro-regions in homodimer assembly, *Science 247*, 1328-1330.

12. Cui, Y., Hackenmiller, R., Berg, L., Jean, F., Nakayama, T., Thomas, G., and Christian, J. L. (2001) The activity and signaling range of mature BMP-4 is regulated by sequential cleavage at two sites within the prodomain of the precursor, *Genes Dev. 15*, 2797-2802.

13. Sopory, S., Nelsen, S. M., Degnin, C., Wong, C., and Christian, J. L. (2006) Regulation of Bone Morphogenetic Protein-4 Activity by Sequence Elements within the Prodomain, *J. Biol. Chem. 281*, 34021-34031.

14. Nachtigal, M. W., and Ingraham, H. A. (1996) Bioactivation of Mullerian inhibiting substance during gonadal development by a kex2/subtilisin-like endoprotease, *Proc. Natl. Acad. Sci. 93*, 7711-7716.

15. R.S. Thies, T. C., M.V. Davies, K.N. Tomkinson, A.A. Pearson, Q.A. Shakey and N.M. Wolfman. (2001) GDF-8 propeptide binds to GDF-8 and antagonizes biological activity by inhibiting GDF-8 receptor binding, *Growth Factors 18*, 251-259.

16. Gregory, K. E., Ono, R. N., Charbonneau, N. L., Kuo, C.-L., Keene, D. R., Bachinger, H. P., and Sakai, L. Y. (2005) The Prodomain of BMP-7 Targets the BMP-7 Complex to the Extracellular Matrix, *J. Biol. Chem. 280*, 27970-27980.

17. Dubois, C. M., Laprise, M.-H., Blanchette, F., Gentry, L. E., and Leduc, R. (1995) Processing of Transforming Growth Factor beta 1 Precursor by Human Furin Convertase, *J. Biol. Chem. 270*, 10618-10624.

18. McDonald, N. Q., and Hendrickson, W. A. (1993) A structural superfamily of growth factors containing a cystine knot motif, *Cell 73*, 421-424.

19. Daopin, S., Piez, K. A., Ogawa, Y., and Davies, D. R. (1992) Crystal structure of transforming growth factor-beta 2: an unusual fold for the superfamily, *Science 257*, 369-373.

20. Liao, W. X., Moore, R. K., Otsuka, F., and Shimasaki, S. (2003) Effect of Intracellular Interactions on the Processing and Secretion of Bone Morphogenetic Protein-15 (BMP-15) and Growth and Differentiation Factor-9.

Implication of the abberant ovarian phenotype of BMP-15 mutant sheep, *J.Biol. Chem. 278*, 3713-3719.

21. Sieber C, Ploger F, Schwappacher R, Bechtold R, Hanke M, Kawai S, Muraki Y, Katsuura M, Kimura M, Rechtman MM, Henis YI, Pohl J, and Knaus P. (2006) Monomeric and dimeric GDF-5 show equal type I receptor binding and oligomerization capability and have the same biological activity., *Biol. Chem. 387*, 451-460.

22. Israel DI, Nove J, Kerns KM, Kaufman RJ, Rosen V, Cox KA, and JM., W. (1996) Heterodimeric bone morphogenetic proteins show enhanced activity in vitro and in vivo., *Growth Factors 13*, 291-300.

23. Keah, H. H., and Hearn, M. T. (2005) A molecular recognition paradigm: promiscuity associated with the ligand-receptor interactions of the activin members of the TGF-β superfamily, *J. Mol. Recognit. 18*, 385-403.

24. Greenwald, J., Le, V., Corrigan, A., Fischer, W., Komives, E., Vale, W., and Choe, S. (1998) Characterization of the Extracellular Ligand-Binding Domain of the Type II Activin Receptor, *Biochemistry 37*, 16711-16718.

25. Kirsch, T., Sebald, W., and Dreyer, M. K. (2000) Crystal structure of the BMP-2-BRIA ectodomain complex, *Nat. Struct. Mol. Biol. 7*, 492-496.

26. Lin, H. Y., Wang, X.-F., Ng-Eaton, E., Weinberg, R. A., and Lodish, H. F. (1992) Expression cloning of the TGF-β type II receptor, a functional transmembrane serine/threonine kinase, *Cell 68*, 775-785.

27. Mathews, L. S., and Vale, W. W. (1991) Expression cloning of an activin receptor, a predicted transmembrane serine kinase, *Cell 65*, 973-982.

28. Chen, F., and Weinberg, R. A. (1995) Biochemical Evidence for the Autophosphorylation and Transphosphorylation of Transforming Growth Factor β Receptor Kinases, *Proc. Natl. Acad. Sci. 92*, 1565-1569.

29. Wrana, J. L., Attisano, L., Wieser, R., Ventura, F., and Massagué, J. (1994) Mechanism of activation of the TGF-β receptor, *Nature 370*, 341-347.

30. Manning, G., Whyte, D. B., Martinez, R., Hunter, T., and Sudarsanam, S. (2002) The Protein Kinase Complement of the Human Genome, *Science 298*, 1912-1934.

31. Reissmann, E., Jornvall, H., Blokzijl, A., Andersson, O., Chang, C., Minchiotti, G., Persico, M. G., Ibanez, C. F., and Brivanlou, A. H. (2001) The orphan receptor ALK7 and the Activin receptor ALK4 mediate signaling by Nodal proteins during vertebrate development, *Genes Dev. 15*, 2010-2022.

32. Chen, Y.-G., and Massagué, J. (1999) Smad1 Recognition and Activation by the ALK1 Group of Transforming Growth Factor-beta Family Receptors, *J. Biol. Chem. 274*, 3672-3677.

33. Brown, M. A., Zhao, Q., Baker, K. A., Naik, C., Chen, C., Pukac, L., Singh, M., Tsareva, T., Parice, Y., Mahoney, A., Roschke, V., Sanyal, I., and Choe, S. (2005) Crystal Structure of BMP-9 and Functional Interactions with Pro-region and Receptors, *J. Biol. Chem. 280*, 25111-25118.

34. Attisano, L., Wrana, J. L., Montalvo, E., and Massague, J. (1996) Activation of signalling by the activin receptor complex, *Mol. Cell. Biol. 16*, 1066-1073.

35. Liu, F., Ventura, F., Doody, J., and Massague, J. (1995) Human type II receptor for bone morphogenic proteins (BMPs): extension of the two-kinase receptor model to the BMPs, *Mol. Cell. Biol. 15*, 3479-3486.

36. Greenwald, J., Groppe, J., Gray, P., Wiater, E., Kwiatkowski, W., Vale, W., and Choe, S. (2003) The BMP7/ActRII Extracellular Domain Complex Provides New Insights into the Cooperative Nature of Receptor Assembly, *Molecular Cell 11*, 605-617.

37. Hart, P. J., Deep, S., Taylor, A. B., Shu, Z., Hinck, C. S., and Hinck, A. P. (2002) Crystal structure of the human TβR2 ectodomain-TGF-β3 complex, *Nat. Struct. Mol. Biol. 9*, 203-208.

38. Laiho, M., Weis, M. B., and Massague, J. (1990) Concomitant loss of transforming growth factor (TGF)-beta receptor types I and II in TGF-beta-resistant cell mutants implicates both receptor types in signal transduction, *J. Biol. Chem. 265*, 18518-18524.

39. Massagué, J. (1998) TGF-beta; signal transduction, *Annu. Rev. Biochem. 67*, 753-791.

40. Attisano, L., and Lee-Hoeflich, S. T. (2001) The Smads, *Genome Biology 2(8)*, 3010.3011-3010.3018.

41. Massagué, J., Seoane, J., and Wotton, D. (2005) Smad transcription factors, *Genes Dev. 19*, 2783-2810.

42. Wrana, J. L. (2000) Regulation of Smad Activity, *Cell 100*, 189-192.

43. Heldin, C.-H., Miyazono, K., and ten Dijke, P. (1997) TGF-β signalling from cell membrane to nucleus through SMAD proteins, *Nature 390*, 465-471.

44. Balemans, W., and Van Hul, W. (2002) Extracellular Regulation of BMP Signaling in Vertebrates: A Cocktail of Modulators, *Developmental Biology 250*, 231-250.

45. Thompson, T. B., Lerch, T. F., Cook, R. W., Woodruff, T. K., and Jardetzky, T. S. (2005) The Structure of the Follistatin:Activin Complex Reveals Antagonism of Both Type I and Type II Receptor Binding, *Developmental Cell 9*, 535-543.

46. Groppe, J., Greenwald, J., Wiater, E., Rodriguez-Leon, J., Economides, A. N., Kwiatkowski, W., Affolter, M., Vale, W. W., Belmonte, J. C. I., and Choe, S. (2002) Structural basis of BMP signalling inhibition by the cystine knot protein Noggin, *Nature 420*, 636-642.

47. Wiater, E., and Vale, W. (2003) Inhibin Is an Antagonist of Bone Morphogenetic Protein Signaling, *J. Biol. Chem. 278*, 7934-7941.

48. SH, P. (2005) Fine tuning and cross-talking of TGF-beta signal by inhibitory Smads, *J Biochem Mol Biol. 38*, 9-16.

49. Jones, C. M., Armes, N., and Smith, J. C. (1996) Signalling by TGF-β family members: short-range effects of Xnr-2 and BMP-4 contrast with the long-range effects of activin, *Current Biology 6*, 1468-1475.

50. Rogulja, D., and Irvine, K. D. (2005) Regulation of Cell Proliferation by a Morphogen Gradient, *Cell 123*, 449-461.

51. Dale, L., and Wardle, F. C. (1999) A gradient of BMP activity specifies dorsal-ventral fates in early Xenopus embryos, *Seminars in Cell & Developmental Biology 10*, 319-326.

52. Hemmati-Brivanlou, A., and Melton, D. A. (1992) A truncated activin receptor inhibits mesoderm induction and formation of axial structures in Xenopus embryos, *Nature 359*, 609-614.

53. Massagué, J. (1996) TGF-β Signaling: Receptors, Transducers, and Mad Proteins, *Cell 85*, 947-950.

Chapter 2. Ternary Structure of BMP-2/BMPRIa-ECD/ActRII-ECD

2.1. Introduction

TGF-β ligands initiate their intracellular signaling responses through interactions with receptors on the cell surface. Determining the exact structural arrangement of the receptors when these complexes form has been a main focus of current research. Recently, several binary structures of TGF-β ligands in complex with their high-affinity receptor ECDs have been determined. These structures include one type I receptor complex, BMP-2/BMPRIa-ECD (*1*), and two type II receptor complexes, TGF-βIII/TGF-βRII-ECD (*2*) and BMP-7/ActRII-ECD (*3*). Based on these structures, two differing models for ternary receptor complex formation can be formed. The TGF-β ternary model of TGF-βIII/TGF-βRII-ECD/BMPRIa-ECD (*2*) suggests a complex in which the type I and type II receptors make contact with each other while the BMP ternary model of BMP-7/BMPRIa-ECD/ActRII-ECD (*3*) predicts the receptors are positioned in such a way that they would not interact with each other. To fully address these competing views of TGF-β receptor complex assembly, the structure of a complete, signaling competent TGF-β ternary complex is required. With this ternary structure, the actual receptor orientation and any conformational changes to the ligand or receptors upon binding will be captured. Additionally, the structure will allow for the identification of the structural determinants controlling differences in TGF-β ligands' affinities for the same receptor.

2.2. BMP-2/BMPRIa-ECD/ActRII-ECD Crystal Structure

To address these lingering questions concerning TGF-β ligand-receptor assembly, the structure of BMP-2 bound to the ECDs of both the type I receptor BMPRIa and the type II receptor ActRII was crystallized and solved to a final resolution of 2.15 Å. BMP-2 was used as the ligand for its ability to bind both receptors with relatively high affinity as well as it is more efficiently refolded from inclusion bodies than other TGF-β ligands (*1*). BMPRIa and ActRII were chosen as the type I and type II receptors, respectively, because they have been shown to be actively expressed in large enough quantities for crystallization trials (*1*, *4*). Crystals for the BMP-2/BMRPIa-ECD/ActRII-ECD complex were found to grow in two independent conditions. The first suitable crystals for x-ray diffraction were found in a 15% Iso-propanol, 0.1M HEPES pH 7.5, 15% PEG 4000 condition at room temperature. However, the diffraction pattern generated from these crystals revealed a major flaw. When orientated down an arbitrary 0° angle, the diffraction pattern looked very good, with symmetric reflections (Figure 2-1). However, when rotatated 90°, the diffraction pattern showed a splitting of the reflections. This splitting there are many imperfections to the crystal (Figure 2-2). This high mosaicity, a measure of crystal uniformity, prevented the indexing of the crystal space group rendering the information useless for structure determination.

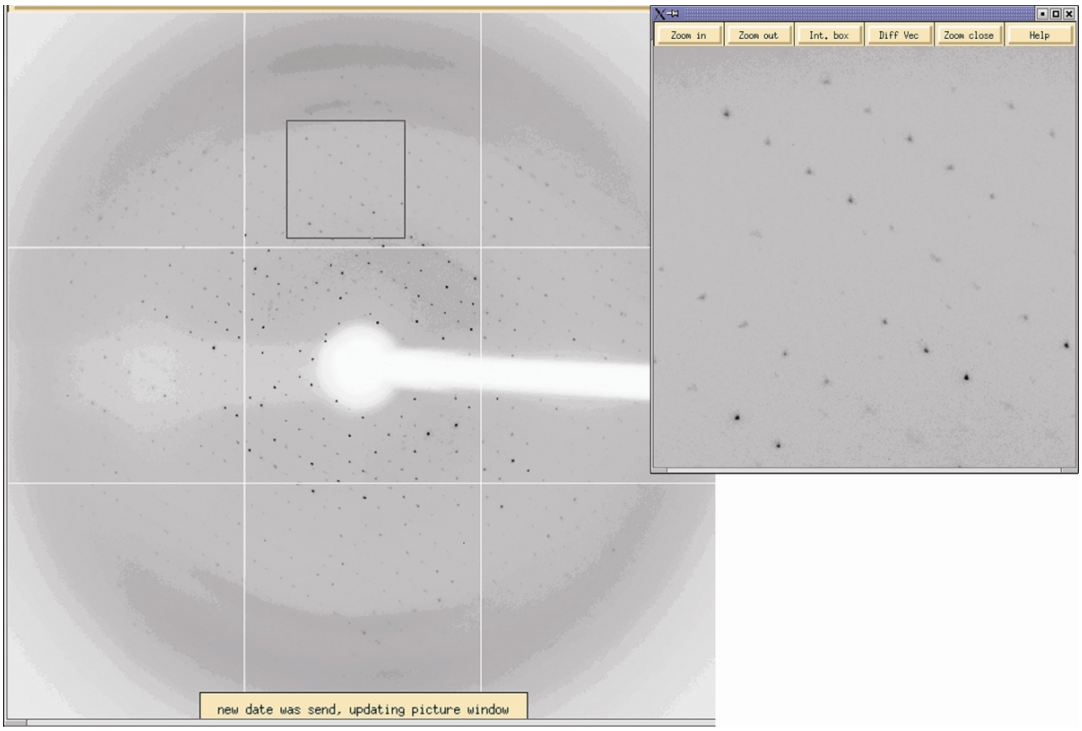

Figure 2-1. X-ray diffraction pattern crystal condition #1. The image represents the diffraction pattern taken down the 0° plane. The inset is a magnification of pattern to show the symmetry of the reflections.

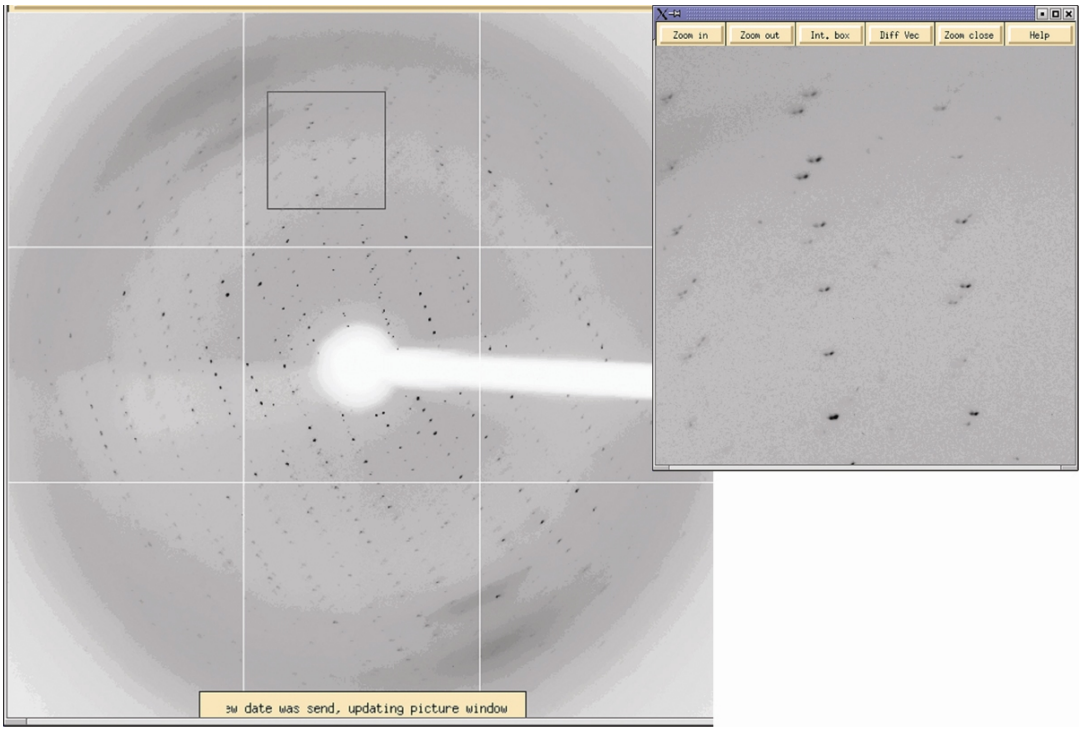

Figure 2-2. X-ray diffraction pattern crystal condition #1. The image represents the diffraction pattern taken down the 90° plane. The inset is a magnification of pattern to show the splitting of the reflections.

A second crystal form was found in a sodium formate condition at 4° C (see Chapter 6 for complete crystallization details). These crystals did not display the same mosaicity problem as the room temperature crystals as both the 0° and 90° reflections show symmetric reflections with no splitting. These crystals were used for subsequent data collection and eventual structure solution. The BMP-2/BMPRIa-ECD/ActRII-ECD complex crystallized in the $P6_522$ space group with a=b=104.8 Å and c=363.3 Å, with $\alpha=\beta=90°$ and $\gamma=120°$. The presence of such a large unit cell dimension, c=363.3 Å, presented a difficult challenge to good data collection. As the distance between the reflections is inversely related to the unit cell dimensions, the long c axis generates closely spaced reflections on the detector. Indeed, the size of the detector in allowing

for resolving of these reflections limited the resolution range for crystal #1 to 2.5 Å. To overcome this limitation, the data for crystal #2 were collected on a large detector, MarMosiac 325, to increase the distance between reflections. By using this large detector the resolution for crystal #2 was increased to 2.15 Å.

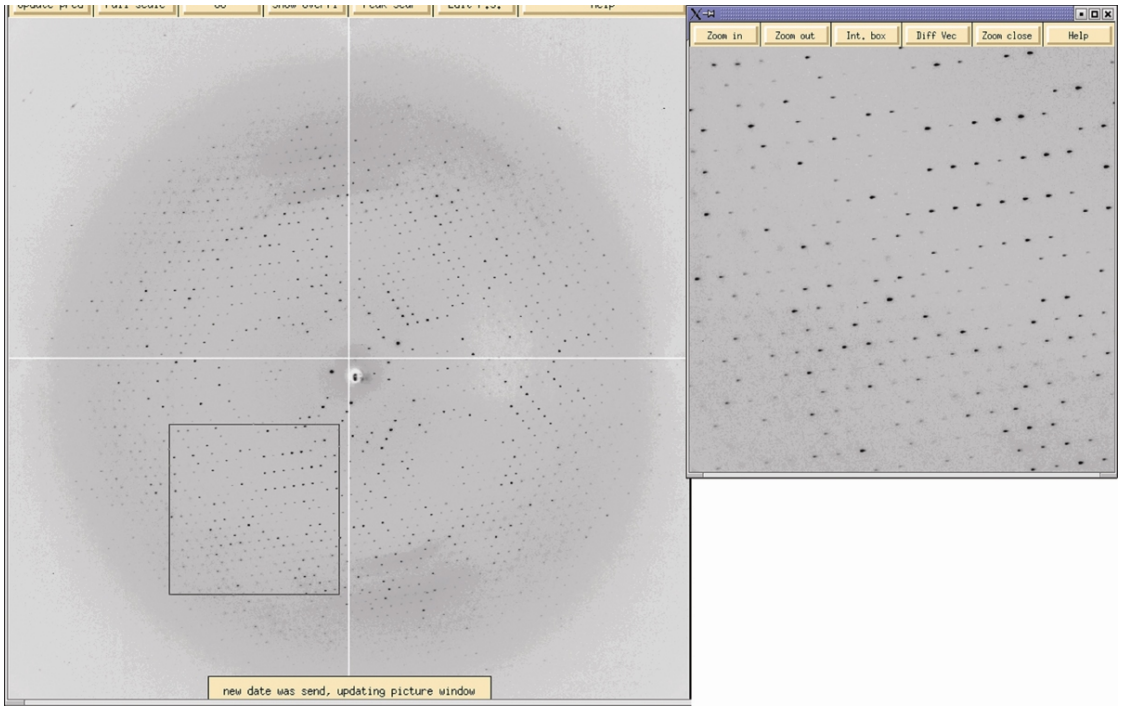

Figure 2-3. X-ray diffraction pattern crystal condition #2. The image represents the diffraction pattern taken down the 0° plane. The inset is a magnification of pattern to show the symmetry of the reflections.

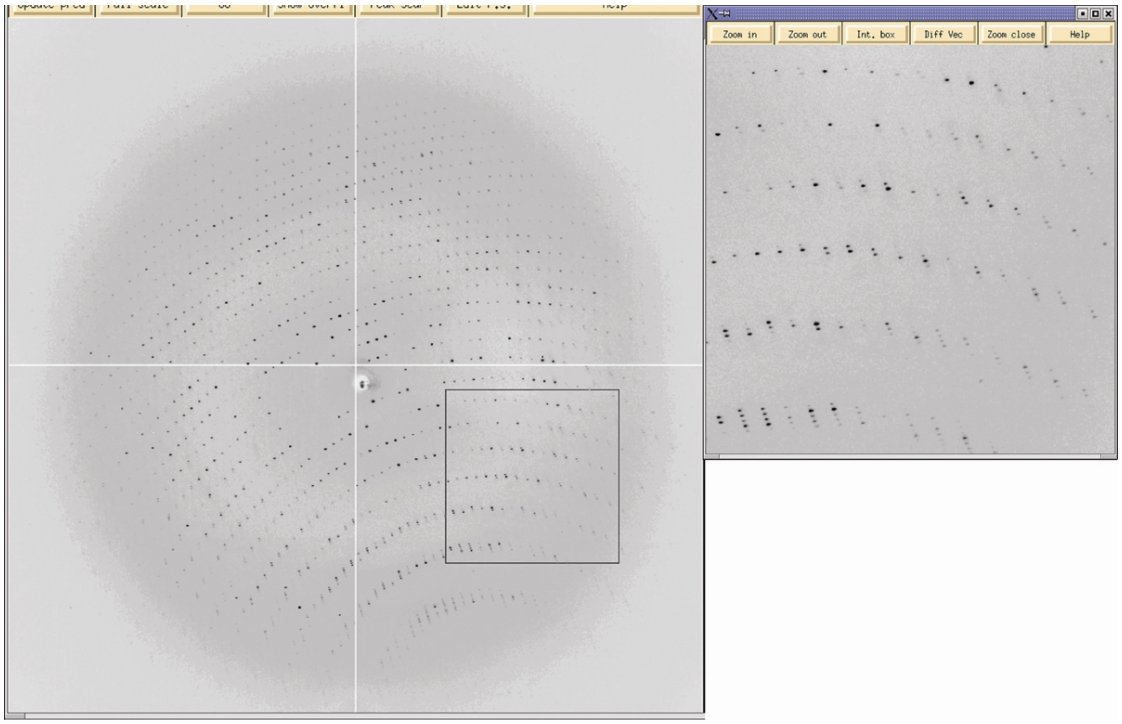

Figure 2-4. X-ray diffraction pattern crystal condition #2. The image represents the diffraction pattern taken down the 90° plane. The inset is a magnification of pattern to show the symmetry of the reflections.

Molecular replacement, using the previously solved BMP-2/BMPRIa-ECD structure (*1*) as the initial model, was used to obtain initial phases for the BMP-2/BMPRIa-ECD/ActRII-ECD ternary structure. Based on the calculated Matthews coefficient, the number of complex monomers (which would include a single ligand monomer associated with one BMPRIa-ECD and one ActRII-ECD molecule) per asymmetric unit could be two, three, or four. The best solution was found by searching for two independent halves (one BMP-2 monomer bound to one BMPRIa molecule) of the BMP-2/BMPRIa-ECD complex. When looking at this initial solution, electron density for the ActRII-ECD molecules was clearly visible. The two ActRII-ECD molecules could then be positioned into the electron density by using a single

ActRII-ECD molecule from the BMP-7/ActRII-ECD complex (*3*) as a search model. The initial molecular replacement solution was found using the lower resolution data set from crystal #1. This data set was used as the reflections have very high redundancy and molecular replacement does not require the highest resolution data. Following a rigid body refinement, the solution for the lower resolution data set was placed into the higher resolution data set of crystal #2 for further refinement, obtaining the final 2.15 Å resolution. The crystal appears to pack loosely with a solvent content greater than 65%. Most of the crystal contacts appear to be generated through side chain interactions between the BMPRIa molecules as well as side chain interactions between ActRII molecules. The final solution reveals that each asymmetric unit contains a complete TGF-β ternary signaling complex consisting of a BMP-2 dimer bound to two BMPRIa-ECD and two ActRII ECD molecules (Figure 2-5). Across the interface between the BMP-2 ligand monomers in the asymmetric unit there exists a 2-fold non-crystallographic symmetry (NCS) plane (Figure 2-5).

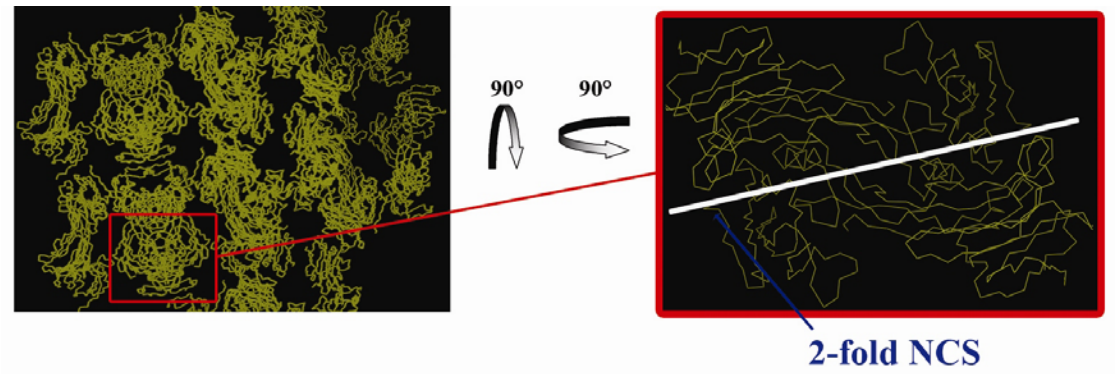

Figure 2-5. Representation of crystal packing. The left image shows the crystal lattice packing for the entire crystal. The right image shows a close up of the asymmetric unit with the 2-fold NCS plane shown in white.

Table 2-1 summarizes the x-ray diffraction and refinement statistics for the BMP-2/BMPRIa-ECD/ActRII-ECD structure. In brief, the ternary complex was refined to a final R factor of 19.0% with a free R factor of 24.0%. The structure displayed good overall geometry with 87.4% of the residues falling in the most favored regions and none in the disallowed regions, as evaluated by a Ramachandran plot. However, the backbone geometry of six residues fell into the generously allowed regions. Closer inspection of these residues finds that they are Ser-72 in both ActRII-ECD molecules, Phe-41 in both BMP-2 ligand molecules, and Asp-89 in both BMPRIa-ECD molecules. Examining the 2Fo-Fc electron density maps contoured at 1σ, the Ser-72 residues of ActRII-ECD are found in strong main-chain but weak side-chain electron density. The location and orientation of the Ser-72 residues positions the side-chain atoms toward solvent and away from the binding interface with BMP-2 (Figure 2-6, 1). There are no contacts to stabilize the side of Ser-72 and the geometry of the residue must be a result of the carbon backbone bending to form the loop connecting beta strands in ActRII-ECD. The Phe-41 residues of BMP-2 are located in finger 1 of each ligand monomer. Similar to Ser-72 of ActRII-ECD, Phe-41 is pointed toward the solvent and is not involved in a receptor interface. However, there is strong electron density for both main chain and side chain atoms and the geometry of the residue is necessary to allow proper stacking of the side-chain ring between the side-chains of Arg-16 and His-39 (Figure 2-6, 2). The side-chain of Val-107 also provides additional stabilizing contacts for this conformation. Residue Asp-89 of the

BMPRIa-ECD molecules is found at the interface with BMP-2. The geometry of the residue is maintained by a hydrogen bond network of the Asp-89 side-chain with a water molecule and a side-chain nitrogen of Arg-97 of BMPRIa (Figure 2-6, 3). Additional Van der Waals interactions are provided by Phe-49 and Leu-66 of BMP-2 to help stabilize the conformation of Asp-89 of BMPRIa-ECD.

Table 2-1. Data collection and refinement statistics for the BMP-2/BMPRIa-ECD/ActRII-ECD crystal structure.

BMP-2 X-ray Data Collection and Refinement Statistics

	Crystal #1	**Crystal #2**
Data Collection		
Beamline	ALS 5-1	SSRL 9-2
Space Group	$P6_522$	$P6_522$
Number of Observations	332,262	454,504
Unique Reflections	39,363	62,054
Resolution Range (Å)[1]	50-2.5 (2.59-2.50)	50-2.15(2.23-2.15)
Average I/σI	24.8 (3.2)	18.8 (4.7)
Completeness (%)	94.7 (96.2)	96.4 (89.4)
R_{sym} (%)	6.8 (40.4)	8.5 (40.2)
Refinement		
Resolution Range	64.7-2.50	84.5-2.15
R_{cryst} (%)	19.9	19.8
R_{free} (%)[2]	24.1	24.0
Average B factor (Å^2)	41.7	40.1
Rms Deviation		
Bonds (Å)	0.013	0.008
Angles (°)	1.442	1.065
Number of Atoms		
Protein		4478
Water		330
Ramachadran plot non –gly, -pro, terminal residues		
most favored regions		437 (87.4%)
Additionally allowed regions		57 (11.4%)
Generously allowed regions		6 (1.2%)

[1] Numbers parentheses correspond to the highest resolution shell

[2] Calculated from 5 % of the data not used in refinement

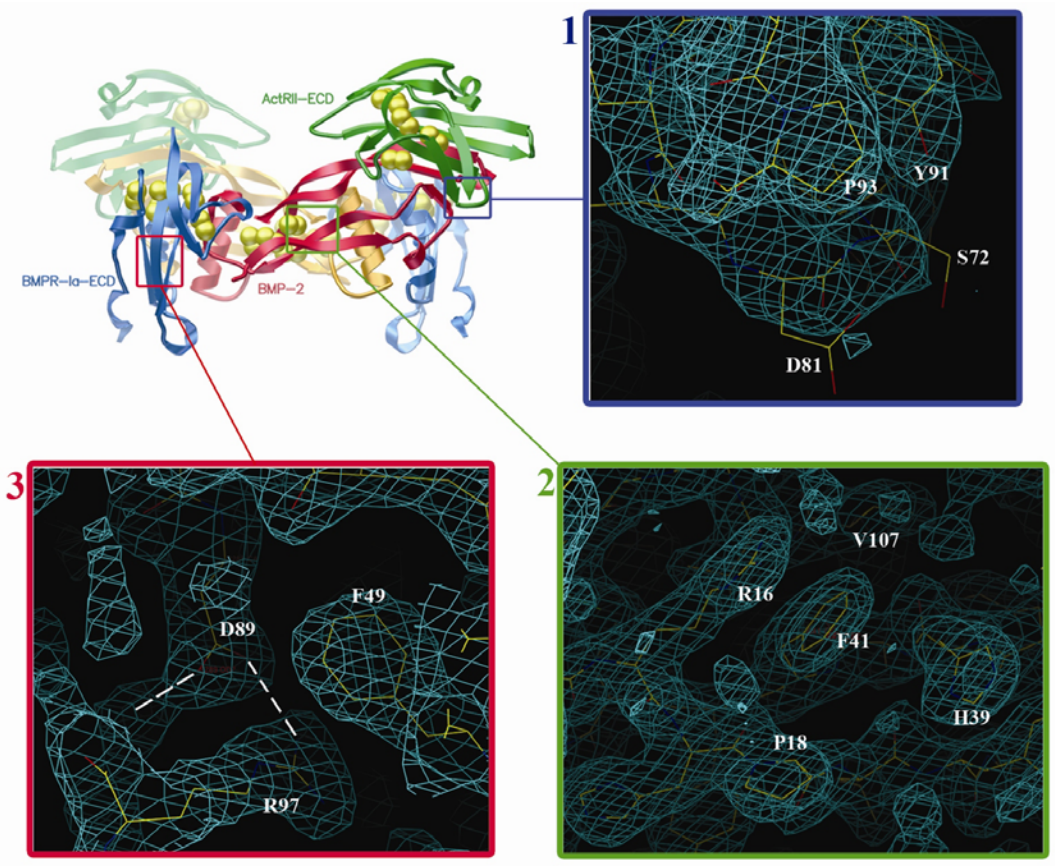

Figure 2-6. Electron density of the generously allowed residues in the BMP-2 ternary complex. Panel 1 shows S72 of ActRII, panel 2 shows F41 of BMP-2, and panel 3 shows D89 of BMPRIa. The white lines in panel 3 indicate hydrogen bonding. Electron density is contoured to 1σ in a 2Fo-Fc map.

As with previously solved crystal structures of TGF-β ligands, the N-terminal residues of the BMP-2 molecules (residues 1-10) are flexible and cannot be seen in the electron density map. Further, the N-terminal and C-terminal residues of BMPRIa-ECD also appear to be flexible, with only residues 33-118 for one BMPRIa-ECD molecule and residues 34-120 for the other visible out of the possible 1-129. Similar

to BMPRIa-ECD, the N-terminal residues (1-6) and the very C-terminal residues (100-102) of the ActRII-ECD molecules could not be found in the electron density maps and are most likely mobile. The BMP-2 ternary complex crystallized in the expected, signaling competent conformation. The BMP-2 dimer is seen in its 'wing spread' or active conformation in which the two fingers of one monomer are pointed almost 180° away from the corresponding fingers in the other monomer (Figure 2-7). The two BMPRIa-ECD molecules are located at opposite sides of the BMP-2 dimer at the junction between the monomers. The BMPRIa-ECD molecules pack tightly against the α-helix H3 and the H3 pre-helix loop of one BMP-2 monomer and the inside of the fingers of the other BMP-2 monomer (Figure 2-7). Conversely, the ActRII-ECD molecules only contact one BMP-2 monomer and are positioned on the outside, concave or knuckle region of fingers 1 and 2 of each BMP-2 monomer (Figure 2-7). The location of the bound receptors positions them such that the C-terminal residues of either ActRII-ECD or BMPRIa-ECD are over 75 Å apart along one BMP-2 monomer (Figure 2-8, a) and ~38 Å apart across the dimer interface (Figure 2-8, b). The BMP-2 ternary structure firmly supports that none of the receptors make contact with each other upon complex formation. Further, the ternary structure confirms the receptor assembly hypothesis based on the BMP-7 homology model (*3*). However, as ~30 N-terminal and ~10 C-terminal residues from the BMPRIa-ECD molecules and ~15 C-terminal residues from the ActRII-ECD molecules are missing, the possibility for receptor-receptor contacts cannot be completely ruled out.

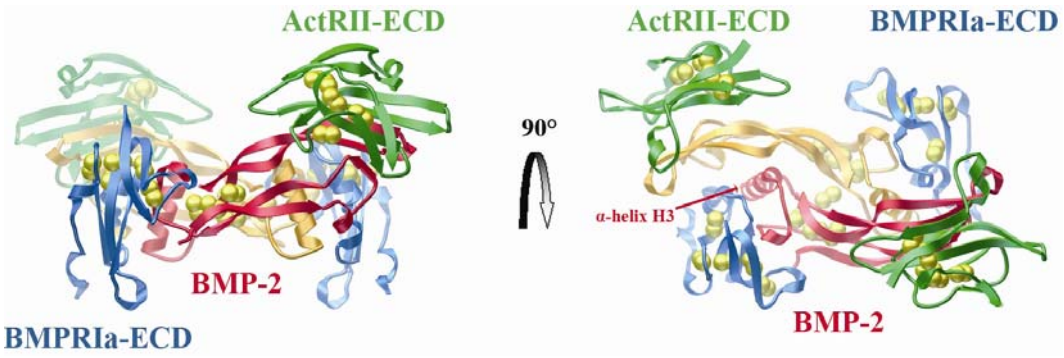

Figure 2-7. Ribbon depiction of BMP-2/BMPRIa-ECD/ActRII-ECD crystal structure. The left image shows the ternary structure as seen on the membrane, while the image on the right is looking down on the membrane from above. The yellow spheres depict sulfur atoms.

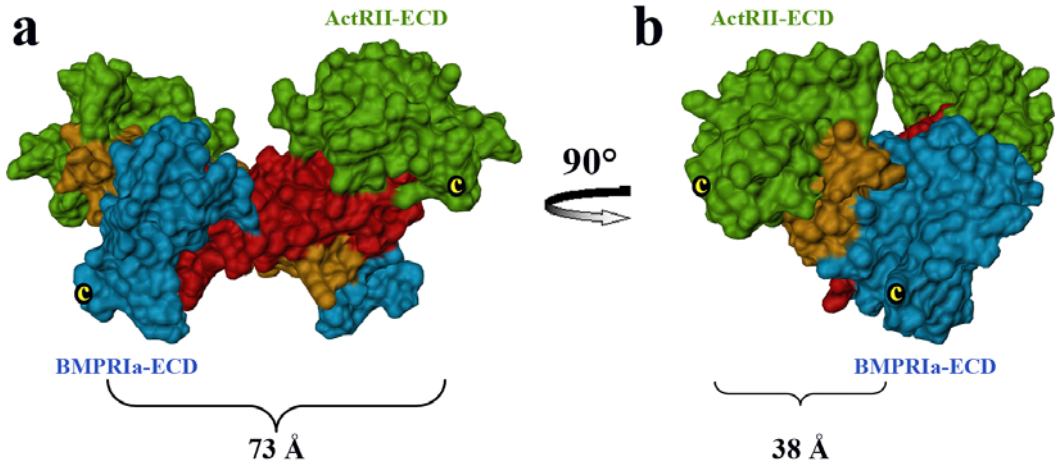

Figure 2-8. Space filling representation of the ternary complex. Panel (a) shows the structure as seen on the membrane. Panel (b) shows the image in panel (a) rotated 90°. The C-terminus of BMPRIa-ECD and ActRII-ECD are labeled.

Focusing on the ternary structure more closely, the two BMP-2 monomers adopt the previously seen TGF-β superfamily architecture. Each monomer has the characteristic 'cystine knot' motif formed by disulfide bonds between Cys-14 to Cys 79, Cys-47 to Cys-113, and Cys-43 to Cys-111 (Figure 2-9, inset). Additionally, in

each monomer there are four beta strands forming two extended fingers, as well as the conserved α-helix H3 (Figure 2-9). The two BMP-2 monomers are covalently linked through an inter-subunit disulfide bond formed between Cys-78 of each monomer. The fold of each BMP-2 monomer gives the dimer the general appearance of a butterfly with the 'cystine knot' as the body and the fingers as the wings (Figure 2-9). When the BMP-2 dimer from the ternary complex is superimposed onto the BMP-2 dimer from the BMP-2/BMPRIa-ECD structure (*1*), few if any backbone shifts are required for a good fit. The Cα RMS deviation is only 0.574 Å over the entire dimer, with the largest deviation in the Cα backbone of 1.30 Å seen in residues Asp-53 and His-54 (5). These residues are located in the H3 pre-helix loop region and while the main-chain atoms may be slightly shifted for these residues between the BMP-2 molecules, the side-chains are still located in similar positions and maintain the same contacts with BMPRIa-ECD. The excellent fit between the BMP-2 dimers of the ternary BMP-2/BMPRIa-ECD/ActRII-ECD complex and the binary BMP-2/BMPRIa-ECD structure reveals that conformational changes to the ligand are not required for type II receptor binding. However, the absence of receptor-receptor contacts combined with the lack of ligand conformational changes leaves the mechanism of the known cooperative receptor binding unanswered.

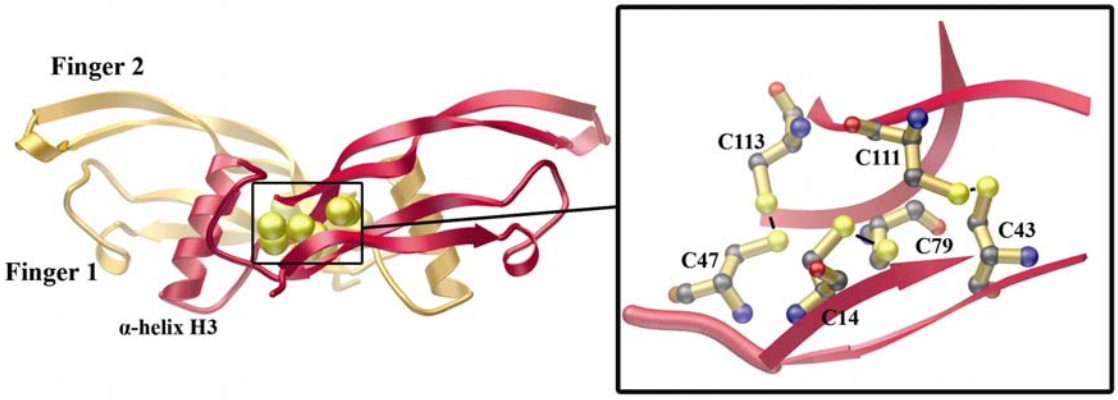

Figure 2-9. Ribbon representation of BMP-2. The inset shows a close-up of the cysteine knot.

As previously mentioned, the BMPRIa-ECD molecules are located at the junction of both monomers of BMP-2. Each BMPRIa-ECD molecule contains five beta strands and the single, short α-helix 1 (Figure 2-10). These five strands form two separate beta sheets, which give the BMPRIa-ECD molecules there distinctive shape, the 3-finger toxin fold (*6*). In both BMPRIa molecules, the electron density can be seen for Loop 3 (L3) (residues 66-70), connecting beta strands 4 and 5, which was not present in the original BMP-2/BMPRIa-ECD structure (*1*). When the BMPRIa-ECD molecules from the BMP-2 ternary structure and the BMP-2/BMPRIa-ECD binary structure (*1*) are overlaid, the BMPRIa-ECD molecules align very well, with a Cα RMS deviation of 0.30 Å (*5*). The largest difference in the alignment between the BMPRIa-ECD molecules is seen in the loop connecting beta strands 1 and 2. However, these residues (46-48) are not found at the interface with BMP-2. The lack of movement in the BMPRIa-ECD molecules, combined with minimal conformational changes in the BMP-2 molecules upon type II receptor binding, suggests that the

receptor interfaces are independent of each other and that conformational changes to the type I receptor interface are not required for type II receptor binding .

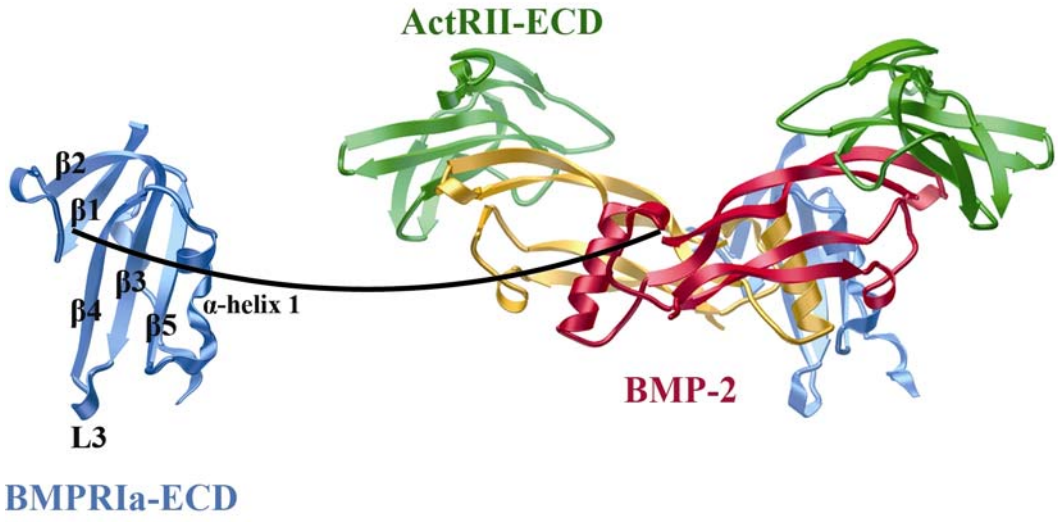

Figure 2-10. Ribbon representation of the ternary complex. One BMPRIa-ECD molecule is peeled away to show the details of the BMPRIa-ECD molecule.

The BMP-2:BMPRIa-ECD interface is fairly large in size and is composed of 26 residues from BMPRIa and 15 residues from monomer A and 12 residues from monomer B of BMP-2 (Figure 2-11). The buried surface at the interface is 1217 $Å^2$, which is ~2-fold larger than the buried surface area for known type II interfaces (*2*, *3*, *7*, *8*). The interface is dominated by residue side-chain contacts between residues on α-helix 1 and beta strands 3 and 4 of BMPRIa-ECD with residues from α-helix H3 and the H3 pre-helix loop of BMP-2 (Figure 2-11). The interface contains a hydrophobic core, which includes ~40% of all residue contacts at the interface, with the surrounding residues consisting primarily of polar or charged contacts (Figure 2-12).

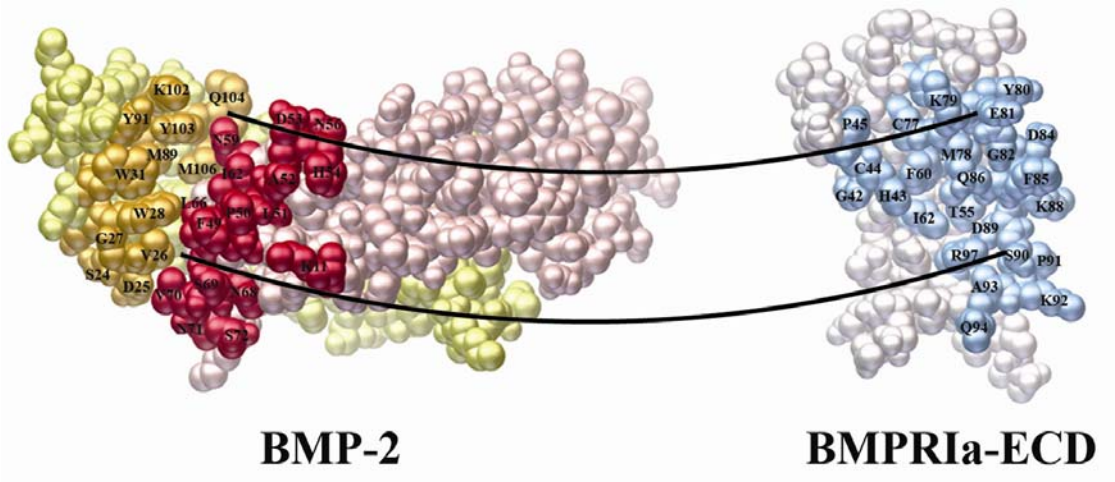

Figure 2-11. Pealed away view of the BMP-2:BMPRIa-ECD interface. The residues involved in the interface are in dark colors and labeled.

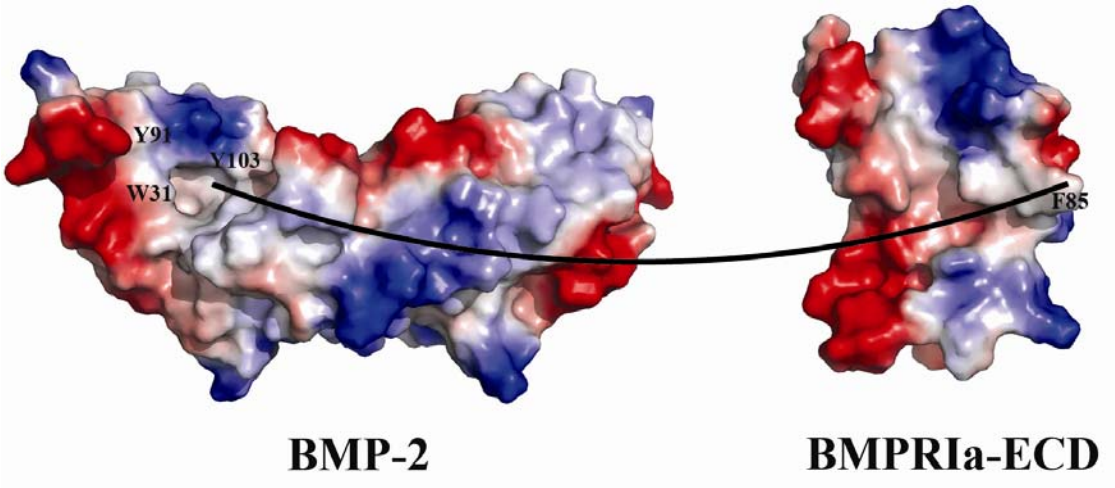

Figure 2-12. Electrostatic potential representation of the BMP-2:BMPRIa-ECD interface. The labeled residues represent key residues forming the hydrophobic pocket at interface.

Unlike the BMPRIa-ECD interface, which is formed by residues from both BMP-2 monomers, the ActRII-ECD interface is found at the outside or concave face of each BMP-2 monomer. In this arrangement, each ActRII-ECD molecule only makes contact with a single BMP-2 monomer (Figure 2-13). Each of the ActRII-ECD

molecules adopts the characteristic 3-finger toxin fold motif (*4*). The seven beta strands found in the ActRII-ECD create three fingers and the overall fold is further stabilized by the presence of eight cysteines, which form four intra-disulfide bonds (Figure 2-13). Since the ActRII-ECDs bind to the outside, concave surface of the BMP-2 fingers, the ActRII-ECDs also have a concave and convex surface. When the ActRII-ECD molecules from the BMP-2/ActRII-ECD interface of the ternary structure are superimposed on either the ActRII-ECD molecules from the BMP-7/ActRII-ECD complex (*3*) or the ActRIIb-ECD molecules from the activin/ActRIIb-ECD structure (*7*), all molecules aligned very well with Cα RMS differences of only 0.66 Å and 0.82 Å, respectively. The major difference between an ActRII-ECD molecule from the ternary complex and an ActRIIb-ECD molecule is seen in the loop 5 region (residues 76-81) connecting beta strands 5 and 6 (Figure 2-14). Between the ActRII-ECD molecules bound to BMP-2 and BMP-7, the only significant difference in the structures is seen in the M-loop (residues 33-38) (Figure 2-14). The minor ActRII-ECD backbone shifts, coupled with the lack of significant movements in the BMP-2 ligand or the BMPRIa-ECD molecules, indicates that the presence of a bound type I receptor does not alter the conformation of the type II receptor interface.

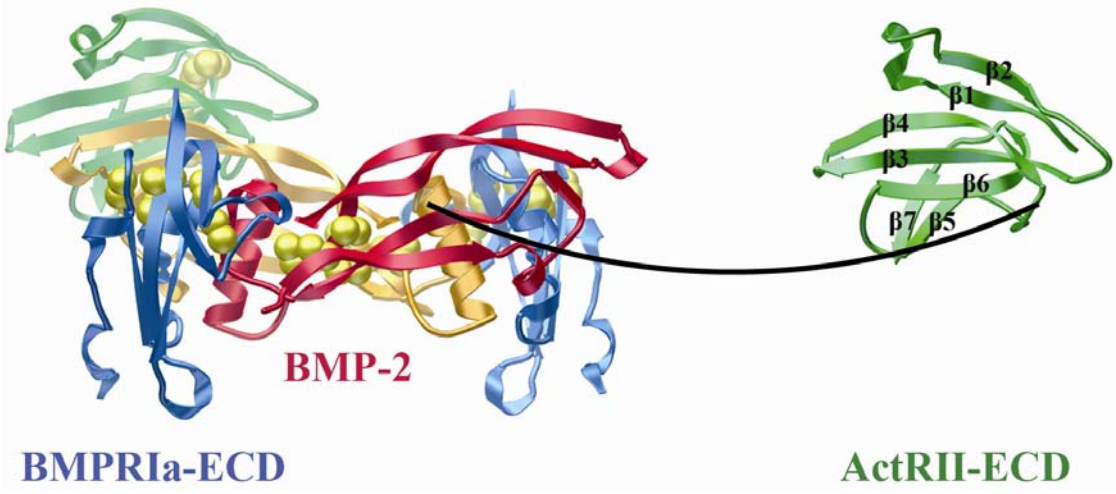

Figure 2-13. Ribbon representation of ternary complex. One ActRII-ECD molecule is peeled away to highlight its structure.

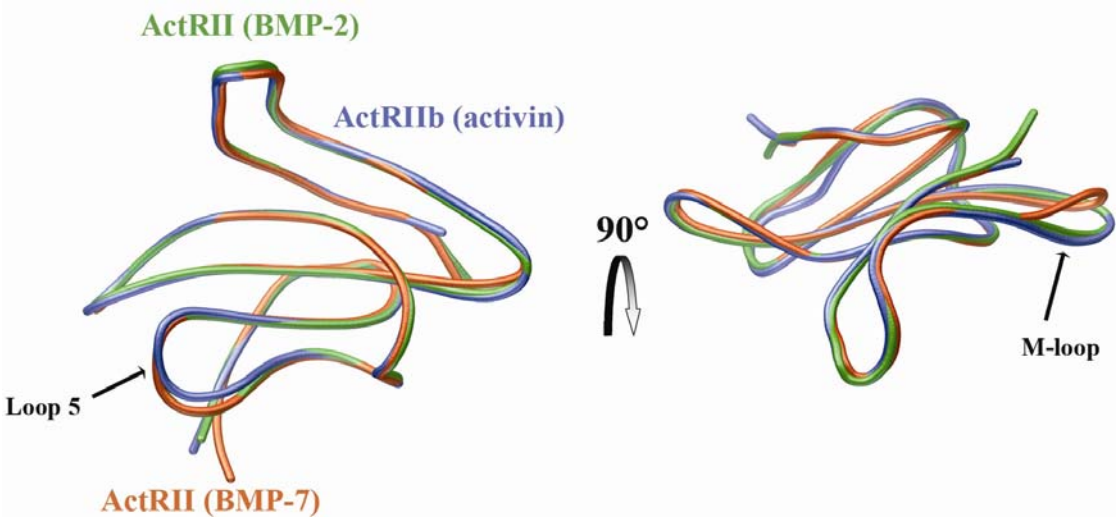

Figure 2-14. Overlay of the known ActRII and ActRIIb structures. The left image shows the differences in the Loop 5 region, while the right image shows the differences in the M-loop.

The BMP-2:ActRII-ECD interface is formed by 12 residues of BMP-2 contacting 10 residues from ActRII with a buried surface area of 670 $Å^2$ (Figure 2-15). As previously mentioned this is roughly half the buried surface area of the BMP-

2:BMPRIa-ECD interface (1217 Å^2). Similar to the BMP-2:BMPRIa-ECD interface, the BMP-2:ActRII-ECD interface consists of a hydrophobic core surrounded by polar and charged residues (Figure 2-16). Using BMP-2 numbering this hydrophobic core is made by residues Ala-34, Pro-35, Ser-86, and Leu-90 of BMP-2 with Phe-42, Trp-60, Leu-61, and Phe-83 of ActRII (Figure 2-15, Figure 2-16). Previous studies have shown that disruption of any of these core residues on ActRII negatively impacts receptor binding (9). Surrounding these core residues are additional, primarily hydrophobic residues, making a majority of the total interface hydrophobic in nature. The contacts found at the edges of the interface are formed almost entirely by polar or charged residues. (Figure 2-16).

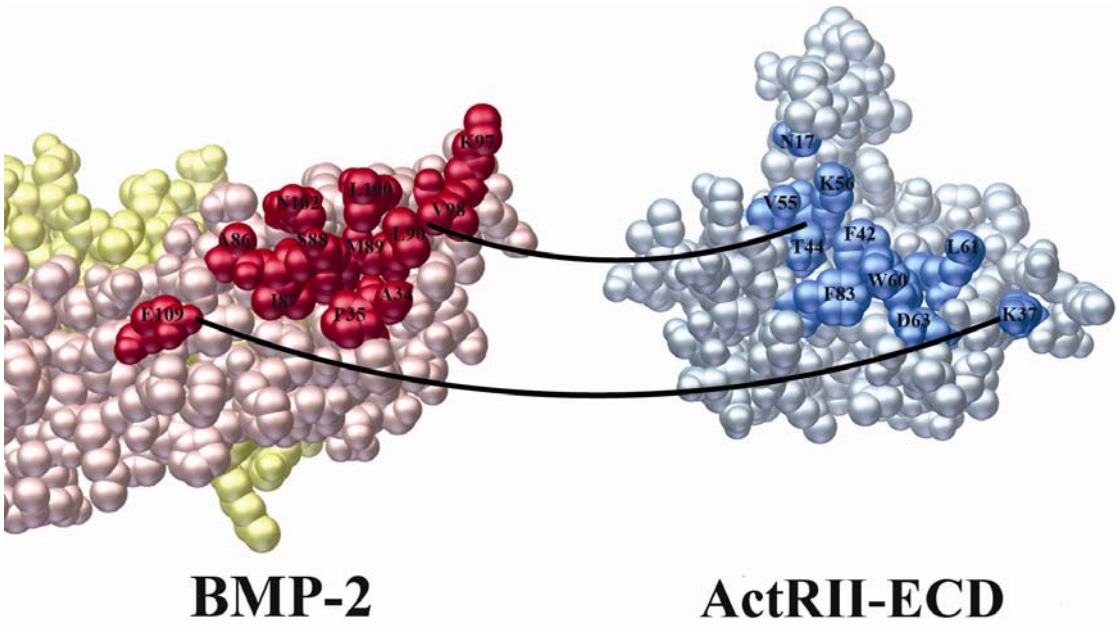

Figure 2-15. Peeled away view of the BMP-2:ActRII-ECD interface. Residues involved in the interface are in darkened colors and labeled. Curved lines show contact points.

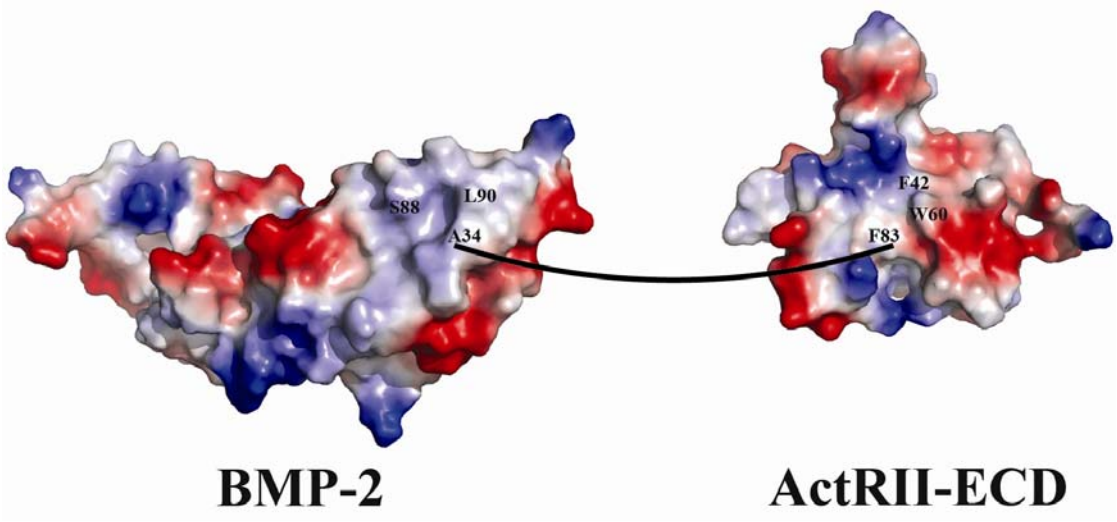

Figure 2-16. Electrostatic representation of the BMP-2:ActRII-ECD interface. The hydrophobic core residues are labeled. The curved line shows a contact point.

As with the type I receptors, the type II receptors exhibit a wide range of ligand binding affinities. The addition of the BMP-2:ActRII-ECD interface, the first structure of a TGF-β ligand bound to its lower affinity receptor, combined with previously solved the high affinity interfaces of BMP-7:ActRII (*3*) and activin:ActRIIb-ECD (*7, 8*) allows for analysis of how TGF-β ligands regulate this wide range of differing affinities. Initial comparison of the three interfaces reveals that they are remarkably similar. As mentioned above, the buried surface area of BMP-2:ActRII-ECD interface is 670 $Å^2$. This is comparable to the size of BMP-7:ActRII-ECD interface, which has a buried surface area of 660 $Å^2$, and the activin:ActRIIb-ECD interface, which is slightly larger with a buried surface area of 774 $Å^2$. The number of contacts are also similar between all three interfaces, with the BMP-7:ActRII-ECD interface formed by 12 residues of BMP-7 contacting 9 residues of ActRII, while the activin:ActRIIb-ECD interface involves 13 residues on both

activin and ActRIIb. Interestingly, the majority of the residues forming theses interfaces are conserved among all three structures. The residues forming the hydrophobic core are structurally equivalent in all three interfaces (Figure 2-17, pink). Surrounding these core residues is a set highly conserved residues (Figure 2-17, green). The residues located at the edges of the interfaces are non-conserved and primarily polar or charged (Figure 2-17, blue). The number, type, and location of these non-conserved residues varies between the different interfaces. For the lower affinity interface of BMP-2:ActRII-ECD there are only three residues, two in BMP-2 and one in ActRII, which are non-conserved. Conversely, the high affinity interface of BMP-7:ActRII-ECD has four ligand and two receptor non-conserved residues and the activin:ActRIIb-ECD interface has six ligand and three receptor residues which are non-conserved (Figure 2-17). The presence of these non-conserved residues makes different interfaces unique and must encode each ligand's type II receptor affinity and specificity.

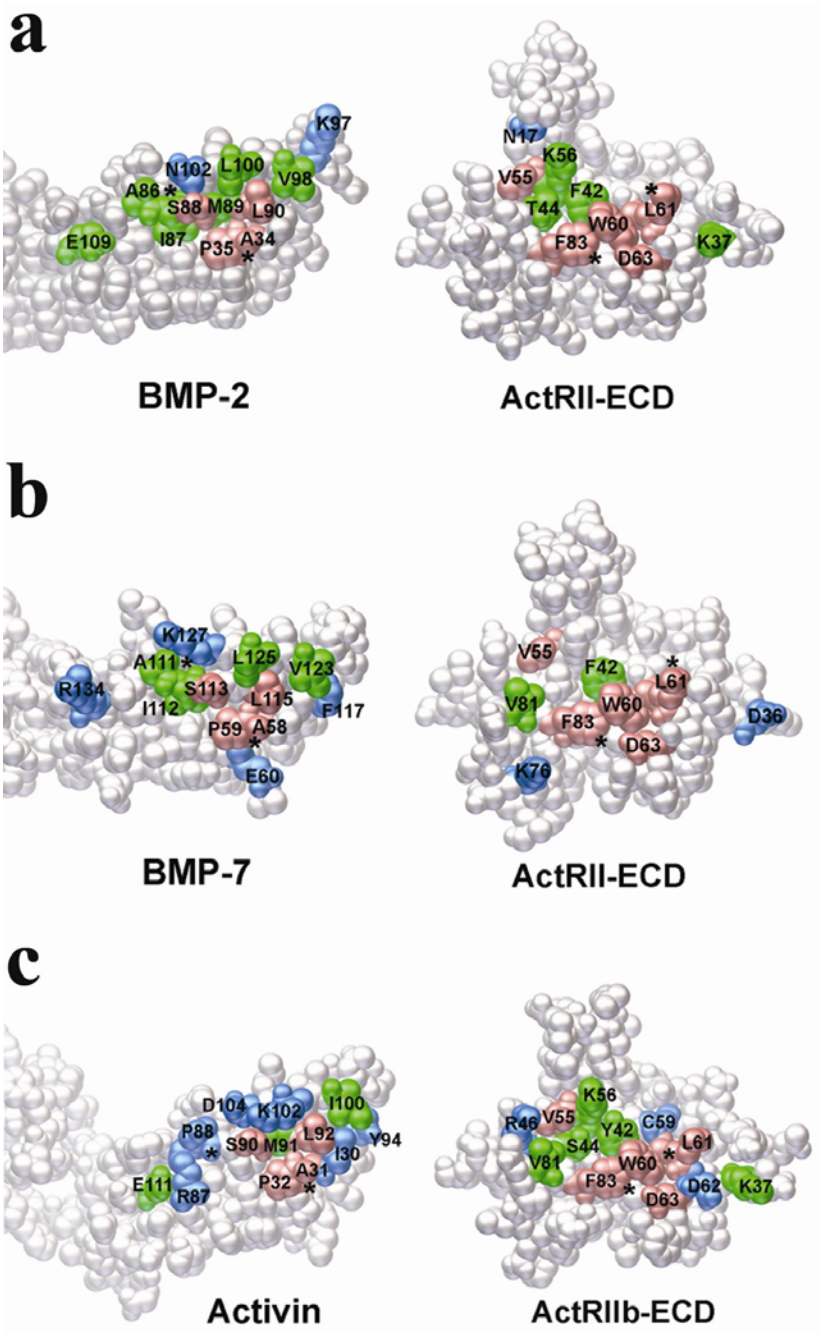

Figure 2-17. Comparison of known type II interfaces. Panel (a) shows the BMP-2:ActRII-ECD interface, panel (b) displays the BMP-7:ActRII-ECD interface and panel (c) depicts the activin:ActRIIb-ECD interface. Residues in pink are identical in all interfaces, green residues are highly conserved, and blue residues are unique.

2.3. BMP-2 Mutagenesis Studies

With ~40 TGF-β ligands and only 12 different TGF-β receptors, a unique feature of the TGF-β receptors is their ability to bind multiple ligands with differing affinity and specificity. Both type I and type II receptors share this large range of ligand affinities. For instance, BMPRIa has been shown to bind BMP-2 with high affinity, K_D ~3 nM, yet binds BMP-7 with much lower affinity, K_D ~1.5 μM (*3*). While subtle conformational changes between the ligands may have an impact on determining ligand-receptor affinity, the major the structural influences must be encoded by the unique residues found in either interface. Therefore, in an attempt to locate the residues responsible for this ~500-fold difference in affinity, the interfaces of BMP-2:BMPRIa-ECD and BMP-7:BMPRIa-ECD were compared. The BMP-7:BMPRIa-ECD was generated by superimposing the BMP-7 ligand from BMP-7:ActRII-ECD (*3*) with the BMP-2 ligand from the ternary structure. This BMP-7 ligand was chosen because its H3 pre-helix loop was reported to be in a more similar conformation to that of BMP-2's H3 pre-helix loop than the H3 pre-helix loop of unbound BMP-7 (*3*). The two ligands superimpose well, with a Cα RMS deviation of 2.18 Å between the two ligands. While not perfect, the close fit between the ligands suggests the BMP-7:BMPRIa-ECD model interface is representative of the true interface.

Previous studies have shown that a single mutation in the H3 pre-helix loop of BMP-2, L51P, can disrupt its binding to BMPRIa (*10*). Based on this information, the the H3 α-helix and the H3 pre-helix loop region was the focus of the comparisons

between the two interfaces. As with the type II interfaces, the residues in this region of the interface are very similar between BMP-2 and BMP-7 (Figure 2-18). However, one small section of the H3 pre-helix loop, residues 52-54 in BMP-2, is significantly different. In BMP-2, these residues are Ala-52, Asp-53, and His-54. The side chain Asp-53 makes a hydrogen bond with the side chain of Thr-55 of BMPRIa, while the side chain of His-54 makes a salt bridge interaction with the main-chain carbonyls of His-44 and Cys-43 of BMPRIa (Figure 2-19). In BMP-7, the structurally equivalent residues are Asn-76, Ser-77, and Tyr-78. Both Ser-77 and Tyr-78 are not predicted to be able to generate the same contacts seen in the BMP-2:BMPRIa-ECD interface. Because these residue differences are all located adjacent to each other, the triple mutant of A52N/D53S/H71Y was introduced into BMP-2 as a single construct.

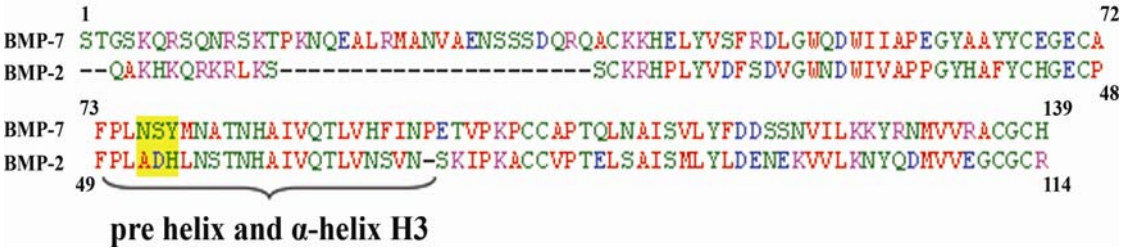

Figure 2-18. Sequence alignment of BMP-2 and BMP-7. In yellow are the three residues mutated to make BMP-2 mimic BMP-7.

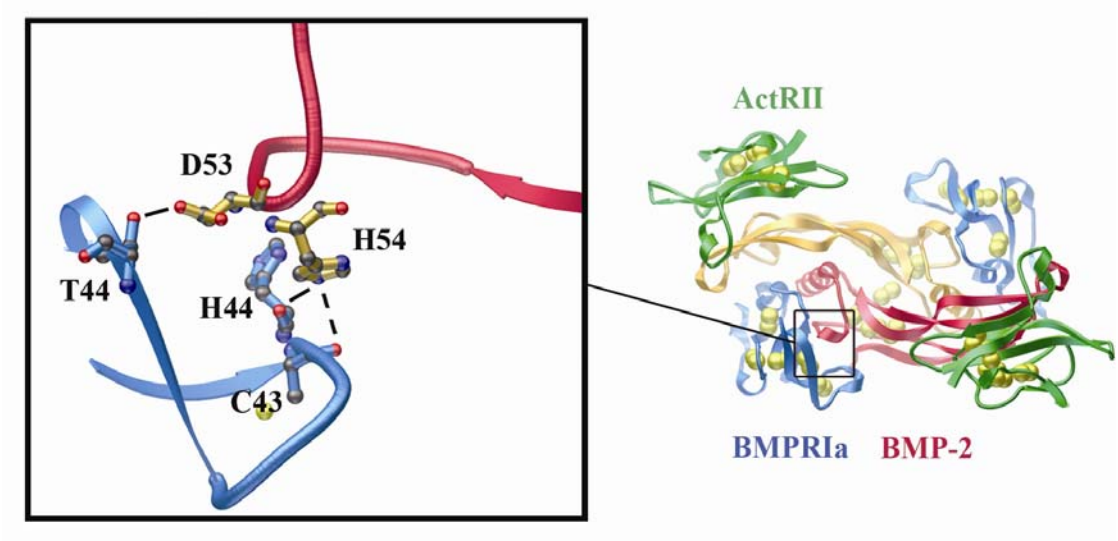

Figure 2-19. Close-up of the BMP-2:BMPRIa-ECD interface. The inset highlights the interactions D53 and H54 of BMP-2 with BMPRIa.

To test the effect this mutation had on BMP-2's affinity for BMPRIa, surface plasmon resonance (BIAcore) was used. The receptor ECD of BMPRIa was immobilized to the chip surface and then the BMP ligands were flowed over the surface. BMP-2_{wt} displayed an affinity of K_D =3.96 nM while BMP-7_{wt} displayed an affinity 400-fold weaker at K_D =1.68 μM (Table 2-2). These are very similar to the previously reported values (*3*). The BMP-$2_{A52B/D53S/H54Y}$ mutant displayed an affinity of K_D =143 nM (Table 2-2). To insure that the mutant was properly folded, it was also flowed over an ActRIIb-ECD surface and showed comparable affinity to that of BMP-$2_{wt.}$ The ~35-fold decrease in affinity for the BMP-$2_{A52B/D53S/H54Y}$ mutant indicates the significant alteration to the H3 pre-helix loop caused by the A52N/D53S/H54Y mutation did alter BMP-2's affinity for BMPRIa-ECD. However, the effect was not the 400-fold difference between BMP-2 and BMP-7. This result suggests that

additional residues or the exact orientation of each ligand's fingers may play a role in determining type I binding affinity.

Table 2-2. BIAcore affinity data for BMP-2 type I mutant The data is shown as the dissociation rate, k_{off}, and the association rate, k_{on}, derived from a global fit using the kinetic model 1:1 Langmuir binding with mass transfer.

Receptor Affinity Data from BIAcore Experiments		
Ligand	**Receptor BMPRIa**	
	k_{off}[1/s]/k_{on}[1/M*s]	**K_D [nM]**
BMP-2_{wt}	$1.72x10^{-3}/4.39x10^{5}$	3.96
BMP-7	$8.10x10^{-2}/4.82x10^{6}$	1684
BMP-$2_{A52N/D53S/H54Y}$	$5.12x10^{-2}/3.57x10^{5}$	143

Similar to BMPRIa, ActRII displays a broad range of binding affinities to a number of different ligands. ActRII has been shown to bind activin with extreme high affinity, K_D ~0.1 nM, BMP-7 with high affinity, K_D ~1 nM, but BMP-2 with much weaker affinity, K_D ~50 nM (*3*). Identification of the residues responsible for binding affinity is now possible with the addition of the low affinity interface of BMP-2:ActRII-ECD from the ternary structure. As previously noted, a quick comparison of this interface with the high affinity interfaces of BMP-7:ActRII-ECD (*3*) or activin:ActRIIb-ECD (*7*) reveals that all three are similar. Since the BMP-2:ActRII-ECD and BMP-7:ActRII-ECD interfaces share the same receptor, these interfaces were more initially compared. Upon detailed inspection, two potentially important residues involved in receptor affinity were identified based on the differences in charge-charge contacts between these interfaces. In BMP-7, Glu-60 makes a favorable hydrogen bond interaction with Lys-76 of ActRII (Figure 2-20, a). However,

in BMP-2 the equivalent residue is Pro-36 and this proline is unable to form any contacts with Lys-76 of ActRII (Figure 2-20, a). The second residue difference involves a charge reversal on both the ligand and the receptor. In BMP-2, Glu-109 forms a favorable salt bridge with Lys-37 of ActRII (Figure 2-20, b). However, in BMP-7, the equivalent residue to Glu-109 is Arg-134 and this arginine makes a larger salt bridge interaction with Asp-36 of ActRII (Figure 2-20, b). For ActRII to accommodate this charge swap between BMP-2 and BMP-7, the M-loop undergoes a large backbone movement. In the BMP-7:ActRII-ECD interface, the top half of the M-loop is positioned facing solvent, which gives the proper orientation to allow the Asp-36 side chain to point towards the interface (Figure 2-20, b). However, in the BMP-2:ActRII-ECD interface, the top of the M-loop is shifted down and closer to the binding interface, allowing the side chain of Lys-37 to be at the interface (Figure 2-20, b). The position of the M-loop in ActRII and the contacts it makes with the ligand might have significant impact of receptor affinity.

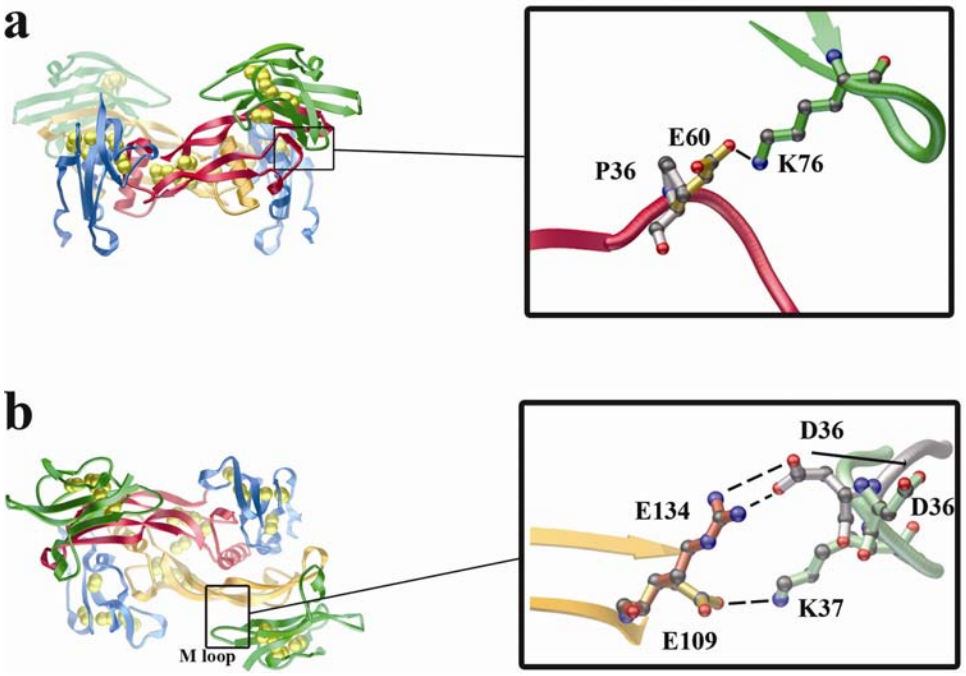

Figure 2-20. Comparison of BMP-7:ActRII and BMP-2:ActRII interfaces. Panel (a) shows the P36E mutation to BMP-2. Panel (b) shows E109R mutation in BMP-2.

Expanding the analysis of receptor binding affinity beyond charged residues, two additional residue differences were identified between BMP-2 and BMP-7 which may influence type II receptor affinity. The first of these residues reveals a potentially important hydrophobic difference. In BMP-7, Phe-117 makes a strong hydrophobic interaction with Val-81 of ActRII (Figure 2-21). This interaction is located at one end of the hydrophobic core and appears to seal closed the pocket. The equivalent residue to Phe-117 in BMP-2 is Leu-92. While Leu-92 is still a hydrophobic residue, the same contact with Val-81 is not present in the BMP-2:ActRII-ECD interface (Figure 2-21). The absence of this Phe-117:Val-81 interaction, reduces the overall buried surface are at the interface which may negatively impact receptor binding and overall affinity.

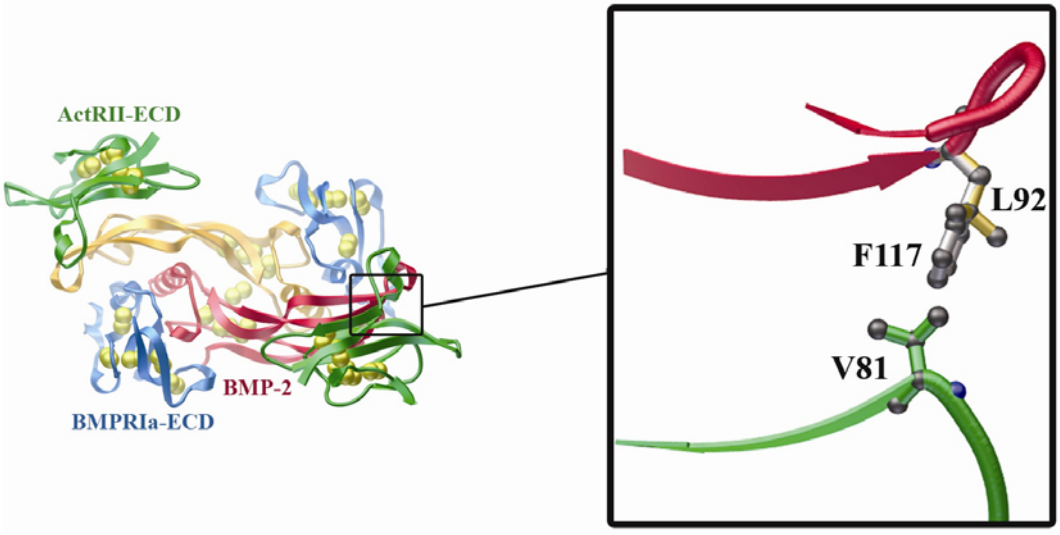

Figure 2-21. Comparison of the BMP-7and BMP-2 interface with ActRII-ECD. Inset shows the close-up of the contacts made by F117 in BMP-7 or L92 in BMP-2 with V81 of ActRII-ECD.

The fourth residue in BMP-2, which may have a direct influence on receptor binding and affinity, was not chosen based on differences in type II receptor contacts. If a ternary model of BMP-7/BMPRIa-ECD/ActRII-ECD, based on the BMP-2 ternary structure, is generated, Arg-48 of BMP-7 can be manipulated to make contacts with residues in both ActRII-ECD and BMPRIa-ECD (Figure 2-22). If Arg-48 indeed forms these contacts *in vivo*, it would be the only ligand residue to make direct contact with residues of both receptor types. The equivalent residue of Arg-48 in BMP-2 is Ser-24 and the short side chain of this residue would not be able to make contact with both receptor types (Figure 2-22). Further, though large ligand backbone conformational changes are not seen upon sequential binding of the receptors, a small conformational change to the main chain of Arg-48 in BMP-7 and the corresponding shift to side-chain atoms following type II binding might have important implications

on type I receptor binding. This interaction, if present, could help explain the cooperative nature of overall receptor binding.

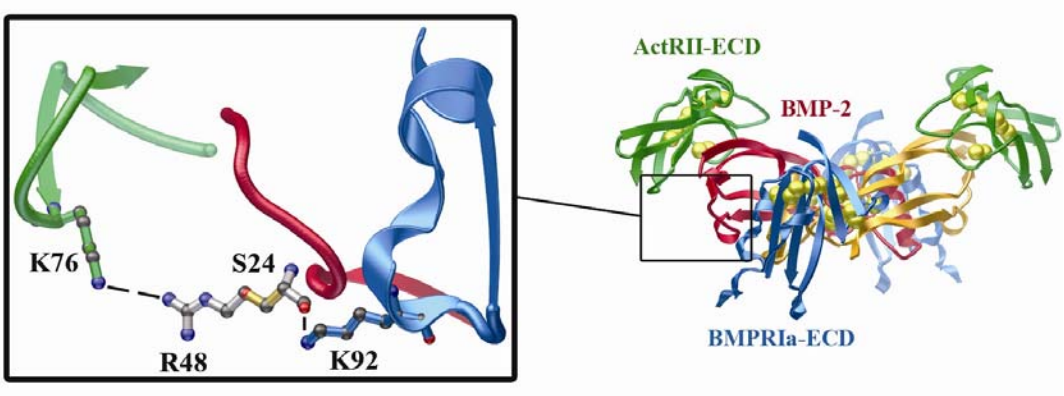

Figure 2-22. Comparison of the BMP-7 and BMP-2 receptor interfaces. Inset is a close-up of the contacts made by S24 of BMP-2 with K92 of BMPRIa and the predicted contacts of R48 of BMP-7 with K76 of ActRII and K92 of BMPRIa.

To test the significance of the above mentioned residues on ActRII binding affinity, all four mutations, S24R, P36E, L92F, and E109R, were inserted into BMP-2 individually. In a similar fashion to the BMP-2 type I mutants, type II receptor binding affinities were monitored using BIAcore. The receptor ECDs of both BMPRIa and ActRII were immobilized onto the chip surface and the ligands were flowed over the surface. All BMP-2 ligands were flowed over the BMPRIa surface to insure that the mutations only affected type II receptor binding and not the type I interface. All mutants, except BMP-2_{P36E}, showed similar affinity for BMPRIa-ECD as BMP-2_{wt}, with K_D ~3 nM. Even though the BMP-2_{P36E} mutant appears to be a single band on a SDS-PAGE gel, the inability to bind to the type I receptor suggests that the protein is not properly folded. This result indicates that the insertion of Pro-36

may have structural implications for proper folding of the BMP-2 ligand. Based on this result, the BMP-2_{P36E} mutant was not further tested for ActRII-ECD binding.

To ensure the activity of the ActRII-ECD surface, BMP-7_{wt} was run over the surface as a positive control. BMP-7_{wt} displayed the expected high affinity for ActRII-ECD with K_D ~3 nM (Table 2-3). BMP-2_{wt} showed a much lower affinity for ActRII-ECD with a K_D ~70 nM (Table 2-3). The affinities of BMP-7_{wt} and BMP-2_{wt} for the ActRII-ECD are comparable to previously reported values (*3*). For the BMP-2_{S24R} mutant, the affinity to ActRII-ECD was unchanged with a K_D ~90 nM (Table 2-3). This suggests that while the BMP-2_{S24R} mutant may be able to form a contact with the ActRII-ECD, either this contact does not form or is transient and does not exert a stabilizing effect on complex formation. When either the BMP-2_{L92F} or the BMP-2_{E109R} mutants were flowed over the ActRII-ECD surface, a small but consistent 2-fold increase in affinity was seen with a K_D ~25 nM (Table 2-3). The addition of the larger hydrophobic group in the BMP-2_{L92F} mutant appears to contribute to a slight increase in overall receptor binding affinity. Further, the presence of a second, partial hydrogen bond between the Arg-109 and Asp-36 of ActRII in the BMP-2_{E109R} mutant must impart greater energetic contributions to binding as compared to the single hydrogen bond found in the wild type Glu-109:Lys-37 contact. These mutations seem to alter the binding affinity in a similar manner. The BMP-2_{L92F} mutant shows a 3-fold decrease in dissociation rate (Table 2-3), while the BMP-2_{E109R} mutant exhibits an 5-fold decrease in dissociation rate (Table 2-3). The difference in the dissociation rate can be clearly in the raw BIAcore traces. In Figure 2-23, panel a shows the very steep

slope for the k_{off}, dissociation, rate of BMP-2_{wt}. In comparison, the traces for BMP-2_{L92F} and BMP-2_{E109R} the k_{off} slopes are much shallower, indicating a slower dissociation rate (Figure 2-23). While displaying small increases in binding affinity to ActRII, neither of these mutations come close to accounting for the ~20-fold difference in affinity between BMP-2 and BMP-7 for ActRII-ECD.

Table 2-3. BIAcore affinity for BMP-2 mutants based on the BMP-7:ActRII interface. The data is shown as the dissociation rate, k_{off}, and the association rate, k_{on}, derived from a global fit using the kinetic model 1:1 Langmuir binding with mass transfer.

Ligand	ActRII		
	k_{off}[1/s]	**k_{on}[1/M*s]**	**K_D [nM]**
BMP-2	$8.56x10^{-2} \pm 2.3x10^{-3}$	$1.51x10^{6} \pm 2.0x10^{4}$	56.6 ± 1.0
BMP-7	$1.19x10^{-2} \pm 4.0x10^{-4}$	$3.44x10^{6} \pm 4.1x10^{5}$	3.49 ± 0.30
BMP-2_{S24R}	$8.38x10^{-2} \pm 5.6x10^{-3}$	$1.03x10^{6} \pm 1.2x10^{5}$	81.9 ± 4.1
BMP-2_{P36E}	No Data	No Data	No Data
BMP-2_{L92F}	$3.66x10^{-2} \pm 1.7x10^{-3}$	$1.28x10^{6} \pm 1.2x10^{5}$	28.8 ± 1.4
BMP-2_{E109R}	$1.59x10^{-2} \pm 1.2x10^{-3}$	$5.72x10^{5} \pm 2.0x10^{3}$	27.6 ± 2.2

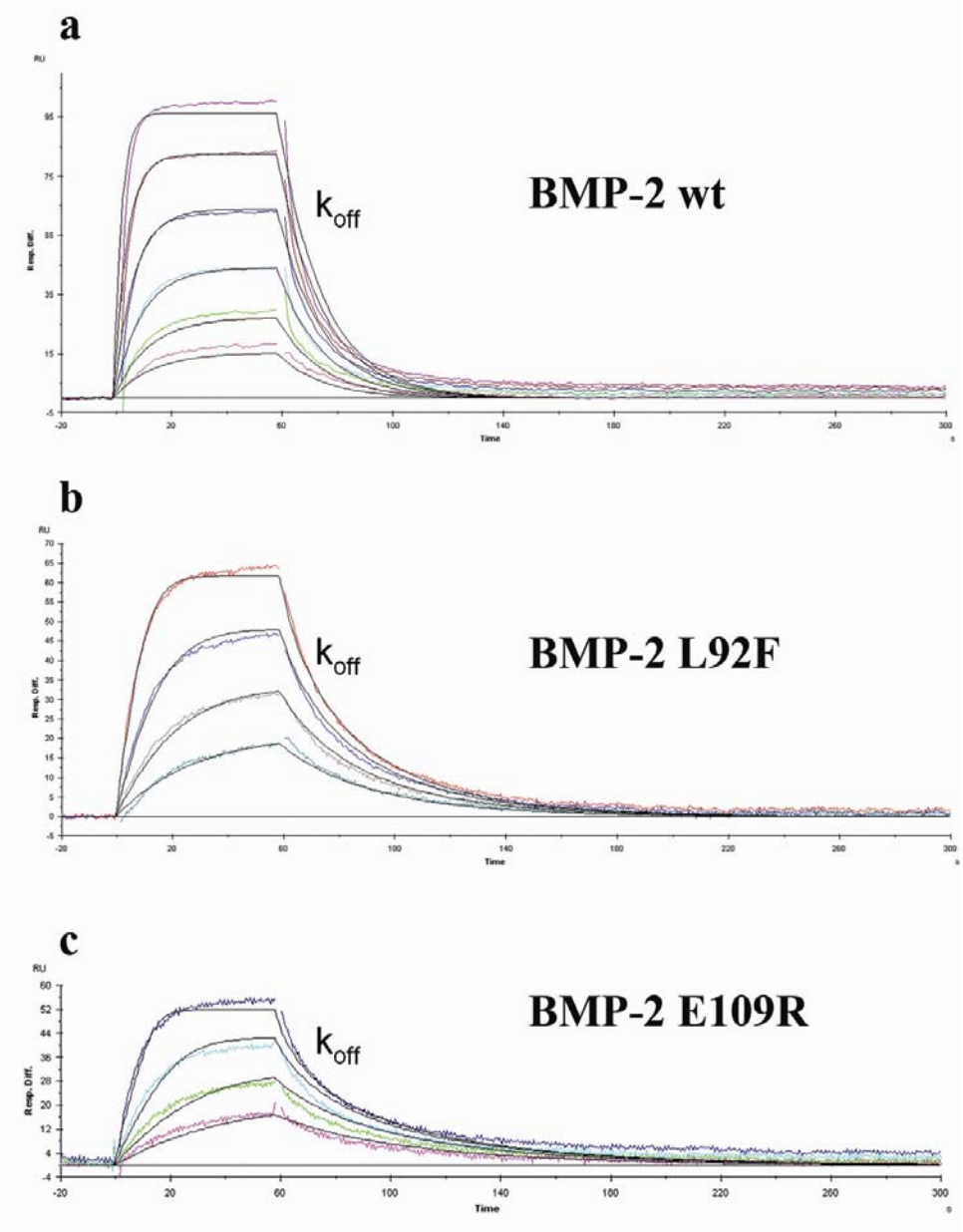

Figure 2-23. Comparison of the BMP-2 BIAcore traces. Panel (a) shows BMP-2_{wt} BIAcore curves. Panel (b) shows the mutant BMP-2_{L92F} curves, while (c) depicts the BMP-2_{E109R} traces. The black lines are the gobal 1:1 Langmuir fit with mass transfer.

Since the four residues chosen based on the comparison of the BMP-2:ActRII-ECD and BMP-7:ActRII-ECD interfaces failed to significantly increase BMP-2 affinity for ActRII, the BMP-2:ActRII-ECD interface was then compared with the

activin:ActRIIb interface (*7*). Since the ECDs of ActRII and ActRIIb are 63% identical and 92% similar, differences seen between the interfaces with the ligands should be important for binding. A detailed analysis of the interfaces revealed two ligand residues predicted to be crucial for high affinity binding. In activin, Arg-87 forms a salt bridge interaction with Asp-62 of ActRIIb (Figure 2-24, a). The equivalent residue in BMP-2, Ser-85, is unable to make a similar contact (Figure 2-24, b). Interestingly, even though Arg-87 and Glu-111 (same as Glu-109 in BMP-2) are found on different strands of finger 2 in activin, spatially their side-chains are positioned directly adjacent to each other. This structural orientation creates a highly charged surface region on activin and forms charge-charge interactions with complimentary surface residues from ActRIIb-ECD (Figure 2-24, a; Figure 2-25). If the S85R mutant is introduced into BMP-2, the arginine side chain is predicted to form a different but similar hydrogen bond network with Asp-34 of ActRII and Glu-83 of BMP-2 (Figure 2-24, b). The concentration of charge residues in this region of the ligand might be important for receptor affinity.

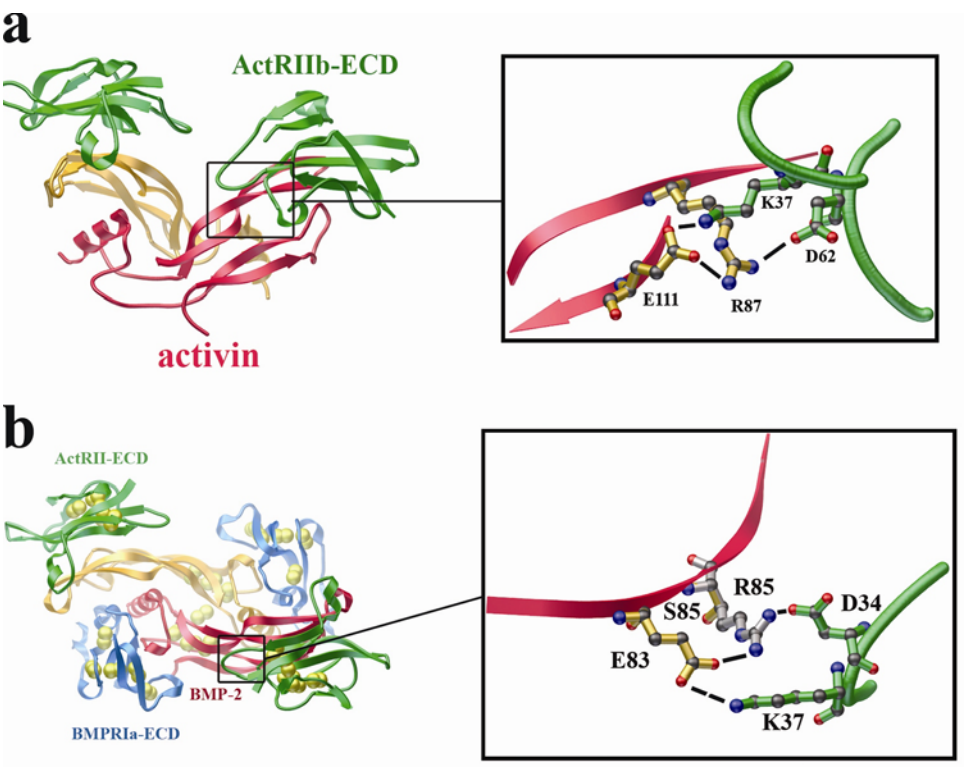

Figure 2-24. Close-up of activin:ActRIIb and BMP-2:ActRII-ECD interfaces. Panel(a) shows the activin:ActRIIb interface. Panel (b) shows the predicted interface of BMP-2 with the S85R mutation.

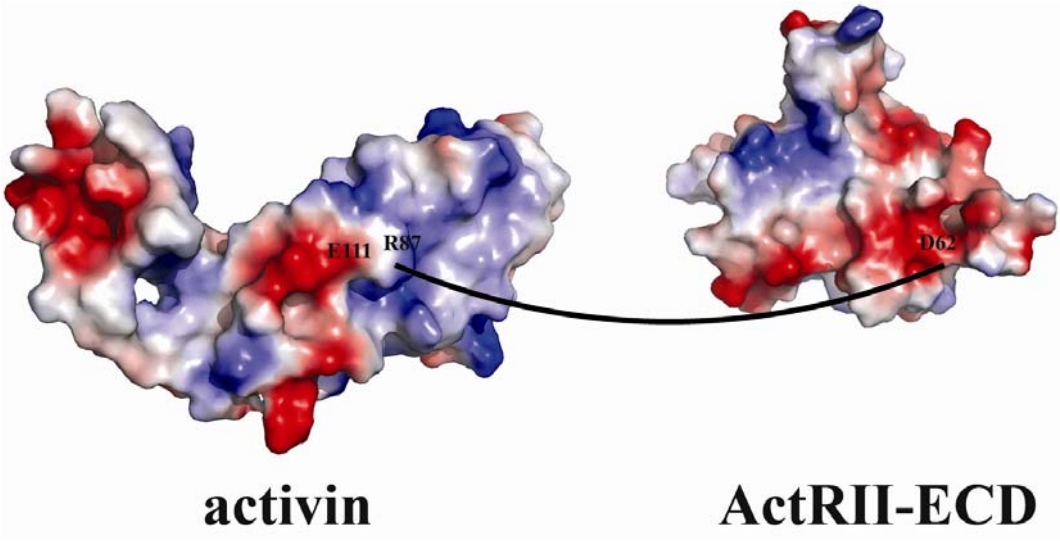

Figure 2-25. Electrostatic representation of the activin:ActRIIb-ECD interface. Residues labeled are found in the charge network mentioned in Figure 2-19.

The second residue difference between BMP-2 and activin with predicted type II receptor binding importance is Lys-102 of activin. Positioned at the top of the hydrophobic core, the side-chain of Lys-102 spans the gap between activin and ActRIIb, making a hydrogen bond with the backbone carbonyl of Cys-59 of ActRIIb as well as a hydrogen bond with Asp-104 of activin (Figure 2-26, a). The equivalent of Lys-102 in BMP-2 is Leu-100 and while Leu-102 maintains similar hydrophobic characteristics to Lys-102 of activin, it is unable to form the same hydrogen bonding interactions found in the activin:ActRIIb interface (Figure 2-26, b). Previous studies have shown the mutation of Lys-102 to either alanine or glutamic acid results in a decrease or loss of binding of activin to ActRIIb (*11*). This diminished receptor binding is most likely the result of the disruption to the hydrogen bond network and the insertion of L100K mutant into BMP-2 may restore these interactions and increase ligand affinity.

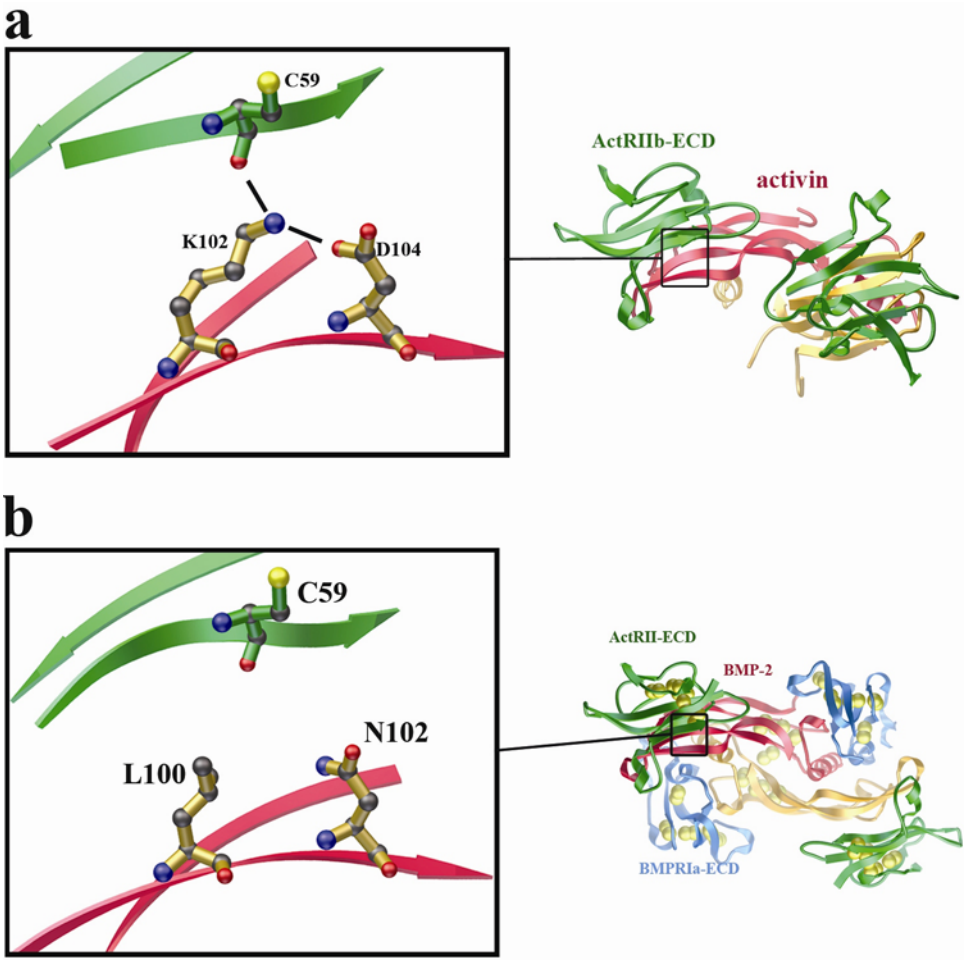

Figure 2-26. Comparison of activin:ActRIIb-ECD and BMP-2:ActRII-ECD interfaces. Panel (a) shows the K102 interface in activin:ActRIIb interface. Panel (b) shows the equivalent L100 residue in the BMP-2:ActRII interface.

As with the previously mentioned mutants derived from the BMP-7:ActRII-ECD complex, the S85R and L100K mutations based on the activin:ActRIIb-ECD structure were introduced into BMP-2 independently and their binding affinity to ActRII-ECD tested using BIAcore. Similar to the BMP-2_{E109R} mutant, the BMP-2_{S85R} mutant showed a small, reproducible 2-fold increase in affinity to ActRII-ECD compared to BMP-2_{wt}, with a K_D =37.2 nM (Table 2-4). Again, the minimal increase

in affinity suggests that only partial or weak contacts are formed with ActRII when the arginine is introduced. The loss of a single, strong hydrogen bond in an interface has been shown to decrease affinity 10 to 100-fold or more (*12*). When the BMP-2_{L100K} mutant was flowed over the ActRII-ECD chip surface, a 5 to 10-fold increase in affinity was seen with a K_D ~9 nM (Table 2-4). This increase in binding affinity was created by the BMP-2_{L100K} mutant having an 8-fold decrease in disassociation rate compared with BMP-2_{wt}, while maintaining the same association rate. This significant increase in affinity by the BMP-2_{L100K} mutant suggests that high affinity type II receptor binding is controlled by hydrogen bond formation between ligand and receptor.

Table 2-4. BIAcore affinity for BMP-2 mutants based on the activin:ActRIIb interface. The data is shown as the dissociation rate, k_{off}, and the association rate, k_{on}, derived from a global fit using the kinetic model 1:1 Langmuir binding with mass transfer.

Ligand	ActRII		
	k_{off}[1/s]	**k_{on}[1/M*s]**	**K_D [nM]**
BMP-2	$8.56x10^{-2} \pm 2.3x10^{-3}$	$1.51x10^{6} \pm 2.0x10^{4}$	56.6 ± 1.0
BMP-7	$1.19x10^{-2} \pm 4.0x10^{-4}$	$3.44x10^{6} \pm 4.1x10^{5}$	3.49 ± 0.30
BMP-2_{S85R}	$3.68x10^{-2} \pm 6.6x10^{-3}$	$1.18x10^{6} \pm 2.6x10^{5}$	31.5 ± 1.4
BMP-2_{L100K}	$1.10x10^{-2} \pm 6.0x10^{-4}$	$1.11x10^{6} \pm 2.0x10^{4}$	9.9 ± 0.7

Since both the E109R and the S85R mutations exhibited a small increase in binding affinity to ActRII-ECD, a double mutant, E109R/S85R, was introduced into BMP-2 to explore if receptor affinity could be enhanced. It was predicted that the

cumulative effect on receptor binding affinity with both mutations present together would be greater than the sum of both mutations alone. That is, the small energetic contributions of each mutation will be enhanced by the presence of the other. Unfortunately, the BMP-$2_{S85R/E109R}$ mutant does not show a further increase in binding affinity to ActRII-ECD over either of the single mutants (Table 2-5). As mentioned earlier, though located on the different strands of BMP-2 finger 2, both E109R and S85R are structurally positioned near each other. Therefore, this result indicates that their contributions to binding energy are highly coupled because their proximity.

Table 2-5. BIAcore affinity data comparing the single and double BMP-2 mutations showing weak increase in affinity. Data analyzed as previously discussed.

Ligand	ActRII		
	k_{off}[1/s]	**k_{on}[1/M*s]**	**K_D [nM]**
BMP-2	$8.56x10^{-2} \pm 2.3x10^{-3}$	$1.51x10^{6} \pm 2.0x10^{4}$	56.6 ± 1.0
BMP-2_{S85R}	$3.68x10^{-2} \pm 6.6x10^{-3}$	$1.18x10^{6} \pm 2.6x10^{5}$	31.5 ± 1.4
BMP-2_{E109R}	$1.59x10^{-2} \pm 1.2x10^{-3}$	$5.72x10^{5} \pm 2.0x10^{3}$	27.6 ± 2.2
BMP-$2_{S85R/E109R}$	$5.0x10^{-2} \pm 1.0x10^{-2}$	$1.80x10^{6} \pm 9.0x10^{4}$	30.9 ± 4.4

2.4. Conclusions

The ternary structure of BMP-2/BMPRIa-ECD/ActRII-ECD is the first look at an intact, signaling competent TGF-β complex. The structural arrangement of the ligand bound to both receptor types is such that the receptors do not make direct contact with each other. This finding is in contrast with the predicted structural arrangement for a TGF-βIII signaling complex in which the different receptor types

would form contacts (*2*). Based on this information, either the TGF-βIII model is incorrect and the receptors do not actually touch, or each TGF-β ligand subfamily has its own unique receptor complex arrangement. Only additional ligand-receptor structures will be able to confirm which hypothesis is correct. Further, in the ternary structure, the BMP-2 ligand is not seen to undergo significant backbone conformational changes compared to the binary structure of BMP-2/BMPRIa-ECD (*1*). This indicates the BMP-2 ligand is preconfigured for type II binding. Therefore, how the known cooperative receptor binding is achieved in the absence of receptor contacts or ligand conformational changes remains unclear.

The ternary structure also contains the first interface of a TGF-β ligand bound to its lower affinity receptor. The comparison of the BMP-2:ActRII-ECD interface with the known high affinity interfaces of BMP-7:ActRII (*3*) and activin:ActRIIb-ECD (*7*) should identify the structural determinants required for high affinity type II receptor binding. One difference between the interfaces is the position of the M-loop of ActRII. This loop appears to shift to facilitate the most favorable residue contacts possible in each interface. Interestingly, mutations made to BMP-2 to generate the same contacts seen in the high affinity interfaces with ActRII, E109R and S85R, only display a minimal impact on overall binding affinity: ~2-fold increase. These results suggest that ligand interactions with the M-loop are most likely transient and other regions of the interface dominate the binding energetics. Further analysis of the interfaces revealed another mutation, L100K, which was able to increase BMP-2's affinity to ActRII-ECD 5 to 10-fold. However, this affinity of ~10 nM is still 10-fold

lower than BMP-7 and 100-fold lower than activin affinity to ActRII-ECD. Therefore, the exact residue composition required for high affinity binding remains elusive.

2.5. References

1. Kirsch, T., Sebald, W., and Dreyer, M. K. (2000) Crystal structure of the BMP-2-BRIA ectodomain complex, *Nat. Struct. Mol. Biol. 7*, 492-496.

2. Hart, P. J., Deep, S., Taylor, A. B., Shu, Z., Hinck, C. S., and Hinck, A. P. (2002) Crystal structure of the human TβR2 ectodomain-TGF-β3 complex, *Nat. Struct. Mol. Biol. 9*, 203-208.

3. Greenwald, J., Groppe, J., Gray, P., Wiater, E., Kwiatkowski, W., Vale, W., and Choe, S. (2003) The BMP7/ActRII Extracellular Domain Complex Provides New Insights into the Cooperative Nature of Receptor Assembly, *Molecular Cell 11*, 605-617.

4. Greenwald, J., Fischer, W. H., Vale, W. W., and Choe, S. (1999) Three-finger toxin fold for the extracellular ligand-binding domain of the type II activin receptor serine kinase, *Nat. Struct. Mol. Biol. 6*, 18-22.

5. Collaborative Computational Project, N., 4. (1994) The CCP4 suite: programs for protein crystallography, in *Acta Crystallographica Section D*, pp 760-763.

6. Greenwald, J., Le, V., Corrigan, A., Fischer, W., Komives, E., Vale, W., and Choe, S. (1998) Characterization of the Extracellular Ligand-Binding Domain of the Type II Activin Receptor, *Biochemistry 37*, 16711-16718.

7. Greenwald, J., Vega, M. E., Allendorph, G. P., Fischer, W. H., Vale, W., and Choe, S. (2004) A Flexible Activin Explains the Membrane-Dependent Cooperative Assembly of TGF-[beta] Family Receptors, *Molecular Cell 15*, 485-489.

8. Thompson, T. B., Woodruff, T. K., and Jardetzky, T. S. (2003) Structures of an ActRIIB:activin A complex reveal a novel binding mode for TGF-β ligand:receptor interactions, *EMBO J. Apr 1*, 1555-1566.

9. Gray, P. C., Greenwald, J., Blount, A. L., Kunitake, K. S., Donaldson, C. J., Choe, S., and Vale, W. (2000) Identification of a Binding Site on the Type II Activin Receptor for Activin and Inhibin, *J. Biol. Chem 275*, 3206-3212.

10. Keller, S., Nickel, J., Zhang, J.-L., Sebald, W., and Mueller, T. D. (2004) Molecular recognition of BMP-2 and BMP receptor IA, *Nat. Struct. Mol. Biol. 11*, 481-488.

11. Wuytens, G., Verschueren, K., de Winter, J. P., Gajendran, N., Beek, L., Devos, K., Bosman, F., de Waele, P., Andries, M., van den Eijnden-van Raaij, A. J. M., Smith, J. C., and Huylebroeck, D. (1999) Identification of Two Amino Acids in Activin A That Are Important for Biological Activity and Binding to the Activin Type II Receptors, *J. Biol. Chem. 274*, 9821-9827.

12. Pons, J., Rajpal, A., and Kirsch, J. F. (1999) Energetic analysis of an antigen/antibody interface: alanine scanning mutagenesis and double mutant cycles on the HyHEL-10/lysozyme interaction, *Protein Sci. 8*, 958-968.

Chapter 3. Nature of cooperative TGF-β receptor binding

3.1. Introduction

Along with the promiscuity exhibited by the TGF-β receptors for their ligands, TGF-β receptors also display a known cooperative binding during complex formation. TGF-β ligands have both high and lower affinity receptors and bind these receptors in a stepwise fashion: High affinity receptors bind first, followed by the lower affinity receptors (*1*). The ligand's affinity for the lower affinity receptor has been shown to be increased in the presence of the bound high affinity receptors. Indeed, both activin and TGF-β ligands are unable to bind their lower affinity receptors in the absence of the high affinity receptors (*2, 3*) While BMP ligands are able to weakly bind their lower affinity receptors, the affinity of this interaction is increased in the presence of high affinity receptors (*4*). While cooperative receptor binding has been consistently observed, the exact mechanism remains unresolved.

The activin/inhibin sub-family of the TGF-β superfamily consists of four activin β-subunits and one inhibin α-subunit, which can be combined into a variety of different homo and heterodimers (*5*). For instance, homodimers of two β_B or two β_A subunits are the most common forms of activin, while inhibin is a hetero-dimer of one α subunit with either one β_B or one β_A subunit (*6*). The β subunits of activin have been shown to bind type I and type II TGF-β receptors while the α subunit has not shown the ability to interact with either of these receptor types (*7*). Since an Inhibin dimer has only one β subunit, it is one capable of binding a single type II receptor, whereas activin dimers with two β subunits can bind the usual two type II and two type I receptors. Inhibin derives its name from its known characteristic function of

antagonizing normal activin signaling (*8*). The predicted mechanism of Inhibin antagonism is by binding a single type II molecule into a non-signaling complex, the receptor is sequestered the away from activin and not available for signaling (*9*). By exploiting the difference in receptor binding capabilities of activin and Inhibin, the underlying mechanism of cooperative receptor binding can be better understood.

3.2. BIAcore Studies for activin and Inhibin

The ternary structure of BMP-2/BMPRIa-ECD/ActRII-ECD shows the cooperative binding of ActRII to BMP-2 following BMPRIa binding is not mediated through major conformational changes to either the ligand or receptors. In light of this finding, the cooperative receptor binding must be a result of other influences. One possibility is the reduced rotational freedom of a TGF-β ligand upon binding to its high affinity receptors. That is, when the ligand binds its high affinity receptors, it becomes locked in the plane of the cell surface, enabling the lower affinity receptors to bind more easily. To analyze if the loss of freedom affects receptor affinity, the binding of activin and inhibin to their type II receptors was compared. Using BIAcore, ActRIIb-ECD was immobilized on a CM5 chip surface at varying receptor densities. On flow cell 2, a high density of ActRIIb-ECD was immobilized on the surface with a final response unit (RU) of 600. To flow cell 3, a low density of ActRIIb-ECD was immobilized with a final RU = 20, while in flow cell 4 a medium density was immobilized with a total RU of 200. While the RU unit is an arbitrary value, it does accurately reflect the relative amount of protein bound to the chip surface. Therefore,

the higher the RU, the more protein that is bound to the CM5 chip surface in a linear relationship. By changing the density of the ActRIIb-ECD on the surface of the flow cells, the average distance between ActRIIb-ECD molecules is varied.

When flowed over all three chip surfaces, activin displayed a changing affinity to ActRIIb-ECD depending on the chip density. For the high density surface (flow cell 2), activin displayed an affinity of K_D =0.244 nM (Table 3-1). This value is comparable to the previously reported affinity value of activin to ActRII-ECD of K_D =0.059 nM (*4*). When passed over the medium density surface (flow cell 4), activin showed a similar binding affinity to flow cell 2 with an observed K_D =0.280 nM (Table 3-1). Interestingly, activin exhibited a 10-fold lower affinity for ActRIIb-ECD on the low density surface (flow cell 4) with a K_D =2.22 nM (Table 3-1). Conversely, Inhibin did not exhibit a similar trend in binding affinities to ActRIIb-ECD with varying surface densities. The affinity of Inhibin to ActRIIb-ECD was K_D =13.1 nM on the high density chip surface and the affinity is virtually unchanged when flowed over the low density surface, which gave an affinity of K_D =15.6 nM (Table 3-1).

Table 3-1. BIAcore affinity for activin and Inhibin to ActRIIb-ECD. The data is shown as the dissociation rate, k_{off}, and the association rate, k_{on}, derived from a global fit using the kinetic model 1:1 Langmuir binding with mass transfer for all three surface densities.

Ligand	**Receptor ActRIIb-ECD**					
	Low Density		Medium Density		High Density	
	k_{off}[1/s]/k_{on}[1/M*s]	**K_D [nM]**	**k_{off}[1/s]/k_{on}[1/M*s]**	**K_D [nM]**	**k_{off}[1/s]/k_{on}[1/M*s]**	**K_D [nM]**
activin	$1.91x10^{-3}/8.61x10^{6}$	2.22	$2.53x10^{-4}/8.95x10^{6}$	0.283	$1.50x10^{-4}/6.14x10^{6}$	0.244
Inhibin	$3.53x10^{-3}/2.26x10^{6}$	15.6	$2.26x10^{-3}/1.82x10^{6}$	12.4	$2.16x10^{-3}/1.65x10^{6}$	13.1

3.3. Basis for Cooperative Receptor Binding

The basis for the observed trends in receptor affinity between activin and Inhibin is based on each of the difference in each ligand's binding properties. As previously stated, activin is a homodimer of β subunits, in this case β_A subunits, where each monomer can independently bind a type II receptor. Type II receptor binding sites are unique compared to the type I receptor sites, which are formed at the junction of both monomers and consist of residues found in both monomers (*10*). With two type II binding sites per dimer, one activin ligand is able to engage in a "bidentate" binding. This form of binding occurs when a molecule, such as activin, is able to bind multiple receptors (ActRIIb) at the same time. However, this "bidentate" binding requires certain spatial parameters for the ActRIIb-ECD molecules immobilized on the chip surfaces.

Previous studies have calculated the protein density on a BIAcore chip surface to be approximately 1ng/mm^2 at 1000 RU (*11*). Based on this determination, the high density surface in flow cell 2 correlates to an average distance of ~57 Å between ActRIIb-ECD molecule. The medium density surface on flow cell 4 was calculated to have an average distance of ~130 Å between ActRIIb-ECD molecules, while the low density surface on flow cell 4 would have much greater distance between ActRIIb-ECD molecules at ~313 Å. Looking at the solved structures of type II receptors bound to BMP and TGF-β ligands (*4, 12*) and the BMP ternary structure, the distance between receptor sites on the ligand ranges from ~70 to 90 Å (Figure 3-1). Based on this distance, the activin and Inhibin ligands can definitely interact with multiple

receptor molecules on flow cell 2 (the high density surface), and most likely interact with multiple ActRIIb-ECD molecules on flow cell 4 (medium density surface), if the ligand has multiple receptor binding sites. However, with such a large distance between ActRIIb-ECD molecules on flow cell 3 (low density surface), both of the ligands will be forced to only interact with a single receptor molecule.

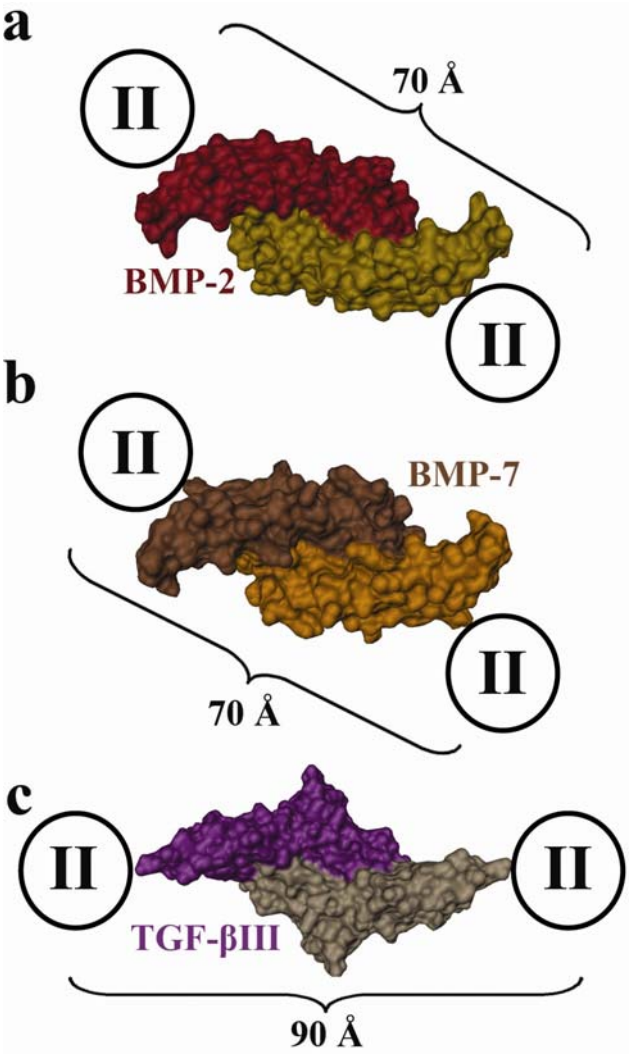

Figure 3-1. Distance between type II receptor binding sites. Panel (a) shows BMP-2, panel (b) shows BMP-7, and panel (c) shows TGF-βIII. The location of the type II receptors are shown as circles and the distances are to the middle of the receptor.

The initial binding of an activin or Inhibin molecule to the chip surface results in an increase in local concentration of the ligands on the chip surface. That is, the ligands are no longer free to move over the remainder of the chip surface, but rather are fixed in one place. Further, the binding event reduces the rotational freedom of the activin dimer. One ligand monomer is locked in a binding position which limits the number of possible conformations of the second monomer. This loss of movement lowers the entropy of binding for the second receptor. On the low density surface, the large distance between ActRIIb-ECD molecules surface forces the activin dimer to only bind one molecule, even though it has the ability to bind two. Therefore, the affinity recorded for flow cell 3 corresponds to a true 1:1 binding event. This indicates that single activin monomer binds an ActRIIb-ECD molecule with K_D ~2nM affinity. However, on the medium and high density surfaces, the initial binding of activin to one ActRIIb-ECD molecule brings the activin dimer in closer to additional receptor molecules. Combined with the loss of ligand freedom, these effects result in easier binding of a second ActRIIb-ECD molecule and the recorded 10-fold increase in binding affinity, K_D ~0.2 nM. The same binding affinity of activin for ActRIIb-ECD on the high and medium density surfaces, indicates activin is able to bind two receptors each of these surfaces. Inhibin's inability to bind two ActRIIb-ECD molecules is consistent with this model for cooperative binding. Since Inhibin can only bind ActRIIb-ECD in a 1:1 interaction, increasing the surface concentration for

the receptor should not alter overall affinity. Indeed, the K_D of Inhibin for ActRIIb-ECD is unchanged for all three surfaces.

The increase in affinity exhibited by activin for ActRIIb-ECD on the more dense surfaces is a result in the decrease in dissociation rate, k_{off}. Activin displays a 10-fold decrease in the k_{off} rate for the medium and high density surfaces compared to the low density surface, exactly equal to the increase in overall K_D. It is the presence of a second bound receptor to activin which is responsible for this change in dissociation rate. The k_{off} rate for Inhibin is unchanged for all three density surfaces confirming this hypothesis. Further, the k_{off} rates for activin and Inhibin are comparable on the low density surface where both ligands can only form a 1:1 complex with ActRIIb-ECD.

3.4. TGF-β Ligand flexibility and Receptor Affinity

Two crystal structures of activin bound to ActRIIb-ECD show that, similar to TGF-βIII, activin is a flexible ligand and can adopt multiple different conformations (*13, 14*). This flexibility does not interfere with the formation of the type II binding sites, only the type I binding sites. This is because the type II receptor sites remain intact in all conformations, while the type I sites become disordered (Figure 3-2, a). The structural data combined with the BIAcore data reveals a model to explain the observed cooperative receptor binding seen on the cell membrane. As the flexible activin ligand moves across the surface, one ligand monomer can bind one type II (ActRIIb in this example) receptor molecule (Figure 3-2, a). This initial step reduces

the mobility of the activin ligand in the cell membrane and increases local concentration of the ligand. This loss of mobility and increased concentration facilitates the binding of a second ActRIIb receptor by the other activin monomer (Figure 3-2, b). The activin ligand is now trapped in its "wing spread" or active conformation with the type I receptor binding site fully formed (Figure 3-2, b). Since the ligand is fixed, the type I receptors do not have to overcome the entropy of capturing the activin dimer on the cell surface or locking it in the correct binding orientation. This ligand formation has more favorable binding energetics, effectively increasing the binding affinity for the type I receptor (Figure 3-2, c).

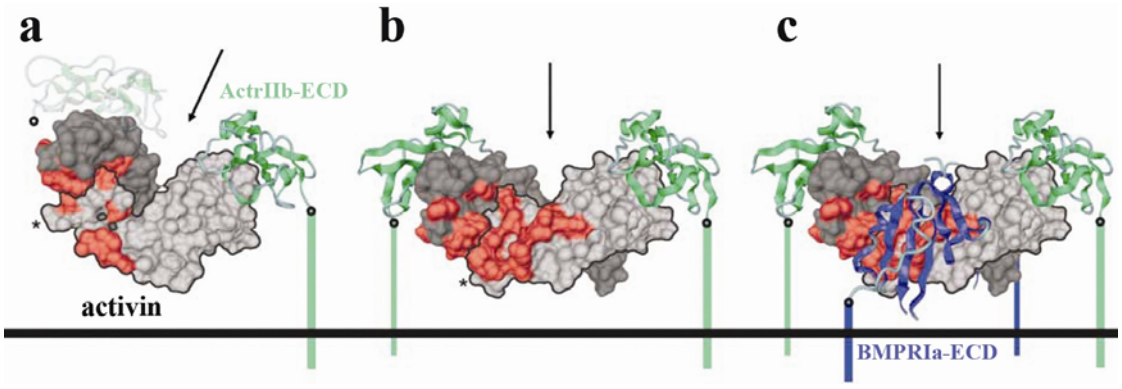

Figure 3-2. Panel (a) depicts the activin-ActRIIb-ECD structure (*13*). Panel (b) models how activin looks when bound to two ActRIIb molecules at the cell surface. Panel (c) shows BMPRIa bound to the complex in panel (b). Activin is shown as surface representation and ActRIIb-ECD as ribbon diagram. The red area in activin represents the type I binding site.

3.5. Conclusion

The BIAcore affinity studies reveal TGF-β ligand-receptor affinity is mediated through both the type and number of interactions found at the cell surface. Activin,

for instance, is able to bind two ActRIIb molecules simultaneously (bidentate), while Inhibin is only able to bind a single ActRIIb molecule (monodentate) (*7*). When activin was flowed over both high and low density surfaces containing ActRIIb-ECD molecules, a 10-fold difference in affinity was recorded. However, inhibin failed to show a significant change in receptor affinity in relation to chip surface density. Extrapolating these results to the cell surface, the binding of the second receptor is a crucial step in the signaling process. This second binding event both increases the ligand's local concentration on the cell surface and locks the ligand in an active conformation. This fixed, active conformation of the ligand bound to its high affinity receptor, reduces the entropy of binding for the lower affinity receptors, resulting in the observed increase in affinity. While the BMP ligands have been shown to be inherently less flexible than either the activin of TGF-β sub-families (*4, 10*), this same model can still explain the cooperative binding they display (*15*). Although the BMPs are already in a conformation to bind their lower affinity receptors, the increase in local concentration and loss of ligand movement upon binding of the high affinity receptors has the same effects on lower receptor binding as described in the activin binding model.

3.6. References

1. Sebald, W., and Mueller, T. D. (2003) The interaction of BMP-7 and ActRII implicates a new mode of receptor assembly, *Trends in Biochemical Sciences 28*, 518-521.

2. Wrana, J. L., Attisano, L., Wieser, R., Ventura, F., and Massagué, J. (1994) Mechanism of activation of the TGF-β receptor, *Nature 370*, 341-347.

3. Mathews, L. S. (1994) Activin receptors and cellular signaling by the receptor serine kinase family, *Endocr. Rev. 15*, 310-325.

4. Greenwald, J., Groppe, J., Gray, P., Wiater, E., Kwiatkowski, W., Vale, W., and Choe, S. (2003) The BMP7/ActRII Extracellular Domain Complex Provides New Insights into the Cooperative Nature of Receptor Assembly, *Molecular Cell 11*, 605-617.

5. Pangas, S. A., and Woodruff, T. K. (2000) Activin Signal Transduction Pathways, *Trends in Endocrinology and Metabolism 11*, 309-314.

6. Thompson, T. B., Cook, R. W., Chapman, S. C., Jardetzky, T. S., and Woodruff, T. K. (2004) Beta A versus beta B: is it merely a matter of expression?, *Molecular and Cellular Endocrinology 225*, 9-17.

7. Woodruff, T. K. (1999) Editorial: Hope, Hypothesis, and the Inhibin Receptor. Does Specific Inhibin Binding Suggest There Is a Specific Inhibin Receptor?, *Endocrinology 140*, 3-5.

8. Lebrun, J. J., and Vale, W. W. (1997) Activin and inhibin have antagonistic effects on ligand-dependent heteromerization of the type I and type II activin receptors and human erythroid differentiation, *Mol. Cell. Biol. 17*, 1682-1691.

9. Martens, J. W. M., de Winter, J. P., Timmerman, M. A., McLuskey, A., van Schaik, R. H. N., Themmen, A. P. N., and de Jong, F. H. (1997) Inhibin Interferes with Activin Signaling at the Level of the Activin Receptor Complex in Chinese Hamster Ovary Cells, *Endocrinology 138*, 2928-2936.

10. Kirsch, T., Sebald, W., and Dreyer, M. K. (2000) Crystal structure of the BMP-2-BRIA ectodomain complex, *Nat. Struct. Mol. Biol. 7*, 492-496.

11. Stenberg, E., Persson, B., Roos, H., and Urbaniczky, C. (1991) Quantitative determination of surface concentration of protein with surface plasmon resonance using radiolabeled proteins, *Journal of Colloid and Interface Science 143*, 513-526.

12. Hart, P. J., Deep, S., Taylor, A. B., Shu, Z., Hinck, C. S., and Hinck, A. P. (2002) Crystal structure of the human TβR2 ectodomain-TGF-β3 complex, *Nat. Struct. Mol. Biol. 9*, 203-208.

13. Greenwald, J., Vega, M. E., Allendorph, G. P., Fischer, W. H., Vale, W., and Choe, S. (2004) A Flexible Activin Explains the Membrane-Dependent Cooperative Assembly of TGF-[beta] Family Receptors, *Molecular Cell 15*, 485-489.

14. Thompson, T. B., Woodruff, T. K., and Jardetzky, T. S. (2003) Structures of an ActRIIB:activin A complex reveal a novel binding mode for TGF-β ligand:receptor interactions, *EMBO J. Apr 1*, 1555-1566.

15. Ebisawa, T., Tada, K., Kitajima, I., Tojo, K., Sampath, T. K., Kawabata, M., Miyazono, K., and Imamura, T. (1999) Characterization of bone morphogenetic protein-6 signaling pathways in osteoblast differentiation, *J. Cell. Sci. 112*, 3519-3527.

Chapter 4. BMP-3 and BMP-6 Structures Illuminate the Nature of Binding Specificity with Receptors

4.1. Introduction

To confirm if the methods for regulating receptor binding is universally conserved throughout the TGF-β superfamily, additional ligand structures and biochemical studies are required. Two less well characterized TGF-β ligands, BMP-3 and BMP-6, were the focus of these continued efforts. BMP-3 is a divergent member of the BMP family and, along with its homologue BMP-3b (GDF-10), shares only ~40% sequence identity with other BMP family members (*1*). In comparison, BMP-2 and BMP-6 share closer to 60% sequence identity. Highly abundant in demineralized bone, BMP-3 was initially thought to be osteoinducive (*2*). However, recent research suggests a different, antagonistic role for BMP-3. Conditioned medium containing BMP-3 was shown to inhibit BMP signaling characteristics in a variety of cell types (*3*). Additionally, in *Xenopus* embryos, BMP-3 exerted actions opposed to those of BMP-2 (*4*). The mechanism for this unique signaling ability of BMP-3 remains unclear. It was suggested that by signaling through the Smad-2/3 (TGF-β/activin) pathway, BMP-3 may be an intracellular antagonist (*3, 5*). More recently, BMP-3 was proposed to be an extracellular antagonist, similar to inhibin, by sequestering type II receptors into non-signaling complexes (*6*). To clarify the functional mechanism of BMP-3 action, further studies with respect to structure, receptor affinity, specificity, and activity are necessary.

BMP-6 is a member of the BMP-5, -6, -7, and -8 sub-family and possesses more traditional BMP signaling functions. Compared to other BMPs, such as BMP-2 or BMP-7, BMP-6 has more potent osteoinducive properties as well as being the

strongest inducer of human mesenchymal stem cell (hMSC) differentiation (*7*). BMP-6 also plays a key role in bone formation and decreased fracture healing (*8*). BMP-6 has been linked to roles in a variety of different cancers, most notably the metastasis of prostate cancer (*9*). While BMP-6 has been shown to form complexes with numerous different receptors in a variety of cell types (*10*), few *in vitro* studies have examined the structural basis for receptor binding and the comparative specificities between these receptors.

4.2. Results and Discussion

4.2.1. Crystal Structure of BMP-3

The unbound BMP-3 ligand dimer was crystallized and its structure solved to a final resolution of 2.20 Å. BMP-3 crystallized in the H3 space group with unit cell dimensions of a=b= 96.8 Å and c= 101.5 Å and α=β= 90° and γ= 120°. To obtain the initial phase information for the BMP-3 structure, molecular replacement was employed using the BMP-2 ligand from the previously solved ternary structure of BMP-2/BMPRIa-ECD/ActRII-ECD as a search model. To estimate the number of molecules or BMP-3 ligand monomers in the asymmetric unit, the Matthews coefficient was calculated. However, both of the most likely asymmetric unit compositions, two or four monomers had very low relative frequencies. Since BMP ligands have been shown to pack in crystals with high solvent content (*11, 12*), the initial search looked for two ligand monomers. The most successful molecular replacement solution was found by taking one BMP-2 ligand monomer and searching

for two independent BMP-3 monomers per asymmetric unit. Based on this packing, the crystals have a solvent content of close to 65%. The average solvent content for a typical protein crystal is around 43% (*13*). Each BMP-3 monomer in the asymmetric unit is related by a 2-fold NCS across the dimer interface. However, the application of NCS restraints to the monomers during refinement did not improve the refinement statistics. Instead, a single translation, libration, and screw (TLS) group for each monomer was seen to help with refinement. This suggests each BMP-3 monomer crystallized in a slightly different arrangement and the TLS parameter allows for modeling these minor displacement differences.

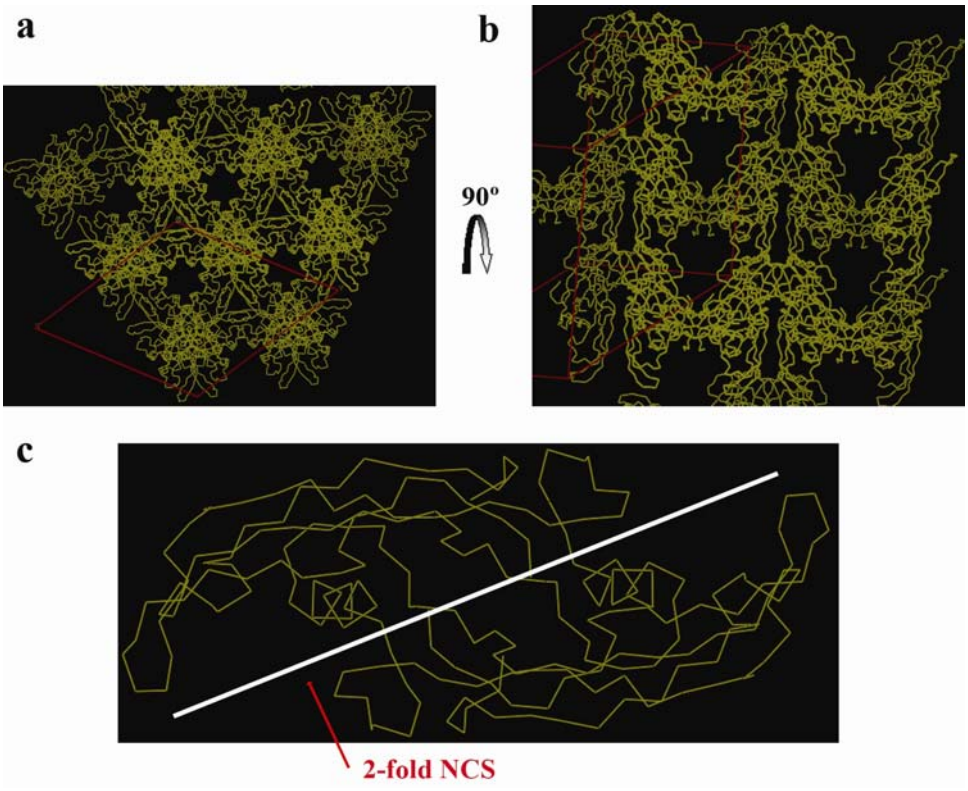

Figure 4-1. BMP-3 Crystal packing. Panel (a) and (b) show the packing of the BMP-3 ligands down the y and z axis. Panel (c) shows the asymmetric unit and the 2-fold NCS separating the two BMP-3 monomers.

As with other previously determined BMP ligand structures, the N-terminal residues of BMP-3 (1-3) are flexible or disordered and are not visible in the electron density maps. The BMP-3 dimer adopts the classic TGF-β family butterfly architecture with each monomer containing a cystine knot motif, four beta strands forming two fingers, and the conserved α-helix H3 (Figure 4-2). The two ligand monomers are connected by an inter-subunit disulfide bond resulting in a covalently linked dimer. The overall fold of the BMP-3 dimer is surprisingly similar to that of BMP-2, including the relative spread angle of the two wings. When overlaid, the structures of BMP-3 and BMP-2 have an average Cα RMS_{dev} of 1.02 Å over the entire

dimer. The regions with largest Cα differences are in the loop regions of the fingers, the H3 pre-helix loop, and the loop directly following the H3 α-helix (Figure 4-3). Not surprisingly, these regions of BMP-3 show the highest B-factors, or greatest amount of flexibility, in the crystal structure and are likely the dynamic parts of the ligand when in solution. Interestingly, the position of the tips of fingers for BMP-3 are more similar to BMP-7 than BMP-2. These regions of BMP-3 and BMP-7 are slightly higher or closer together than the finger tips regions of BMP-2 (Figure 4-3). Further, the H3 pre-helix loop of BMP-3 adopts a more similar conformation to the H3 pre-helix loop of BMP-7 than the H3 pre-helix loop of BMP-2 (Figure 4-3). Since BMP-2 and BMP-7 bind type I receptors with vastly different affinities, it is possible the position of the fingers and intrinsic differences in the H3 pre-helix loop orientation are a mechanism by which TGF-β ligands regulate receptor affinity and binding.

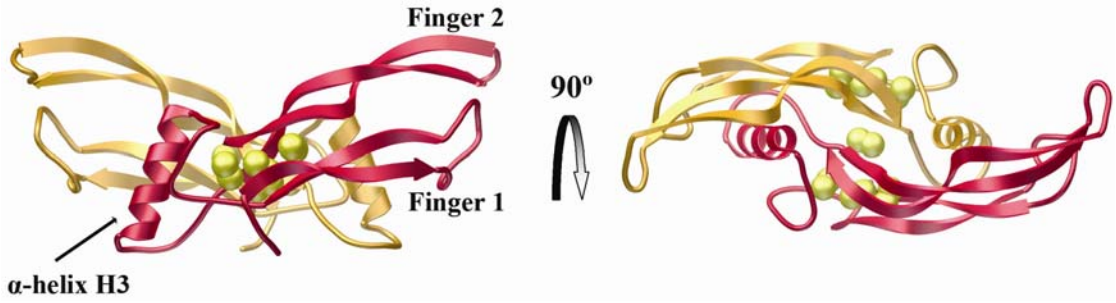

Figure 4-2. Ribbon Structure of BMP-3. Highlighted are the major structural features of TGF-β architecture. Sulfur atoms are shown as yellow spheres.

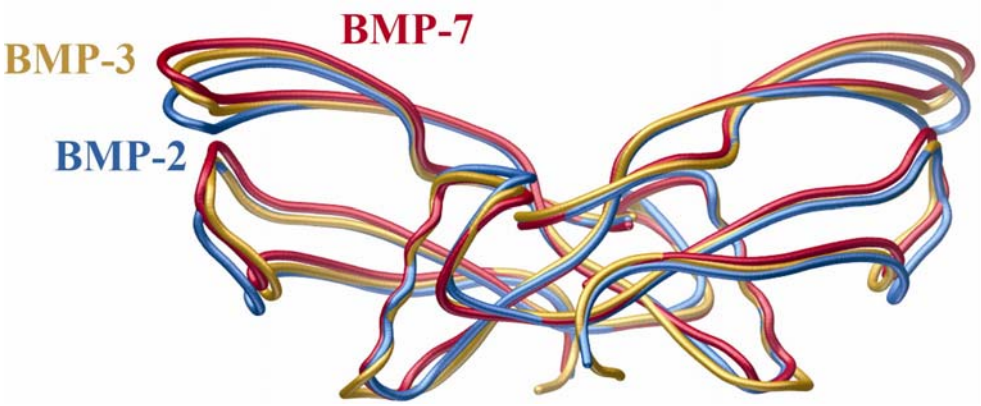

Figure 4-3. Superimposition of BMP-2, BMP-3, and BMP-7. The coil representation of the ligands highlights the differences in backbone conformations.

Table 4-1 summarizes the x-ray diffraction data and refinement statistics for BMP-3. The BMP-3 structure was refined to a final R-factor of 22.8% with a free R-factor of 25.7%. Overall, the structure displayed good geometry with ~89% of all residues found in the most favored region and none seen in the disallowed regions as determined by Ramachandran plot (Table 4-1). There were, however, four residues, Val-67 and Tyr-35 in each monomer, which could only be placed into generously allowed geometric conformations. Residue Val-67 is found in the loop region directly following α helix H3. Compared to BMP-2, this loop region of BMP-3 has a two amino acid residue insertion. Looking at a 2Fo-Fc electron density map contoured at 1σ, the loop region appears to be flexible as the electron density maps are weaker and the atoms possess higher B-factors than compared to other regions of the ligand. However, there are no gaps or breaks in the main chain backbone density and the side chain density for Val-67 can be clearly seen (Figure 4-4, a). Since the position of the Val-67 side chain is positioned facing away from the predicted type I binding interface,

the reason for the residue to adopt this generously allowed conformation is not entirely clear. Residue Tyr-35 is located in the middle of finger one with its side chain pointed into solvent. Unlike Val-67, the 2Fo-Fc electron density for Tyr-35 is strong for both main chain and side chain atoms (Figure 4-4, b). The conformation of the residue is stabilized by a water mediated hydrogen bond with Asp-33 as well as hydrophobic stacking with Arg-10 (Figure 4-4, b). If a type II receptor is modeled onto the BMP-3 surface, Tyr-35 is positioned such that it is close to making contacts with the receptor. Based on its location and conformation, Tyr-35 may play a role in type II receptor binding.

Table 4-1. X-ray diffraction and refinement statistics for BMP-3.

X-ray Data Collection and Refinement Statistics

	BMP-3
Data Collection	
Beamline	ALS 8.3.1
Space Group	H3
Number of Observations	50312
Unique Reflections	17488
Resolution Range (Å)[1]	50-2.2 (2.28-2.20)
Average I/σI	15.9 (6.2)
Completeness (%)	97.9 (99.9)
R_{sym} (%)	5.5 (31.3)
Refinement	
Resolution Range	64.7-2.20
R_{cryst} (%)	22.8
R_{free} (%)[2]	25.7
Average B factor (Å^2)	46.5
Rms Deviation	
Bonds (Å)	0.012
Angles (°)	1.327
Number of Atoms	
Protein	1682
Water	98
Number of TLS groups	2
Ramachadran plot non –gly, -pro, terminal residues	
most favored regions	163 (89.1%)
Additionally allowed regions	16 (8.7%)
Generously allowed regions	4 (2.2%)

[1] Numbers parentheses correspond to the highest resolution shell

[2] Calculated from 5 % of the data not used in refinement

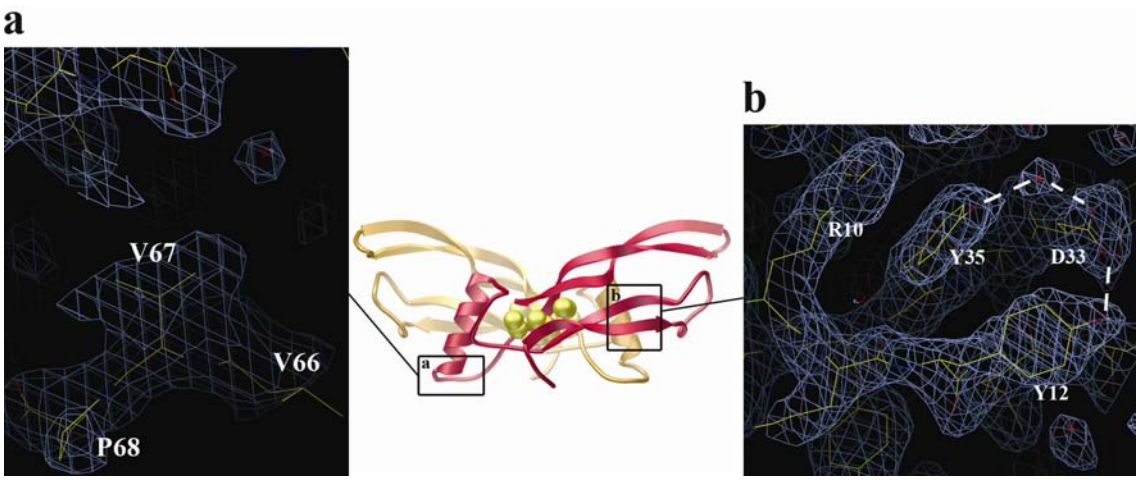

Figure 4-4. Close-up of the BMP-3 residues which are found in generously allowed regions. Panel (a) shows electron density environment for V67 while panel (b) shows Y35. Electron density is contoured at 1σ in a 2Fo-Fc map.

4.2.2. BMP-3 Homology Models

The ligand structure of BMP-3 was used as the building block to generate a complete, 6-member homology model by combining it with the previously solved ternary structure of BMP-2 bound to BMPRIa-ECD and ActRII-ECD. As mentioned previously, the BMP-3 ligand superimposes well with BMP-2, so no significant adjustments are needed to accurately place BMP-3 into the ternary complex. This close fit suggests that the homology model of BMP-3 with BMPRIa-ECD and ActRII-ECD is a good approximation of how the receptors will be positioned when actually bound to BMP-3. Looking at the overall structural arrangement of the BMP-3 ternary complex, no contacts between the different receptor types are predicted (Figure 4-5). While a previous study suggested BMP-3 may bind its type II receptors in a unique region of the ligand (*6*), the well fit interface of BMP-3 with ActRII-ECD suggests otherwise. Further, the BMPRIa-ECD molecules are positioned at the junction of the

two BMP-3 monomers in the same conformation as seen in the BMP-2:BMPRIa-ECD interface (Figure 4-5) (*12, 14*). The predicted buried surface area of the BMP-3:BMPRIa-ECD interface is 1268 $Å^2$, which is comparable to the 1217 $Å^2$ buried surface area seen at the BMP-2:BMPRIa-ECD interface. To generate the type I interface, twenty-three residues of BMPRIa make contact with fourteen residues of monomer A and ten residues of monomer B of BMP-3 (Figure 4-6, a). In comparison, the BMP-2:BMPRIa interface is formed by twenty-six residues of BMPRIa contacting twelve residues of monomer B and fifteen residues of monomer A of BMP-2 (Figure 4-6, b). While the total number of contacts and the size of the two interfaces are similar, the residues involved in the interfaces appear to vary greatly. While over half the residues making contact with BMPRIa in monomer B of BMP-3 are identical or highly conserved compared to residues in monomer B of BMP-2, only ~33% of the residues are identical or conserved between monomer A of BMP-3 and BMP-2. The majority of residue differences are found in contacts formed between α-helix 1 of BMPRIa and the α-helix H3 and the H3 pre-helix loop in monomer A of BMP-3. Residues in this region have been shown to have a significant impact on type I receptor binding (*15, 16*).

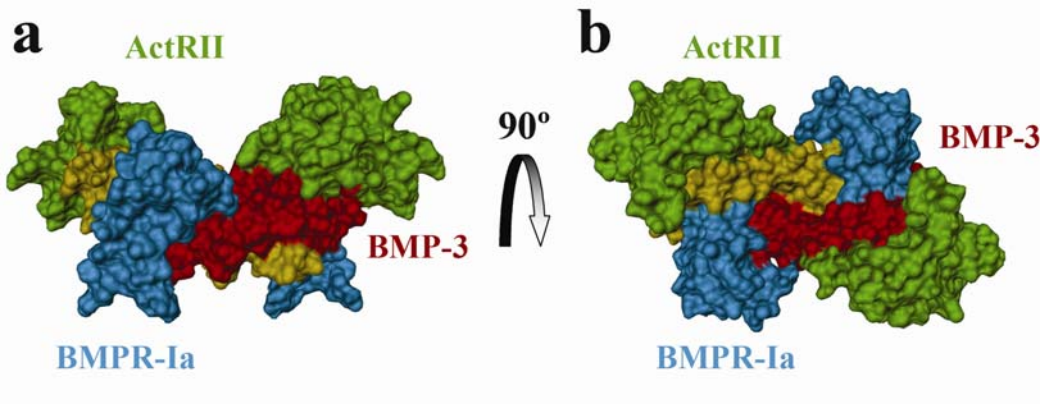

Figure 4-5. Ternary model of BMP-3/BMPRIa-ECD/ActRII-ECD. The space filling representation shows the predicted position of the different receptor types.

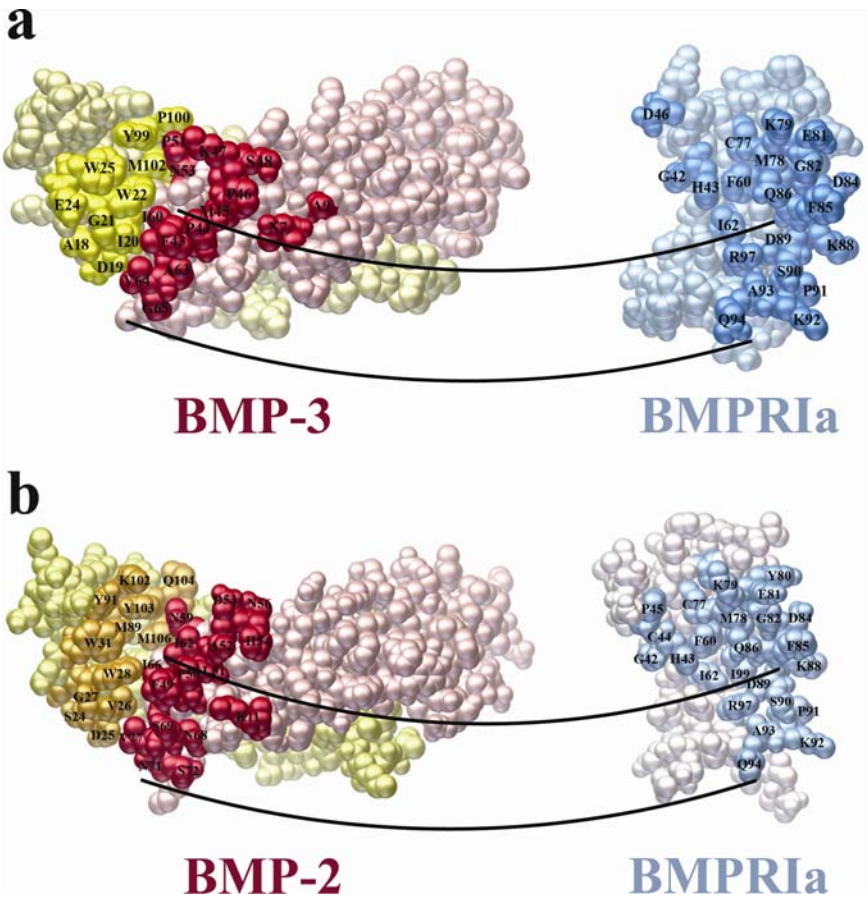

Figure 4-6. Comparison of ligand/type I receptor interfaces. Panel (a) shows the predicted BMP-3:BMPRIa interface and (b) depicts the known BMP-2:BMPRIa interface. The residues at the interface are labeled in each molecule.

Looking more closely at the predicted interface of BMP-3 with ActRII, it is very similar to other previously solved type II interfaces. The BMP-3:ActRII interface is formed from fifteen residues of one ActRII molecule making contact with seventeen residues of one BMP-3 monomer, with a buried surface area of 778 $Å^2$ (Figure 4-7, a). This makes the BMP-3:ActRII interface slightly larger than either the BMP-2:ActRII or the BMP-7:ActRII interfaces with buried surface areas of 660 $Å^2$ and 670 $Å^2$, respectively. The increased surface area is accounted for by the presence of five additional residue contacts seen only in the BMP-3:ActRII interface. A detailed look at the residues forming all three interfaces reveals the conserved type II binding motif is present in the predicted BMP-3:ActRII interface. The residues that form the hydrophobic core, as well as additional highly conserved residues, are present in all three interfaces (Figure 4-7, pink and green). Positioned at the periphery of the interfaces are the non-conserved or unique residues (Figure 4-7, blue). Interestingly, there appears to be a larger number of unique or non-conserved residues in the BMP-3 interface compared to the other type II interfaces. As the BMP-3:ActRII interface is only a model, these additional contacts maybe real or artifacts of the homology model. However, the high degree of similarity between all three type II interfaces suggests that one or a few of these unique residues in BMP-3 most likely determines type II receptor binding.

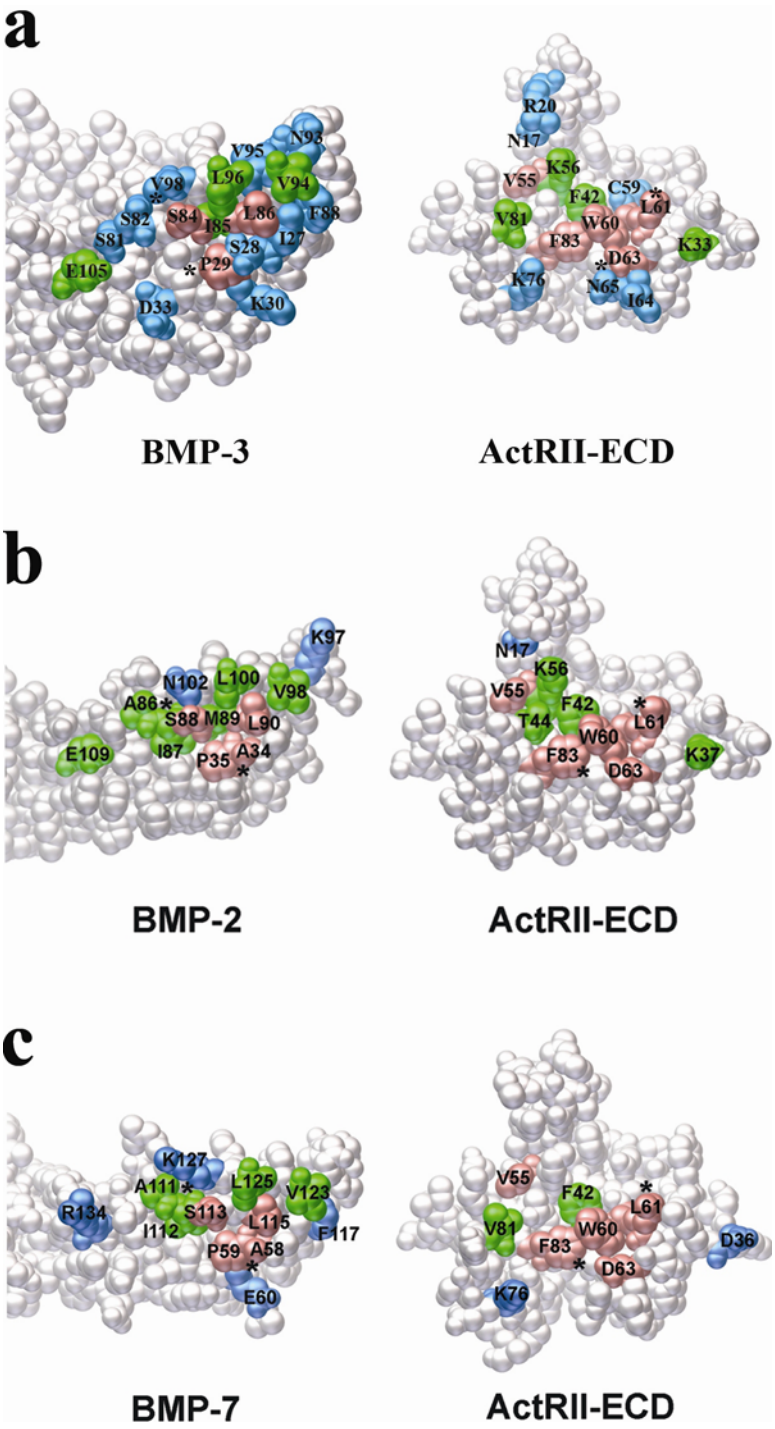

Figure 4-7. Comparison of BMP type II receptor interfaces. Panel (a) highlights the predicted BMP-3:ActRII interface, while panels (b) and (c) show the known BMP-2:ActRII and BMP-7:ActRII interfaces. Pink residues are identical, green are highly conserved, and blue are non-conserved between the interfaces.

4.2.3. Crystal Structure of BMP-6

Similar to BMP-3, the unbound BMP-6 ligand dimer was crystallized and its structure solved to a final resolution of 2.49 Å. BMP-6 crystallized in the space group $P3_121$ with unit cell dimensions of a=b= 97.4 Å and c= 87.4 Å and α=β= 90° and γ= 120°. To obtain a solution for the BMP-6 structure, molecular replacement was utilized with BMP-7 (*11*) as the search model. Based on the Matthews coefficient calculation, four ligand monomers were predicted per asymmetric unit. However, as BMP crystals pack with high solvent content, multiple asymmetric unit compositions were searched. As with BMP-3, the best molecular replacement solution was found by taking one BMP-7 monomer and searching for two independent BMP-6 monomers per asymmetric unit. This packing arrangement for the BMP-6 crystals yields extremely high solvent content at close to 70%. The BMP-6 ligands pack such that large pores or channels are formed in the crystal in the z-axis (Figure 4-8, a), as well as large spaces between ligands when stacking along the y-axis (Figure 4-8, b). The BMP-6 ligand monomers in each asymmetric unit are related by a 2-fold NCS, also seen in the BMP-3 crystals. During refinement, the quality of the model was improved by the use of a single TLS group per monomer, rather than the use of NCS restraints. The addition of a TLS group seemed to allow for adjustment of the two monomers relative to each other.

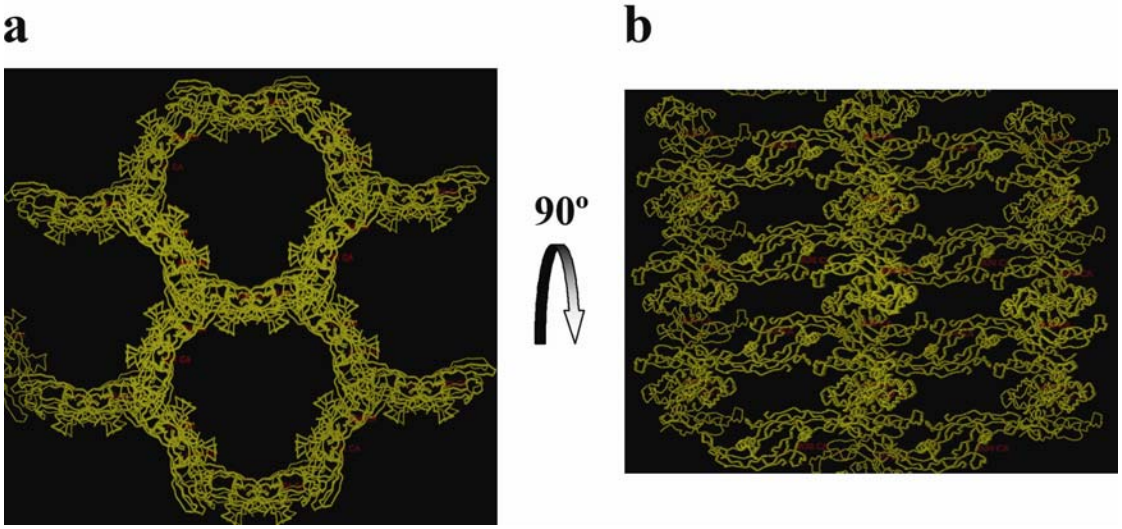

Figure 4-8. Packing arrangement of the BMP-6 crystal. Panel (a) depicts the large channels in the crystal, while (b) is the stacking arrangement.

The N-terminal residues of BMP-6 (1-28) appear to be flexible and disordered, and are not visible in the electron density maps. As with BMP-3, the BMP-6 ligand dimer crystallized in the active or "wings spread" conformation. This highly conserved TGF-β scaffold places fingers of each monomer pointing away from each other and the α-helix H3 at the junction between the monomers (Figure 4-9). The overall fold of the BMP-6 dimer is comparable that of the free BMP-7 dimer (*11*) and when the two structures are superimposed, the average Cα RMS_{dev} is 1.72Å. This is slightly higher than the Cα RMS_{dev} seen between BMP-3 and BMP-2. Interestingly, it appears the monomers of BMP-6 are in noticeably different conformations. When the monomers of BMP-6 are overlaid, the overall Cα RMS_{dev} is 1.74 Å, with a maximum difference of 6.9 Å. The differences in monomer conformations are easier to see when compared to BMP7. Monomer A of BMP-6 seems to overlay well with the corresponding monomer of BMP-7 (Figure 4-10). However, the tip region of finger 2

for monomer B of BMP-6 is in a more open position than finger 2 of the corresponding BMP-7 monomer (Figure 4-10). Equivalent residues in this region exhibit up to a 5 Å shift between structures. Also, the H3 pre-helix loop between the monomers of BMP-6 are found in different conformations. In monomer A of BMP-6, the H3 pre-helix loop is in a similar position to the H3 pre-helix loop found monomer A of BMP-7 (Figure 4-10). However, compared to the H3 pre-helix loop position of monomer B of BMP-7, the H3 pre-helix loop of BMP-6 B undergoes a large movement by pinching in toward the predicted type I receptor binding site. The corresponding residues at the top of the loop between BMP-6 and BMP-7 are shifted by as much as 9.5 Å (Figure 4-10). The differing conformations of the H3 pre-helix loop region between the two monomers of BMP-6 highlights an area of innate flexibility. This flexibility may impact type I receptor binding of BMP-6 and presents a general mechanism by which type I receptor binding can be regulated throughout the TGF-β superfamily. Yet, apart from the local conformational flexibility visualized in the loop regions of one BMP-6 monomer, this structure reiterates the backbone inflexibility of BMP family members. Compared to activin (*17, 18*) or TGF-β (*19*), BMP family members have only been crystallized in the wing spread conformation and this rigidity may be important for BMP function.

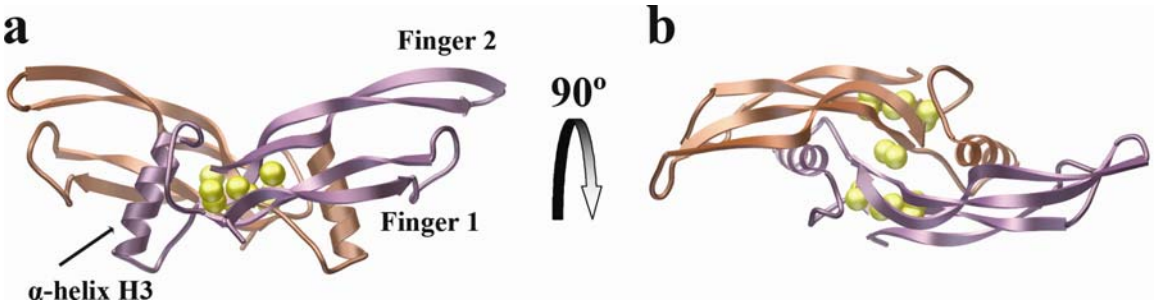

Figure 4-9. Ribbon structure of the BMP-6. Panel (a) shows the side view and panel (b) depicts the top view. Sulfur atoms are shown as yellow spheres.

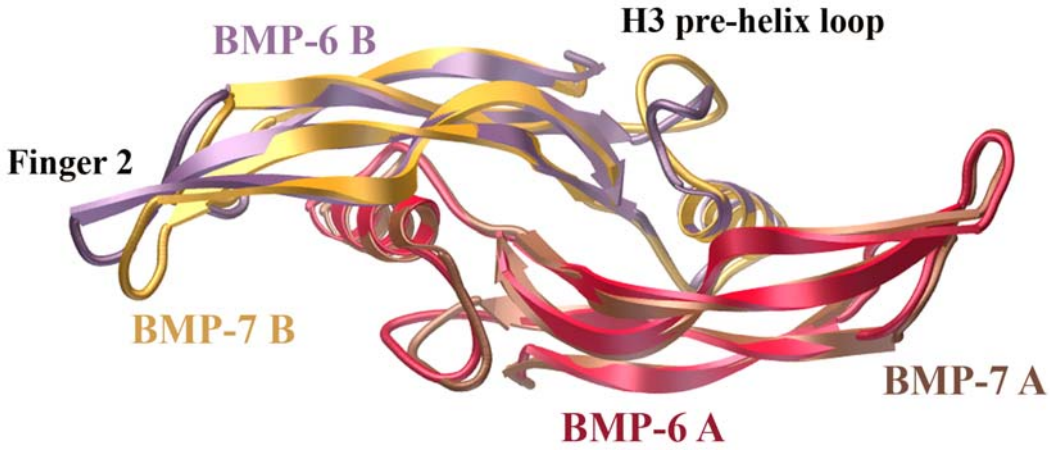

Figure 4-10. Comparison of BMP-6 and BMP-7. The ribbon structures highlight the differences in the B monomers of the each ligand.

Table 4-2 summarizes the x-ray diffraction and refinement statistics for BMP-6. The final BMP-6 structure refines to an R-factor of 23.3% and a free R-factor of 27.6% and displays good overall geometry with ~86% of the residues found in the most favored regions and none in the disallowed regions, as calculated by Ramachandran plot. As with the BMP-3 refinement, there are a few residues which fall into the generously allowed regions for residue geometry. Located in the H3 pre-helix loop region, Asn-73 of both monomers of BMP-6 is found in a generously allowed conformation. Analyzing the 2Fo-Fc electron density map, contoured to 1σ,

the geometry of the Asn-73 is stabilized through interactions with Asn-69 (Figure 4-11, 1). A second residue in both monomers found in a generously allowed orientation is Asn-58. As with Asn-73, the conformation of this residue is stabilized by side chain hydrogen bond interactions with residues on other strands of the fingers (Figure 4-11, 2). The stabilizing contacts coupled with the strong electron density seen for both residues indicates their backbone orientations are not artifacts of the refinement. Two additional residues located only in monomer B, Met-72 and Asn-88, are also seen in a generously allowed conformation. Met-72 is located in the H3 pre-helix loop region, while Asn-88 is found in the loop region directly following the H3 helix. These regions have the weakest electron density in a 2Fo-Fc map for the entire BMP-6 structure and, unlike Asn-58 and Asn-73, the geometry seen in Met-72 or Asn-88 does not appear to be stabilized by inter-residue interactions.

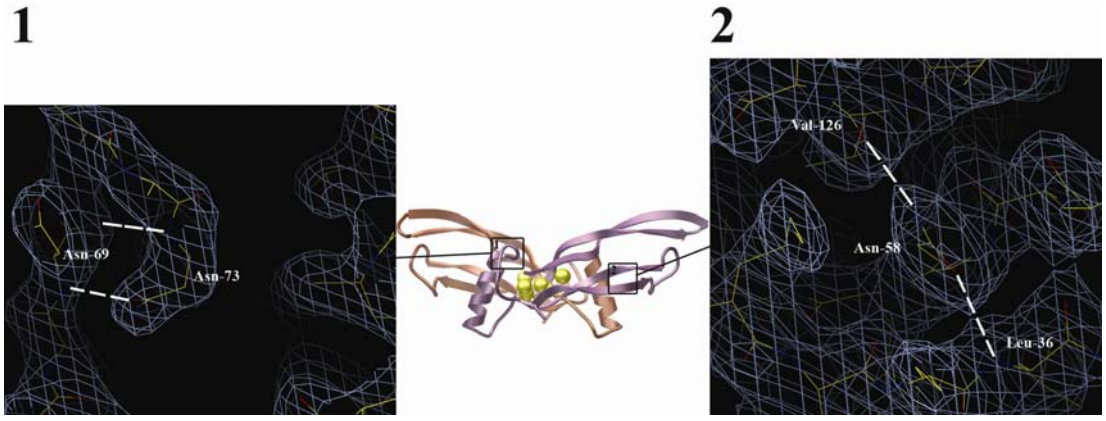

Figure 4-11. Close-up of the BMP-6 structure. Shown are the residues found in the generously allowed regions of both monomers. Electron density environment for (1) Asn-73 and (2) Asn-58. Electron density is contoured at 1σ in a 2Fo-Fc map.

Table 4-2. X-ray diffraction and refinement statistics for BMP-6.

X-ray Data Collection and Refinement Statistics

	BMP-6
Data Collection	
Beamline	SSRL 9-2
Space Group	$P3_121$
Number of Observations	87590
Unique Reflections	16044
Resolution Range (Å)[1]	50-2.49 (2.59-2.49)
Average I/σI	23.9 (2.0)
Completeness (%)	93.0 (57.0)
R_{sym} (%)	5.3 (43.7)
Refinement	
Resolution Range	84.5-2.49
R_{cryst} (%)	23.3
R_{free} (%)[2]	27.6
Average B factor (Å^2)	63.3
Rms Deviation	
Bonds (Å)	0.010
Angles (°)	1.396
Number of Atoms	
Protein	1646
Water	66
Number of TLS groups	2
Ramachadran plot non –gly, -pro, terminal residues	
most favored regions	159 (86.4%)
Additionally allowed regions	21 (11.4%)
Generously allowed regions	4 (2.2%)

[1] Numbers parentheses correspond to the highest resolution shell

[2] Calculated from 5 % of the data not used in refinement

4.2.4. BMP-6 Homology Models

The BMP-6 ligand structure can be superimposed onto the BMP-2 ligand of the ternary complex with only minor adjustments to the ligand backbone. Again, this high degree of structural agreement between the ligands suggests the modeled ligand-

receptor interfaces accurately represent the true interfaces. As with BMP-3, the position of the BMPRIa and ActRII molecules in the ternary model generate well fit interfaces with the BMP-6 dimer. As with the BMP-2 ternary structure and the BMP-3 ternary model, the arrangement of the receptors when bound to BMP-6 presents a signaling complex in which there are no receptor-receptor interactions (Figure 4-12). Although the overall BMP-6 ternary model is well fit, there is one region which does not appear to be an accurate. As mentioned above, the H3 pre-helix loops of monomers A and B of BMP-6 are in different conformations. When a BMPRIa-molecule is modeled into the binding site with monomer B, the movement of the H3 pre-helix loop places the atoms from main chain backbone within ~4 Å of the main chain backbone atoms of BMPRIa. This backbone closeness creates numerous side-chain/side-chain close contacts and one side-chain/main chain clash between BMP-6 and BMPRIa (Figure 4-13, inset). With so many unfavorable interactions present, it is not plausible for a BMPRIa molecule to bind BMP-6 if the H3 pre-helix loop remained in this conformation. To bind a type I receptor, the H3 pre-helix loop region would have to adopt a conformation more similar to the loop found in monomer A (Figure 4-13).

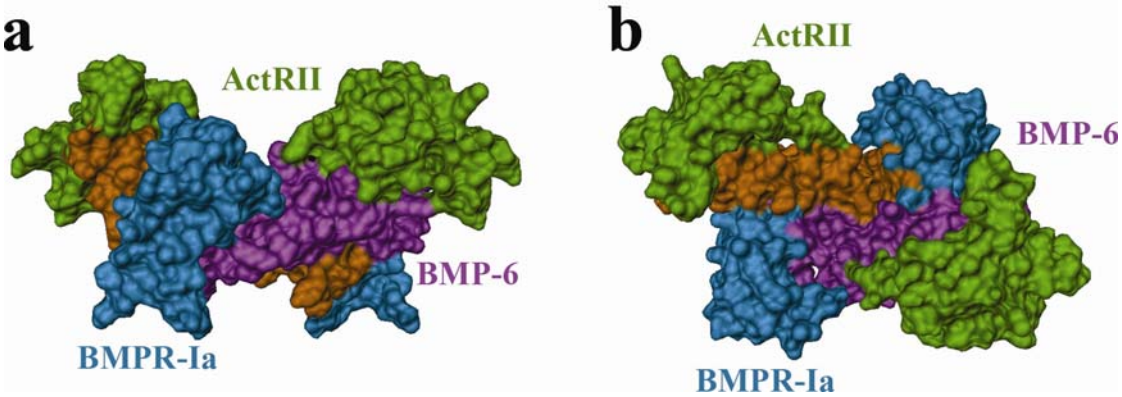

Figure 4-12. Space filling ternary model of BMP-6 with BMPRIa-ECD and ActRII-ECD.

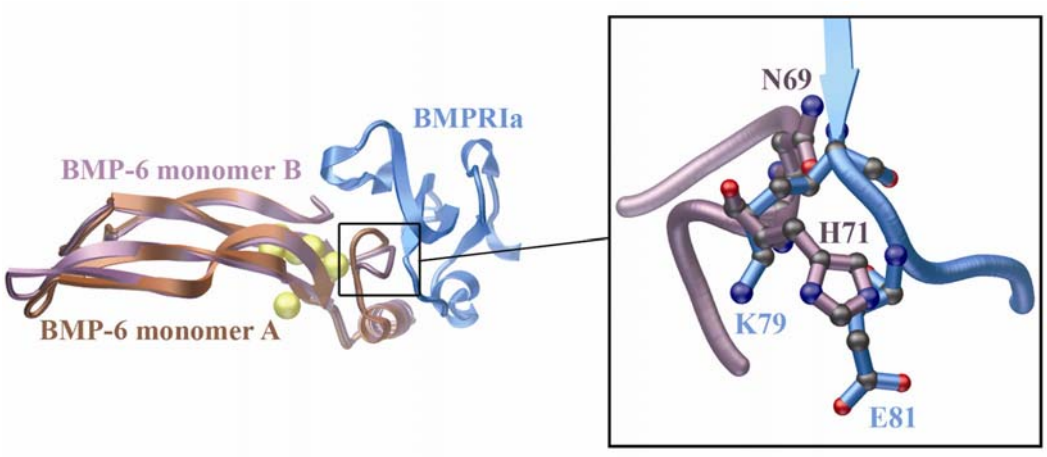

Figure 4-13. Comparison of the BMP-6 monomers. The inset highlights the interface of the H3 pre-helix loop of monomer B with BMPRIa.

Since monomer A appears to be in a conformation more suitable to receptor binding, it was used as the structural basis to analyze the receptor interfaces of BMP-6 with BMPRIa and ActRII. The buried surface area of the predicted BMP-6:BMPRIa interface is 1137 $Å^2$, which is very close to the buried surface area of 1217 $Å^2$ for the BMP-2:BMPRIa interface. To create the BMP-6:BMPRIa interface, twenty-one residues from BMP-6, eight from monomer B and thirteen from monomer A, make

contact with 18 residues from one BMPRIa molecule (Figure 4-14, a). The slightly reduced buried surface area of the BMP-6:BMPRIa interface is a result of six less ligand and five less receptor contacts than the BMP-2:BMPRIa interface (Figure 4-14, b).

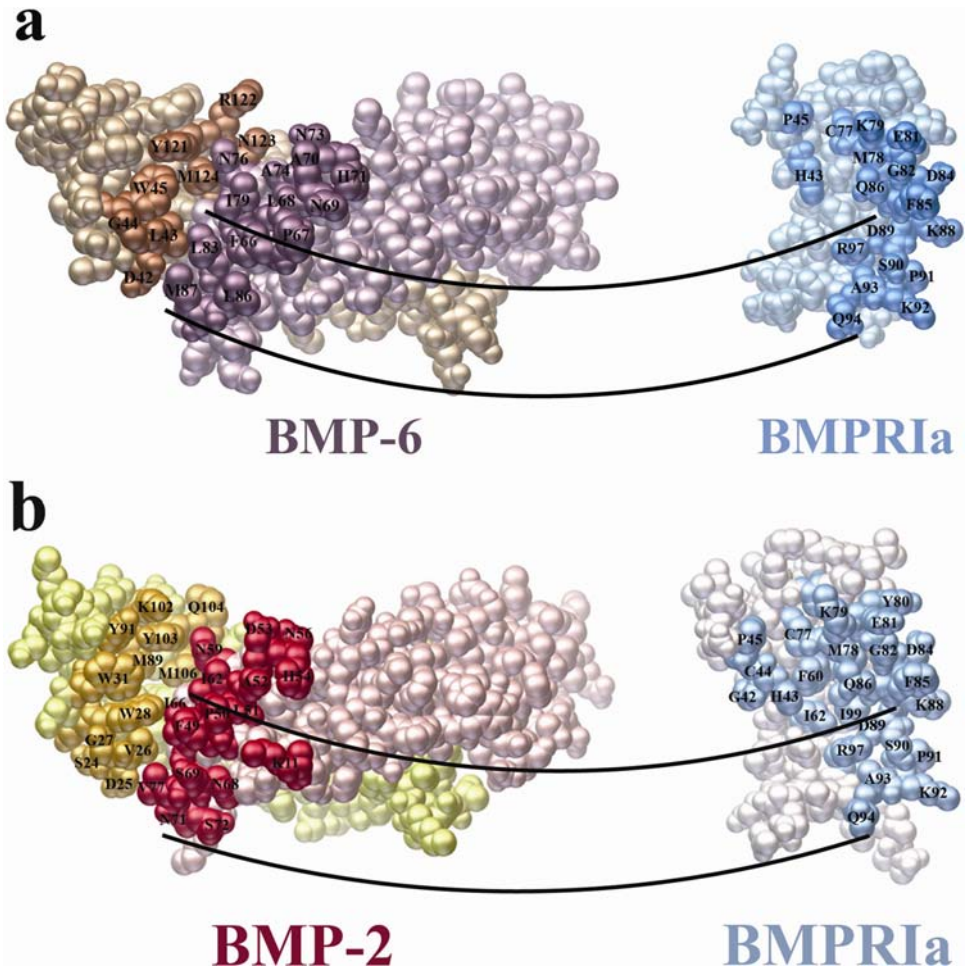

Figure 4-14. Space filling representation of type I interface. Panel (a) shows the predicted type I interface of BMP-6 with BMPRIa. Panel (b) shows the known type I interface of BMP-2:BMPRIa. Labeled are the residues at the interface.

Switching to look at the type II interface, the predicted BMP-6:ActRII interface has a buried surface area of 663 $Å^2$, which is almost identical to the buried

surface areas of BMP-2:ActRII and BMP-7:ActRII at 660 $Å^2$ and 670 $Å^2$, respectively. Fourteen residues from one ActRII and fifteen residues from one BMP-6 monomer are found at the interface (Figure 4-15, a). The BMP-6:ActRII interface appears to share the same binding motif seen in other type II interfaces, including the predicted BMP-3:ActRII interface. The hydrophobic core of the BMP-6:ActRII interface is formed by the equivalent residues found in the BMP-2 and BMP-7 interfaces (Figure 4-15, pink). Additional, highly conserved contacts are also found in the central region of the BMP-6:ActRII interface, while the non-conserved or unique residue contacts appear to be located at the edge of the binding interface (Figure 4-15). Though similar in size to the known type II BMP interfaces, the BMP-6:ActRII interface is predicted to have a large number of non-conserved residues. BMP-6 is predicted to have seven non-conserved residues, while BMP-2 has only two and BMP-7 has four (Figure 4-15, blue). The additional unique residues in the BMP-6 interface may play a role in type II receptor specificity and binding affinity.

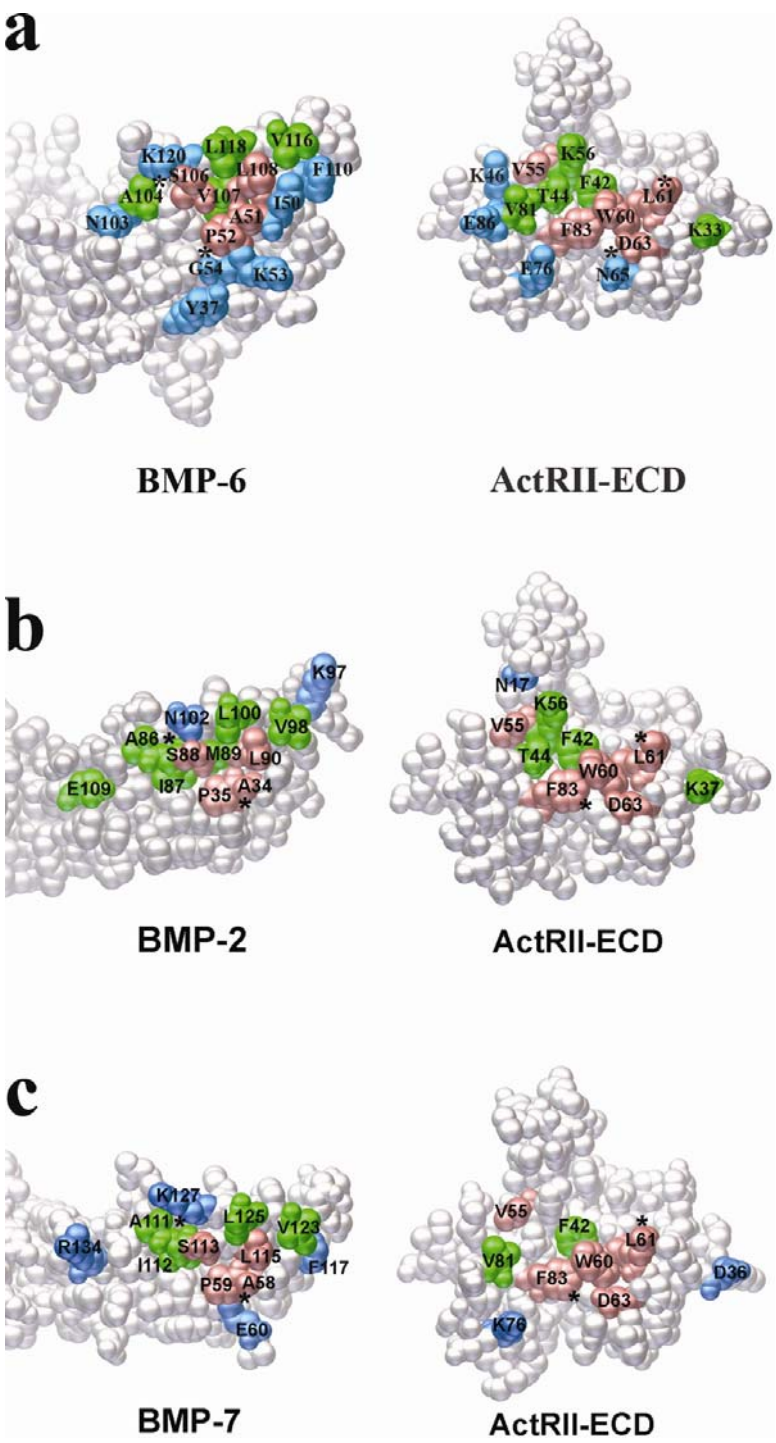

Figure 4-15. Comparison of BMP type II interfaces. Panel (a) shows the predicted BMP-6:ActRII interface, while panels (b) and (c)depict the known BMP-2:ActRII and BMP-7:ActRII interfaces, respectively. Pink residues are identical, green are highly conserved and blue are non-conserved between the interfaces.

4.2.5. Surface Plasmon Resonance (BIAcore) Studies

Since both BMP-3 and BMP-6 are predicted to share similar receptor binding motifs with other BMP ligands, it was important to determine the affinity with which these new ligands bind their receptors. Based on the BMP-2 mutagenesis studies, the determinants for receptor affinity and specificity reside in the non-conserved residues of the interfaces. While BMP-3 has been shown to interact with ActRIIb and Alk-4 in pull down assays (*6*), the affinity to these receptors as well as the actual receptor preference of BMP-3 remains unknown. Even though, the receptor preferences of BMP-6 have been better studied than BMP-3 (*10*), the actual affinity of BMP-6 to these various receptors has not been determined.

To calculate the affinity of BMP-3 and BMP-6 to a range of different receptors, we utilized surface plasmon resonance (BIAcore). For these experiments, receptor ECDs were immobilized onto the chip surface and the BMP ligands flowed over the surface. For the initial round of affinity experiments, BMPRIa-ECD and ActRII-ECD were immobilized onto the chip surface. BMP-3 was shown to bind BMPRIa-ECD with relatively low affinity, K_D= 307 nM (Table 4-3). This affinity is 3 to 6-fold weaker than a typical BMP lower affinity receptor interaction range of K_D= 50-100 nM. The affinity of BMP-3 to ActRII-ECD was even weaker still with a K_D= 1.84 μM (Table 4-3). This extreme low affinity was unexpected as BMP-3 has been shown to bind ActRIIb in other experiments (*5, 6*). The initial BIAcore data suggests neither BMPRIa nor ActRII-ECD are the high affinity receptors for BMP-3. BMP-6 was seen

to bind ActRII-ECD with high affinity, K_D= 7.4 nM, and bind BMPRIa-ECD with lower affinity, K_D= 67 nM (Table 4-3). These affinities are in agreement with previous studies showing BMP-6 binds more tightly to type II receptors than type I receptors (*10*). The affinity of BMP-6 to ActRII-ECD, K_D= 7.4 nM, is comparable to the affinity of BMP-7 to ActRII-ECD, K_D= 3.5 nM (Table 4-3). Interestingly, the affinity of BMP-6 for BMPRIa-ECD, K_D= 67 nM, is 25-fold higher than the affinity of BMP-7 to BMPRIa-ECD, K_D=1.68 μM (Table 4-3). However, it is known BMP-7 prefers Alk-2 as its type I receptor (*20*) and this receptor specificity difference between BMP-6 and BMP-7 may have biological significance.

Table 4-3. BIAcore affinity for BMP-3 and BMP-6 ligands. The data is shown as the dissociation rate, k_{off}, and the association rate, k_{on}, derived from a global fit using the kinetic model 1:1 Langmuir binding with mass transfer.

Ligand	BMP-2	BMP-6	BMP-7	BMP-3_{wt}
Receptor BMPRIa				
k_{off}[1/s]	$1.85x10^{-3} \pm 1.7x10^{-4}$	$1.06x10^{-2} \pm 1.2x10^{-3}$	$7.21x10^{-2} \pm 1.6x10^{-3}$	$5.18x10^{-2} \pm 2.3x10^{-3}$
k_{on}[1/M*s]	$7.06x10^{5} \pm 1.6x10^{4}$	$1.58x10^{5} \pm 8.0x10^{3}$	$4.33x10^{4} \pm 8.0x10^{3}$	$1.69x10^{5} \pm 3.0x10^{3}$
K_D [nM]	**2.61 ± 0.18**	**67.2 ± 4.4**	**1680 ± 145**	**307 ± 19**
Receptor ActRII				
k_{off}[1/s]	$7.65x10^{-2} \pm 8.6x10^{-3}$	$3.54x10^{-3} \pm 1.7x10^{-3}$	$1.19x10^{-2} \pm 4.0x10^{-4}$	$1.78x10^{-1} \pm 2.6x10^{-2}$
k_{on}[1/M*s]	$1.60x10^{6} \pm 3.0x10^{4}$	$4.60x10^{5} \pm 1.9x10^{5}$	$3.44x10^{6} \pm 4.1x10^{5}$	$9.91x10^{4} \pm 2.4x10^{4}$
K_D [nM]	**47.5 ± 6.5**	**7.39 ± 0.71**	**3.49 ± 0.30**	**1840 ± 180**

Since previous BMP-3 studies have utilized ActRIIb as the type II receptor, ActRIIb-ECD was immobilized onto the chip surface. The presence of both ActRII and ActRIIb ECDs on the chip surface will capture any differences in receptor binding affinity of BMP-3. When BMP-3 was flowed over the chip surface, it bound ActRIIb-ECD with a staggering 30-fold higher affinity, K_D= 53 nM, than to ActRII-ECD, K_D= 1.84 μM (Table 4-4). This result is very surprising given the ECD domains of ActRII

and ActRIIb are 63% identical and 92% similar. Further, this discrimination in affinity of BMP-3 for different receptors of the same type is the largest seen for all previously analyzed ligand-receptor interactions. BMP-2, BMP-6, and BMP-7 all bind ActRII-ECD and ActRIIb-ECD with the comparable affinity (Table 4-4). Activin displays the next largest difference, a 4-fold difference, in affinity between ActRII and ActRIIb (*11*). Since BMP-3 has such a strong preference for ActRIIb over ActRII, it is possible BMP-3 also has preferences for other receptors. To assess BMP-3's receptor preferences, the ECDs of type I receptors Alk-2 and BMPRIb (Alk-6) as well as the ECD for type II receptor BMPRII were immobilized onto additional chip surfaces. Unfortunately, binding of BMP-3 to any these receptors was not seen. However, the proper folding and activity of the three receptor ECDs could not be confirmed so it remains unclear what BMP-3's true affinity and specificity is for the remaining TGF-β receptors.

Table 4-4. BIAcore affinity for the comparison of ActRII and ActRIIb affinity. The data is shown as the dissociation rate, k_{off}, and the association rate, k_{on}, derived from a global fit using the kinetic model 1:1 Langmuir binding with mass transfer.

Ligand	**BMP-2**	**BMP-6**	**BMP-7**	**BMP-3$_{wt}$**
Receptor ActRII				
k_{off}[1/s]	$7.65x10^{-2} \pm 8.6x10^{-3}$	$3.54x10^{-3} \pm 1.7x10^{-3}$	$1.19x10^{-2} \pm 4.0x10^{-4}$	$1.78x10^{-1} \pm 2.6x10^{-2}$
k_{on}[1/M*s]	$1.60x10^{6} \pm 3.0x10^{4}$	$4.60x10^{5} \pm 1.9x10^{5}$	$3.44x10^{6} \pm 4.1x10^{5}$	$9.91x10^{4} \pm 2.4x10^{4}$
K_D [nM]	**47.5 ± 6.5**	**7.39 ± 0.71**	**3.49 ± 0.30**	**1840 ± 180**
Receptor ActRIIb				
k_{off}[1/s]	$4.34x10^{-2} \pm 7.0x10^{-4}$	$6.32x10^{-3} \pm 1.2x10^{-3}$	$1.67x10^{-2} \pm 1.1x10^{-3}$	$6.82x10^{-2} \pm 1.7x10^{-2}$
k_{on}[1/M*s]	$1.18x10^{6} \pm 8.0x10^{4}$	$9.17x10^{5} \pm 3.8x10^{4}$	$2.14x10^{6} \pm 2.0x10^{4}$	$1.29x10^{6} \pm 2.7x10^{5}$
K_D [nM]	**36.1 ± 1.3**	**6.87 ± 1.0**	**7.72 ± 0.53**	**52.6 ± 2.0**

4.2.6. BMP-6 type I Receptor Mutagenesis Studies

Based on BIAcore results, it was important to understand the structural basis for the ligands' varying receptor affinities. Since each receptor type appears to have a conserved binding motif throughout the BMP family, receptor affinity and binding specificity must be determined by the unique residues found at each interface. While BMP-6 and BMP-7 share the same high affinity for ActRII and ActRIIb, they have a 25-fold difference in affinity to BMPRIa. As such, the type I interface between these ligands was compared. To generate the BMP-7:BMPRIa interface, the BMP-7 ligand from the BMP-7/ActRII structure (*11*) was overlaid with the BMP-2 ligand bound to BMPRIa-ECD from the ternary structure. This BMP-7 ligand was chosen as its H3 pre-helix loop has been shown to be most similar to that of bound BMP-2 (*11*). The BMP-7 ligand required little backbone adjustment when superimposed with BMP-2, generating a well fit and fairly accurate representation of the type I binding interface.

Comparison of the predicted interfaces of BMP-6:BMPRIa-ECD and BMP-7:BMPRIa-ECD reveals only two residues, both in the H3 pre-helix loop, which appear to be dramatically different between the interfaces. In BMP-6, residues 70 and 71 are an alanine and histidine, respectively, while in BMP-7 the equivalent residues are a serine and a tyrosine. The position of His-71 in BMP-6 is conserved among BMP ligands that bind type I receptors with high affinity. The placement of an alanine residue at position 70 is less conserved throughout the BMP family. These residues in BMP-6 are equivalent to the residues mutated in BMP-2 to probe for type I binding affinity. Previous studies have found residues in the H3 pre-helix loop region

to be important for type I receptor binding. The insertion of a L51P mutation into BMP-2 prevents BMPRIa binding (*15*), and in GDF-5 a mutation of a single residue Arg-57 controls the receptor specificity between BMPRIb and BMPRIa (*16*). Additional residue differences between the interfaces did occur, but these were probably a result of experimental conditions. For instance, Asp-54 and Try-55 of BMP-7 are predicted to contact BMPRIa, yet the structurally equivalent residues in BMP-6, Asp-47 and Try-48 are not. Since the residues were the same in both ligands, their importance to receptor binding could not be tested.

To test if the residues Ser-70 and His-71 play a role in determining low affinity for BMPRIa, the mutations A70S and H71Y were introduced either independently or together into BMP-6. Unfortunately, none of the BMP-6 mutants displayed decreased or altered affinity for BMPRIa. This result suggests type I receptor affinity may be more complex than type II receptor binding and receptor affinity is governed by the combined structural arrangement of multiple residues over both ligand monomers.

4.2.7. BMP-3 type II receptor Mutagenesis Studies

Unlike BMP-6 and other BMP ligands, which displayed equal affinity to both ActRII and ActRIIb, BMP-3 exhibits a previously unseen 30-fold difference in type II receptor affinity. Therefore, to locate the structural basis for the extreme low affinity of BMP-3 to ActRII, the predicted interface of BMP-3:ActRII-ECD was analyzed and compared to the previously solved type II interfaces (*11, 17*), as well as the BMP-2:ActRII-ECD interface from the ternary structure. This analysis led to the

identification of two residues, Ser-28 and Asp-33, of BMP-3 that are only found at the BMP-3:ActRII-ECD interface. BMP-3 is the only BMP to have Ser-28 located in this position. All other known BMPs have an alanine located in the equivalent residue position (Figure 4-16). Ser-28 is located in the loop region connecting the two beta strands that form finger 1 of BMP-3 (Figure 4-17, 1). Based on the previously solved type II interfaces, the placement of an alanine residue at this position appears to be critical for type II binding. Phe-83 of ActRII packs closely to this alanine found in the BMPs, forming the bottom of the conserved hydrophobic core (Figure 4-17, 1). Disruption to this hydrophobic core region is detrimental to type II binding (*21*). A serine at this position in the ligand would introduce a potential steric hindrance as well as a charge repulsion to the tight packing of Phe-83 of ActRII (Figure 4-17, 1). The second potentially important residue, Asp-33 of BMP-3 is also an alanine in all other BMPs that bind type II receptors with high affinity (Figure 4-16). This residue is located near the loop region containing Ser-28, though it is positioned such that it is predicted to make contacts on the edge of the binding interface with ActRII and not in the hydrophobic core region. In the BMP-3:ActRII interface, Asp-33 is predicted to pack closely and interact with Ile-64 of ActRII (Figure 4-17, 2). As with Ser-28, the presence of Asp-33 presents potential stereochemical and charge barriers to receptor binding. Having an alanine in this position would allow Ile-64, located in a loop region of ActRII, to pack more tightly to the BMP ligand, acting as a clip to secure the receptor to the ligand. Loss of this contact may result in the decreased type II receptor affinity seen in BMP-3.

```
BMP-2   -------------QAKHKQRKRLKS------------SCKRHPLYVDFSDVGWNDWIVAPPGYHAFYCHGEC 47
BMP-4   ------------SPKHHSQRARKKNK-----------NCRRHSLYVDFSDVGWNDWIVAPPGYQAFYCHGDC 49
BMP-5   -------NQNRNKSSSHQDSSRMSSVGDYNT-SEQKQACKKHELYVSFRDLGWQDWIIAPEGYAAFYCDGEC 64
BMP-6   -------QQSRNRSTQSQDVARVSSASDYNS-SELKTACRKHELYVSFQDLGWQDWIIAPKGYAANYCDGEC 64
BMP-7   STGSKQRSQNRSKTPKNQEALRMANVAENSS-SDQRQACKKHELYVSFRDLGWQDWIIAPEGYAAYYCEGEC 71
BMP-8   -AVRPLRRRQPKKSNELPQANRLPGIFDDVHGSHGRQVCRRHELYVSFQDLGWLDWVIAPQGYSAYYCEGEC 71
BMP-10  ---------------NAKGN---------------YCKRTPLYIDFKEIGWDSWIIAPPGYEAYECRGVC 40
BMP-3   ---------------QWIEPR--------------NCARRYLKVDFADIGWSEWIISPKSFDAYYCSGAC 41
BMP-15  --------QADGISAEVTASSSKHSGPENN-------QCSLHPFQISFRQLGWDHWIIAPPFYTPNYCKGTC 57

BMP-2   48 PFPLADHLNSTNHAIVQTLVNSVN--SKIPKACCVPTELSAISMLYLDENEKVVLKNYQDMVVEGCGCR 114
BMP-4   50 PFPLADHLNSTNHAIVQTLVNSVN--SSIPKACCVPTELSAISMLYLDEYDKVVLKNYQEMVVEGCGCR 116
BMP-5   65 SFPLNAHMNATNHAIVQTLVHLMFP-DHVPKPCCAPTKLNAISVLYFDDSSNVILKKYRNMVVRSCGCH 132
BMP-6   65 SFPLNAHMNATNHAIVQTLVHLMNP-EYVPKPCCAPTKLNAISVLYFDDNSNVILKKYRNMVVRACGCH 132
BMP-7   72 AFPLNSYMNATNHAIVQTLVHFINP-ETVPKPCCAPTQLNAISVLYFDDSSNVILKKYRNMVVRACGCH 139
BMP-8   72 SFPLDSCMNATNHAILQSLVHLMKP-NAVPKACCAPTKLSATSVLYYDSSNNVILRKHRNMVVKACGCH 139
BMP-10  41 NYPLAEHLTPTKHAIIQALVHLKNS-QKASKACCVPTKLEPISILYLDKGVVTYKFKYEGMAVSECGCR 108
BMP-3   42 QFPMPKSLKPSNHATIQSIVRAVGVVPGIPEPCCVPEKMSSLSILFFDENKNVVLKVYPNMTVESCACR 110
BMP-15  58 LRVLRDGLNSPNHAIIQNLINQLVD-QSVPRPSCVPYKYVPISVLMIEANGSILYKEYEGMIAESCTCR 125
```

Figure 4-16. Alignment of BMP ligand sequences. Cysteines are shown in yellow and the mutated residues of BMP-3 are shown in green and purple.

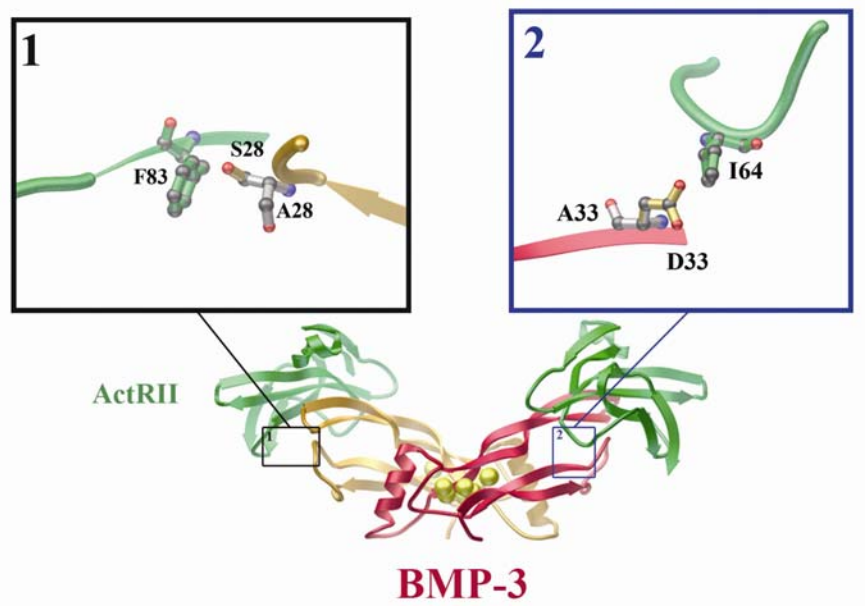

Figure 4-17. Close-up of the BMP-3 type II mutants. Panel 1 shows the S28A mutant interface, while panel 2 shows the D33A mutant interface.

To test if either of these residues have a direct influence on BMP-3's type II binding affinity, the S28A and D33A mutations were inserted into BMP-3

independently and together. When these two potentially unfavorable interactions were removed by individually mutating the residues to alanine, both the BMP-3_{S28A} and BMP-3_{D33A} mutants showed a large, 20-fold increase in affinity for ActRII-ECD compared to BMP-3_{wt} (Table 4-5). The BMP-3_{S28A} mutant displays a K_D= 96.5 nM and the BMP-3_{D33A} mutant has a K_D= 124 nM. Furthermore, BMP-3_{S28A} and BMP-3_{D33A} showed a 5 to 10-fold increase in affinity to ActRIIb-ECD. The affinity of BMP-3_{S28A} and BMP-3_{D33A} to ActRIIb-ECD is K_D = 11.3 nM and K_D= 4.06 nM, respectively (Table 4-5). These affinities make their binding to ActRIIb-ECD near-high affinity interactions. As with the BMP-2 type II mutants, the BMP-3 type II mutants exert their influence through slower dissociation rates. The difference between the dissociation, k_{off}, rates can be seen in the BIAcore traces for BMP-3_{wt} compared to the mutants (Figure 4-18). Interestingly, a double mutant of BMP-$3_{S28A/D33A}$ does not show a further increase in binding affinity over the single mutants (Table 4-5). This indicates their contributions to the binding energy are highly coupled because of the proximity between them. Since both mutants show an equal enhancement in affinity for ActRII-ECD, the ActRII molecule must be able to make minor conformational shifts to adopt the most favorable side chain interactions possible. The position of the M-loop in ActRII was previously shown to have a small overall impact on binding affinity. While the BMP-3_{S28A} and BMP-3_{D33A} mutants account for a significant increase in overall affinity to both ActRII and ActRIIb, the residues responsible for the 30-fold affinity difference in affinity of BMP-3 for ActRII and ActRIIb remains unresolved. Further, the residues responsible for this

discrimination may be encoded on the receptor interacting with a specific residue or residues in the BMP-3 ligand.

Table 4-5. BIAcore affinity data for the BMP-3 mutants. The data is shown as the dissociation rate, k_{off}, and the association rate, k_{on}, derived from a global fit using the kinetic model 1:1 Langmuir binding with mass transfer.

Ligand	**BMP-3_{wt}**	**BMP-3_{S28A}**	**BMP-3_{D33A}**	**BMP-$3_{S28A/D33A}$**
Receptor ActRII				
k_{off}[1/s]	$1.78x10^{-1} \pm 2.6x10^{-2}$	$7.71x10^{-2} \pm 5.4x10^{-3}$	$1.73x10^{-1} \pm 5.8x10^{-2}$	$4.31x10^{-2} \pm 5.8x10^{-3}$
k_{on}[1/M*s]	$9.91x10^{4} \pm 2.4x10^{4}$	$8.13x10^{5} \pm 1.3x10^{5}$	$1.34x10^{6} \pm 2.8x10^{5}$	$2.83x10^{5} \pm 1.1x10^{5}$
K_D [nM]	**1840 ± 180**	**96.5 ± 9.5**	**124 ± 16**	**152 ± 22**
Receptor ActRIIb				
k_{off}[1/s]	$6.82x10^{-2} \pm 1.7x10^{-2}$	$4.36x10^{-3} \pm 9.8x10^{-4}$	$5.39x10^{-3} \pm 1.5x10^{-3}$	$4.03x10^{-3} \pm 1.0x10^{-3}$
k_{on}[1/M*s]	$1.29x10^{6} \pm 2.7x10^{5}$	$3.91x10^{5} \pm 7.0x10^{3}$	$1.41x10^{5} \pm 1.2x10^{5}$	$4.68x10^{5} \pm 8.0x10^{4}$
K_D [nM]	**52.6 ± 2.0**	**11.3 ± 2.8**	**4.08 ± 1.5**	**8.68 ± 2.0**

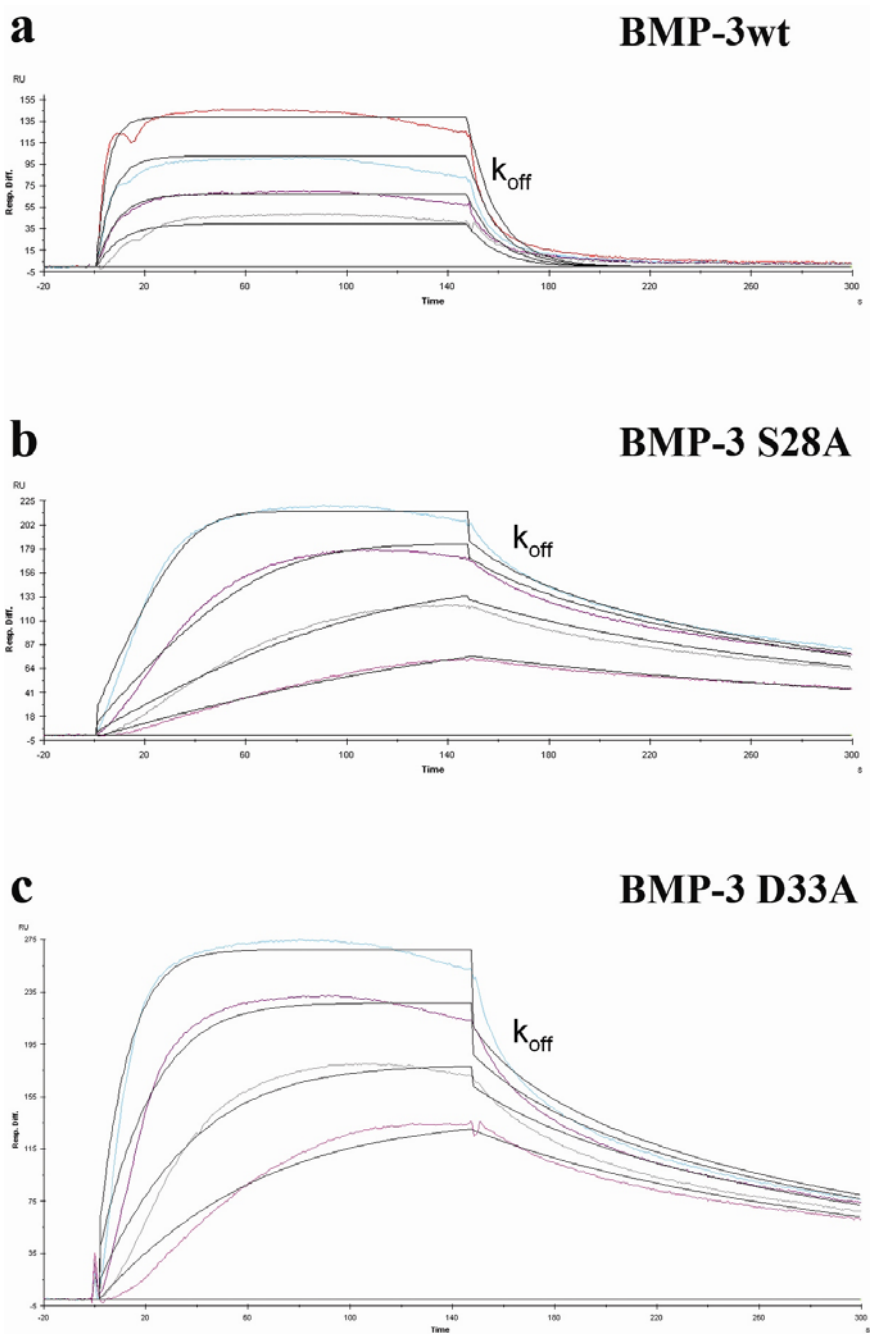

Figure 4-18. BMP-3 BIAcore traces to ActRIIb. Panel (a) shows BMP-3_{wt}, while (b) and (c) show the mutants BMP-3_{S28A} and BMP-3_{D33A}, respectively. The black lined depict the global fit of the data to a 1:1 Langmuir model with mass transfer.

To address the question of receptor specificity, the interfaces of BMP-3:ActRII and BMP-3:ActRIIb needed to be directly compared. The BMP-3:ActRIIb interface

was generated by superimposing one BMP-3 ligand monomer onto one activin monomer bound to ActRIIb (*17*). Even though activin is distinct from the BMP family, the conserved TGF-β architecture present in both monomers allowed for a good fit of the ligands with minimal adjustment to the backbone. The backbone Cα RMS_{dev}= 1.43 Å was very low between the BMP-3 and BMP-2 dimers, suggesting the BMP-3:ActRIIb-ECD is an accurate representation of the true interface. With the ECDs of ActRII and ActRIIb being so similar in sequence, significant differences between the interfaces were not expected. Even though the BMP-3:ActRII-ECD interface has additional contacts compared to the BMP-3:ActRIIb-ECD interface, these differences are most likely dependent on the experimental criteria used to determine contacts. For instance, though residues Asn-65 and Lys-33 are only seen in the ActRII-ECD interface, these are identical in ActRIIb-ECD (Figure 4-19). However, there was a single residue difference between the interfaces which appeared to be important. In ActRII residue 76 is a lysine, while in ActRIIb the structurally equivalent residue is a glutamic acid. While the Glu-76 of ActRIIb is positioned to make favorable hydrogen bond interactions with Lys-30 of BMP-3, Lys-76 of ActRII would create an unfavorable charge repulsion, as well as a potential steric clash with Lys-30 of BMP-3 (Figure 4-20). Therefore, to see if the charge reversal would abolish BMP-3's specificity preference between the receptors, the E76K mutation was inserted into ActRIIb.

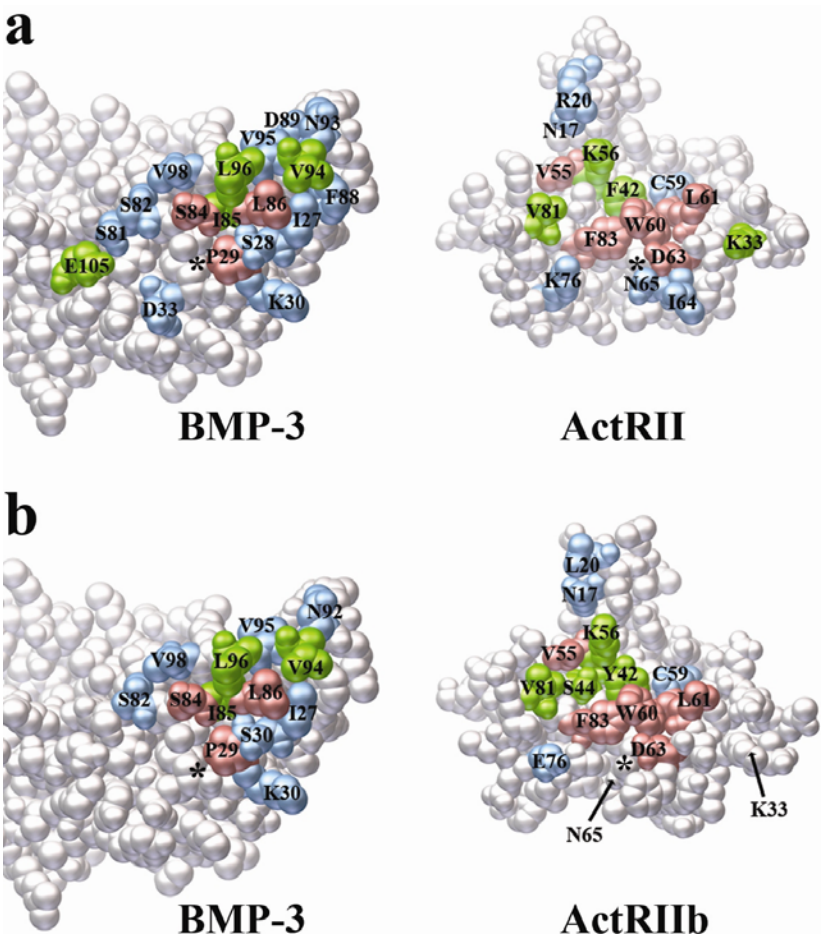

Figure 4-19. Comparison of the BMP-3 type II interfaces. Panel (a) shows BMP-3:ActRII interface and panel (b) shows BMP-3:ActRIIb interface. Color scheme is from comparison with known type II receptors.

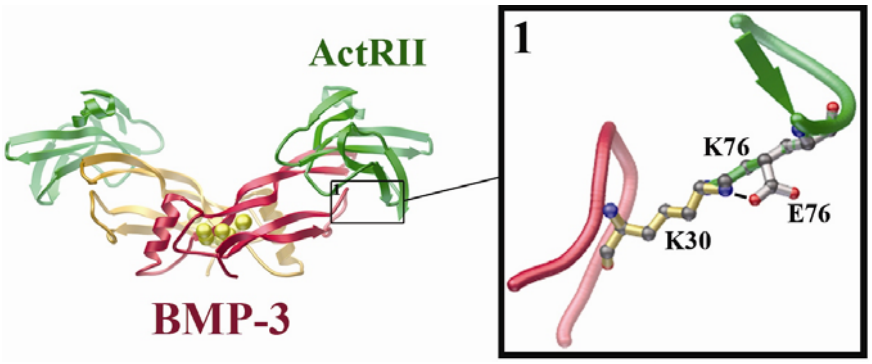

Figure 4-20. Close-up of the BMP-3:ActRII interface. The inset shows E76K mutation made to ActRIIb.

To test the effect this mutation had on BMP-3 binding affinity, the ActRIIb$_{E76K}$-ECD was immobilized onto a BIAcore chip surface. Because the dissociation rate of BMP-3$_{wt}$ to ActRII-ECD was at the measurement limit for the BIAcore 3000 instrument, the BMP-3$_{S28A}$ mutant, a high-affinity ligand to ActRII-ECD, was used to compare its affinity more readily to the ActRIIb$_{E76K}$-ECD surface. The affinity of BMP-3$_{S28A}$ for ActRIIb-ECD was K_D= 11.3 nM but this affinity decreased to K_D= 137 nM for ActRIIb$_{E76K}$-ECD (Table 4-6). With this 10-fold decrease in affinity, BMP-3$_{S28A}$ affinity for ActRIIb$_{E76K}$-ECD is now the same or weaker than its affinity to ActRII-ECD. In comparison, BMP-2, which has a proline at the equivalent position of Lys-30 in BMP-3, does not show any change in affinity between ActRIIb-ECD and ActRIIb$_{E76K}$-ECD (Table 4-6). This result supports the hypothesis that type II receptor specificity for BMP-3 is controlled by the interaction receptor residues with Lys-30 of BMP-3.

Table 4-6. BIAcore affinity comparison of ActRII, ActRIIb, and ActRIIb$_{E76K}$. The data is shown as the dissociation rate, k_{off}, and the association rate, k_{on}, derived from a global fit using the kinetic model 1:1 Langmuir binding with mass transfer.

Ligand	**BMP-2**	**BMP-3$_{wt}$**	**BMP-3$_{S28A}$**
Receptor ActRII			
k_{off}[1/s]	$7.65x10^{-2} \pm 8.6x10^{-3}$	$1.78x10^{-1} \pm 2.6x10^{-2}$	$7.71x10^{-2} \pm 5.4x10^{-3}$
k_{on}[1/M*s]	$1.60x10^{6} \pm 3.0x10^{4}$	$9.91x10^{4} \pm 2.4x10^{4}$	$8.13x10^{5} \pm 1.3x10^{5}$
K_D [nM]	**47.5 ± 6.5**	**1840 ± 180**	**96.5 ± 9.5**
Receptor ActRIIb			
k_{off}[1/s]	$4.34x10^{-2} \pm 7.0x10^{-4}$	$6.82x10^{-2} \pm 1.7x10^{-2}$	$4.36x10^{-3} \pm 9.8x10^{-4}$
k_{on}[1/M*s]	$1.18x10^{6} \pm 8.0x10^{4}$	$1.29x10^{6} \pm 2.7x10^{5}$	$3.91x10^{5} \pm 7.0x10^{3}$
K_D [nM]	**36.1 ± 1.3**	**52.6 ± 2.0**	**11.3 ± 2.8**
Receptor ActRIIb$_{E76K}$			
k_{off}[1/s]	$3.59x10^{-2} \pm 9.0x10^{-3}$	No Data	$4.11x10^{-2} \pm 2.0x10^{-3}$
k_{on}[1/M*s	$6.98x10^{5} \pm 8.0x10^{4}$		$3.02x10^{5} \pm 1.9x10^{4}$
K_D [nM]	**50.3 ± 6.6**		**137 ± 15**

4.2.8. BMP-3 Mutants can Activate the SMAD-1/5/8 Pathway

Even though the mutagenesis and BIAcore experiments shed insight into how BMP-3 regulates receptor affinity and specificity, the mechanism of BMP-3 function remains unclear. Using medium from whole cells, it has been suggested that BMP-3, by signaling through the Smad-2/3 pathway, could antagonize BMP-2 function intracellularly (*5*). A second mechanism, of extracellular antagonism, has also been proposed as BMP-3's function (*6*). However, previous studies have failed to show signaling activity with recombinant BMP-3 (*1*). Based on the above mentioned receptor affinity data, the lack of function for recombinant BMP-3 may have been a result of the poor affinity BMP-3 has for ActRII. To evaluate if the increased affinity to ActRII of the BMP-3 mutants correlates into higher signaling activity, the mutants'

activity was tested in whole cell luciferase assays. The C2C12 cell line was chosen as it is known to express a wide range of TGF-β receptors (*22*). The Id1-Luc reporter clone was chosen as BMP receptors signal through the Smad-1/5/8 pathway and the Id1 promoter contains a well-characterized Smad1-binding site, which responds to activated Smad-1 (*23*). Removal of this site (Id1-Luc mut) abolishes any response, demonstrating that the Id1-Luc is a Smad-1 dependent reporter (*24*). Because fetal bovine serum (FBS) is known to contain BMP-like activity (*25*), low serum concentration, 0.1% FBS, was used in order to minimize any interference on the assay.

The signaling activities of various wild type ligands were tested first to obtain a signaling benchmark. As previously reported, BMP-2 shows strong signaling activity in a concentration-dependent manner with a 40-fold increase in activity at 30 ng/mL (Figure 4-21). This result corresponds with our data showing BMP-2's high affinity for BMPRIa-ECD. BMP-7 also displays strong stimulation of the Smad-1 dependent pathway, similar to BMP-2, with a 55-fold increase in activity at 30 ng/mL (Figure 4-21). Despite its relatively low affinity to BMPRIa-ECD, BMP-7 is still able to signal because C2C12 cells express ALK-2 which BMP-7 is known to bind and also can activate Smad-1 (*26*). In contrast to BMP-2 and BMP-7, BMP-6 shows much weaker signaling activity with only a 9-fold Id1-Luc stimulation at 100 ng/ml (Figure 4-21). This stimulation is approximately 12% of the Id1-Luc activation by the same concentration of BMP-2. BMP-3 shows an insignificant and non-concentration dependent level of signaling through the Smad-1 pathway (Figure 4-21). This finding

is consistent with the previous reports showing lack of recombinant BMP-3 signaling (*1*).

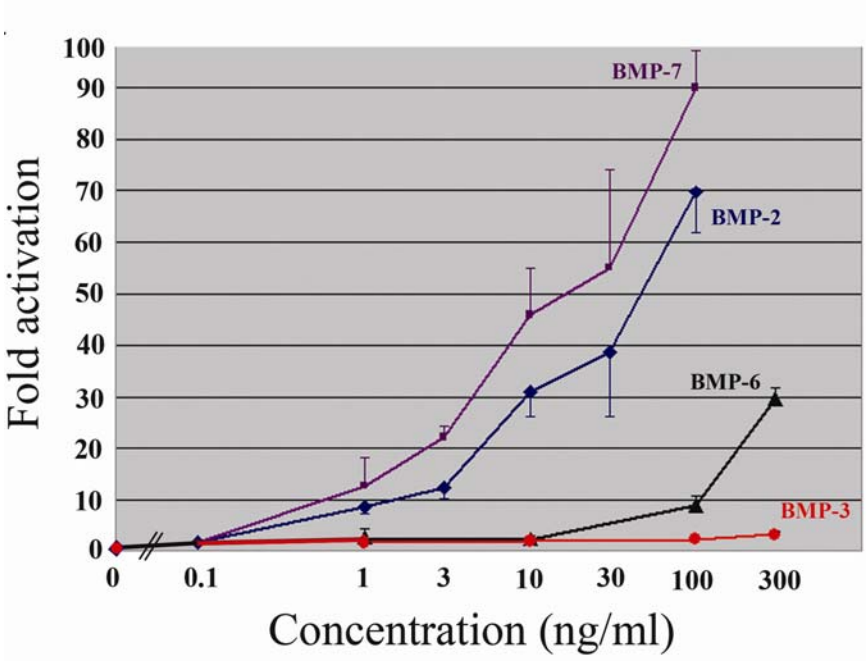

Figure 4-21. Luciferase assay of BMP ligand activity. The graph reports fold activation above background at increasing concentration of ligand.

With baseline signaling established, the BMP-3 mutant ligands were tested in the same Smad-1 dependent reporter assay. The BMP-3_{S28A} mutant shows a significant increase in its ability to activate the Id1-Luc reporter and stimulated reporter activity 13.7-fold at 300 ng/mL (Figure 4-22). The BMP-3_{S28A} mutant now displays a similar level of activity to that of BMP-6. Although the BMP-3_{D33A} mutant has similar affinity for ActRII-ECD as BMP-3_{S28A}, BMP-3_{D33A} did not exhibit as significant an activation of the Id1-Luc reporter, with only a 3.2-fold stimulation at 300 ng/ml (Figure 4b). This activation is ~25% of the activation by the BMP-3_{S28A}

mutant. A third mutant, BMP-3_{K30E}, was also tested in this assay. The insertion of a glutamic acid at residue 30 is predicted to increase the affinity of BMP-3 to ActRII by generating a favorable interaction with Lys-76 of ActRII (Figure 4-23). Unfortunately, the BMP-3_{K30E} mutant did not generate reproducible signaling activity results (Data not shown). Based on this data, we predict BMP-3_{wt} will signal through ActRIIb in a similar manner as BMP-3_{S28A} with ActRII because they share comparable receptor binding affinities. The apparent lack of activity of BMP-3_{wt} in our assays is most likely due to the absence of ActRIIb expression in C2C12 cells.

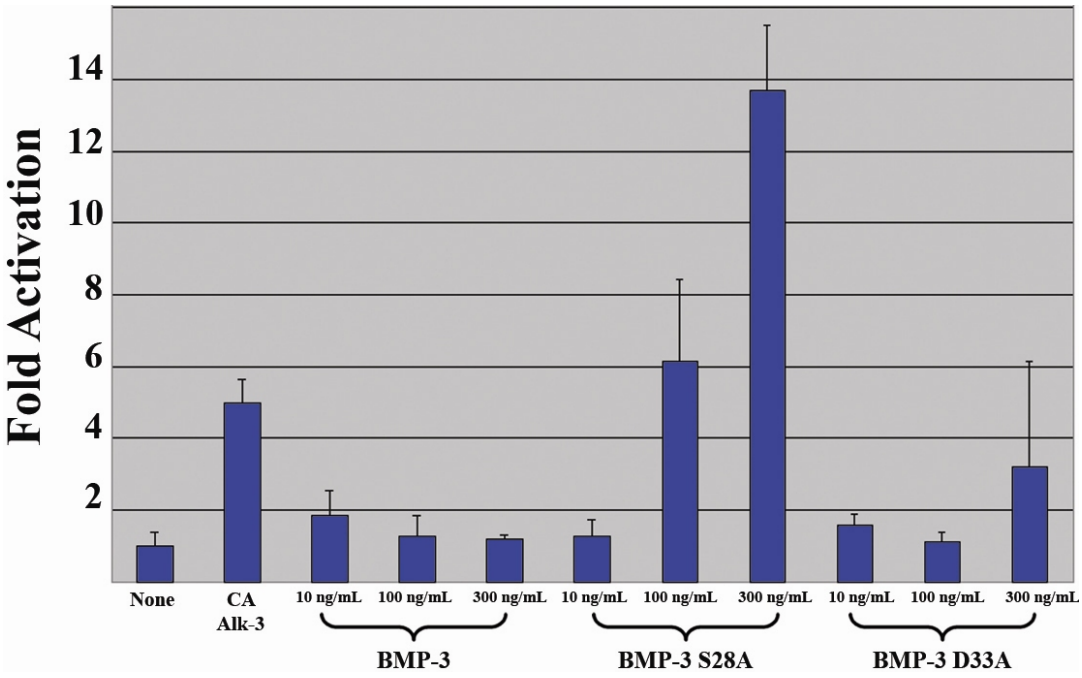

Figure 4-22. Fold increase in luciferase activity at 300 ng/mL for BMP-3, BMP-3_{S28A}, and BMP-3_{D33A}.

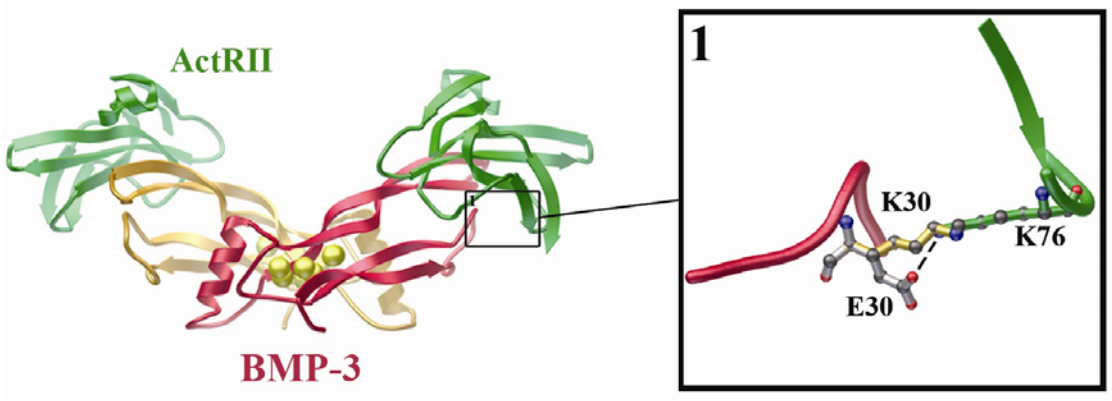

Figure 4-23. BMP-3:ActRII interface. The insert shows the predicted K30E mutation when inserted into BMP-3.

As several studies suggested BMP-3 functions as a BMP antagonist *in vivo* (*1*, *3*, *5*), this additional property of BMP-3 was also tested. One suggested method BMP-3 antagonism is its ability to signal through the Smad-2/3 (TGF-β/activin) pathway (*5*). As such, we repeated the C2C12 experiments, this time transfecting a Smad-2 reporter clone. None of the BMP-3_{wt} or the BMP-3 type II mutants showed any dose dependent activation (Figure 4-24). BMP-2 and BMP-7 were also tested and did not show any Smad-2 reporter activation, confirming the BMP ligands are specific to the Smad-1/5/8 pathway. Both activin and TGF-β1 showed a small but dose dependent activation of the Smad-2 reporter (Figure 4-24). The second proposed mechanism for BMP-3 function was by acting as an extracellular antagonist (*6*). Therefore, a competition assay was performed to see if BMP-3 could antagonize BMP-2 signaling. Using a constant amount of BMP-3, the amount of BMP-2 was increased from a 1:100 starting ratio up to a final ratio of 1:1 of BMP-2:BMP-3. The activity of BMP-2 did not show any significant decrease in response to the presence of BMP-3 (Figure 4-25).

As the BMP-3 type II mutants were shown to activate the Smad-1/5/8 pathway, they were not tested in the competition assay.

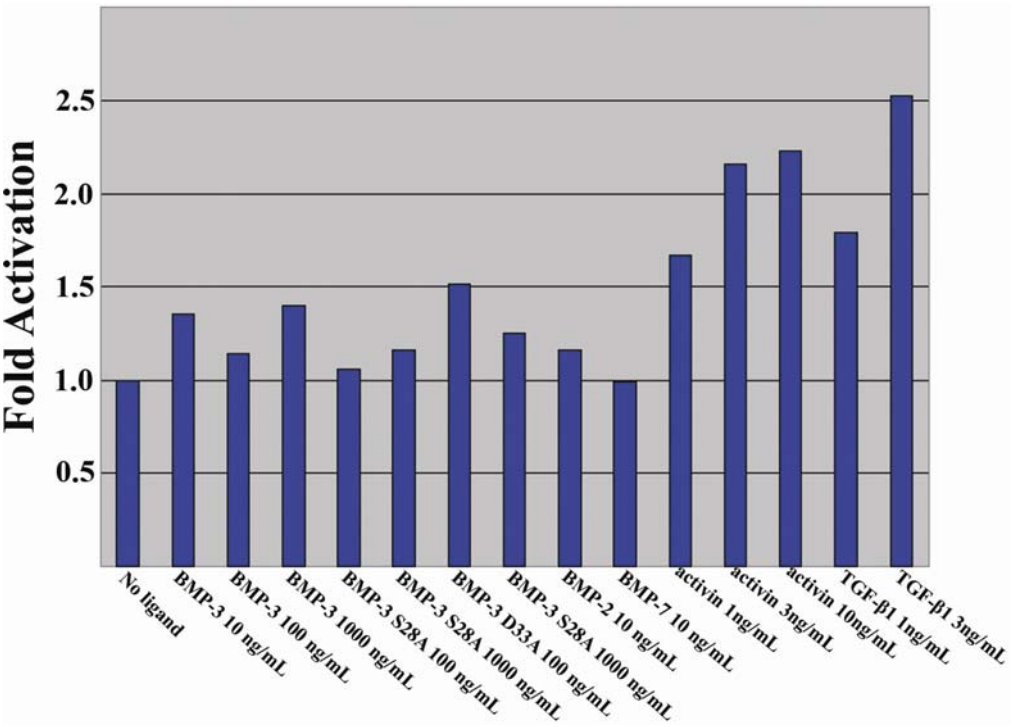

Figure 4-24. Smad-2 luciferase assay. The fold activation of the Smad-2 reporter in the presence of different ligands. The baseline with 'No ligand' was normalized to 1.

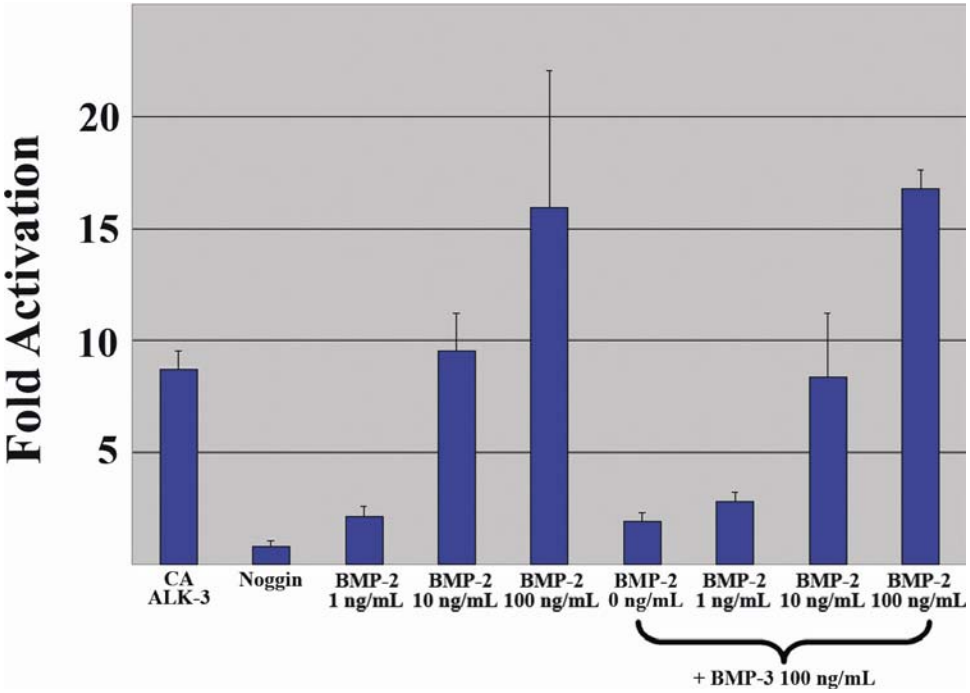

Figure 4-25. BMP-3 competition assay. BMP-2 response was tested in the absence and presence of BMP-3 and the fold-activation compared. The signaling response was normalized in absence of ligand and given a value of 1.

4.2.9. BMP-3 type I receptor Binding Analysis

Similar to BMP-6, the predicted type I interface of BMP-3 with BMPRIa was analyzed to identify residues involved in determining binding affinity. BMP-3_{wt} binds to BMPRIa-ECD with K_D ~300 nM affinity. This affinity is ~100-fold weaker than the high affinity binding of BMP-2 and ~5-fold weaker than the low affinity binding with BMP-6. In an effort to increase BMP-3 affinity for BMPRIa, the sequences of BMP-2 and BMP-3 were aligned and their sequences compared (Figure 4-26). Since residues in the H3 pre-helix loop have been shown to be important for type I receptor binding (*15*), this region was focused on for differences between the ligands.

However, this region has little conservation between BMP-2 and BMP-3 (Figure 4-26). Since there are numerous residue differences, the same region chosen for the BMP-2 and BMP-6 type I mutants was also chosen BMP-3 (Figure 4-26, yellow). To make BMP-3 mimic BMP-2, the P46A and K47D mutations were inserted individually and together into BMP-3.

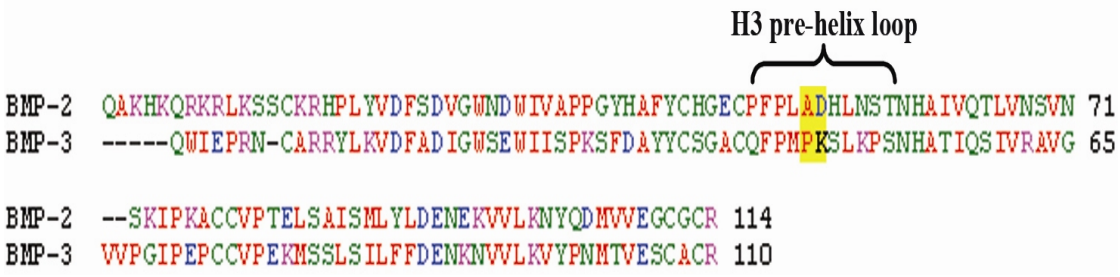

Figure 4-26. Sequence alignment of BMP-2 and BMP-3. The H3 pre-helix loop is identified and the mutated residues are labeled in yellow.

To test if these mutations had any impact on type I receptor affinity, BIAcore was again employed. BMPRIa-ECD was chosen as the type I receptor and immobilized onto the chip surface and the BMP-3 ligands were then flowed over the surface. BMP-3_{wt} showed an affinity of K_D = 398 nM to BMPRIa-ECD, which is comparable to the affinity seen in the previous BIAcore studies (Table 4-7). When the single mutants were flowed over the surface, the affinity for BMPRIa-ECD dropped significantly. The BMP-3_{P46A} affinity fell ~7-fold, while the BMP-3_{K47D} affinity was almost 20-fold lower (Table 4-7). Interestingly, the double mutant, BMP-$3_{P46A/K47D}$, showed comparable affinity to BMPRIa-ECD as did BMP-3_{wt} with K_D = 498 nM (Table 4-7). The restored type I affinity for the double mutant suggests the residues

are coupled during type I receptor binding, but are not responsible for the high affinity binding seen in BMP-2.

Table 4-7. BIAcore affinity comparison of BMP-3 type I mutants. The data is shown as the dissociation rate, k_{off}, and the association rate, k_{on}, derived from a global fit using the kinetic model 1:1 Langmuir binding with mass transfer.

Ligand	BMPRIa		
	k_{off}[1/s]	**k_{on}[1/M*s]**	**K_D [nM]**
BMP-3	$4.6x10^{-2}$	$1.16x10^{6}$	288
$BMP\text{-}3_{P46A}$	$6.7x10^{-2}$	$2.4x10^{5}$	280
$BMP\text{-}3_{K47D}$	$5.6x10^{-2}$	$2.1x10^{5}$	267
$BMP\text{-}3_{P46A/K47D}$	$3.5x10^{-2}$	$7.11x10^{4}$	498

Even though the BMP-3 mutants did not display an increase in affinity for BMPRIa-ECD, they were still tested for signaling activity in a Smad-1 luciferase assay. Similar to the type II signaling assay, $BMP\text{-}3_{wt}$ did not show any activity up to 1000 ng/mL (Figure 4-27). However, all three mutants showed a dose dependent signaling response (Figure 4-27). While the activity is only 5-10% of the signaling activity of BMP-2 at the same ligand concentration, the results suggest that the BMP-3 mutants can bind type I receptors, but not necessarily BMPRIa. To see if the BMP-3 mutants could bind other type I receptors, the ECDs of Alk-2 and Alk-6 (BMPRIb) were immobilized to a chip surface and the ligands' affinities tested. While no binding response was seen for any of the mutants for either receptor, the activity of the receptors could not be confirmed.

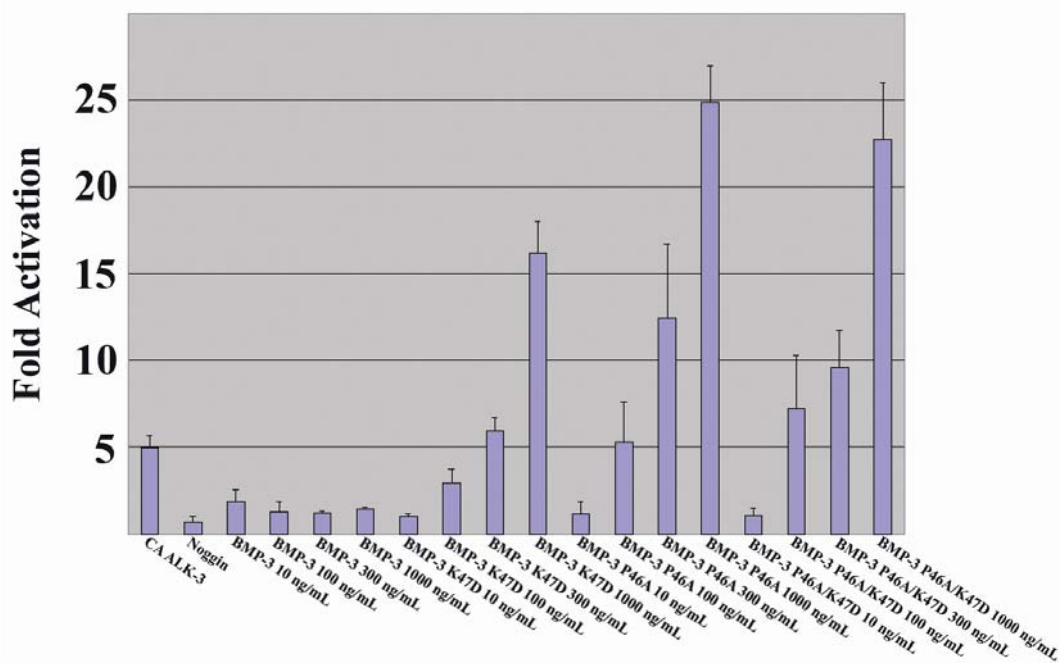

Figure 4-27. BMP-3 type I mutant signaling assay. Signaling response of the various ligands was measured as fold-luciferase response. The assay was normalized to the signaling in absence of ligand and given a response of 1.

4.3. Conclusions

The ability of BMP-3 mutants to signal through the SMAD 1/5/8 pathway as well as function a BMP antagonist is unclear. BMP-3 was shown to complex with ActRIIb and ALK-4 (*6*), which is similar to the activin signaling complex known to signal through the Smad-2/3 pathway (*26*). It has been suggested BMP-3, by signaling through the Smad-2/3 pathway, could antagonize BMP-2 function intracellulary (*27*). However, BMP-3 failed to show any response in the Smad-2 assays and by increasing the affinity to ActRII, the BMP-3_{S28A} mutant was able to signal at a level comparable to BMP-6 in the Smad-1 assays. It is possible the

antagonistic effects previously reported for BMP-3 are a result of BMP-3 forming weaker signaling complexes with the tested receptors. A BMP-3 complex formation would sequester type II receptor, ActRIIb primarily, and prevent this type II receptor from binding to other BMPs. The weaker signaling from the BMP-3:ActRIIb complex would result in a decrease in overall BMP signaling levels throughout the organism.

Another potential key may be the prodomain of BMP-3. It has been shown BMP prodomains can regulate signaling activity, stability, and signaling range of the mature domains (*28, 29*). Much of the functional work with BMP-3 has been performed using conditioned medium containing BMP-3. This medium may contain the prodomain, as well as the mature domain of BMP-3, which could alter BMP-3's function if the two domains interact. In the case of BMP-9, crystallized from conditioned medium, the prodomain was shown to be present and form a tight non-covalent complex with the mature BMP-9 dimer (*30*). The prodomains of numerous other BMP ligands have also been shown to non-covalently bind the mature ligand, as well as other proteins in the extracellular matrix (*31, 32*).

A third possible mode of regulation for BMP-3 could be the presence of unknown co-receptors on the cell surface. Cripto and Betaglycan are known TGF–β ligand co-receptors important for modulating receptor binding and signaling (*33*). The binding of BMP-3 to either one of these molecules, or a similar molecule, might effect downstream signaling. Finally, we cannot exclude the possibility that the binding of BMP-3 to different type II receptors (ActRII vs. ActRIIb) may affect type I receptor

recruitment. These differences in final complex formation may result in changes to downstream signaling.

The same principle of increased receptor affinity leading to increased BMP-3 signaling for the type II mutations also applies to the type I mutants. The type I mutations inserted into BMP-3 did not increase affinity to BMPRIa-ECD but did show increased signaling activity. Although the receptor responsible for this signaling remains unknown for our assays, the signaling response is directly correlated to type I receptor binding. Further work to identify the type I receptor combined with known type II receptor information will allow for tailored BMP-3 receptor binding and downstream signaling. These mutants will also help in pinpointing the true *in vivo* role of BMP-3 in the overall TGF-β signaling cascade.

4.4. References

1. Takao, M., Hino, J., Takeshita, N., Konno, Y., Nishizawa, T., Matsuo, H., and Kangawa, K. (1996) Identification of Rat Bone Morphogenetic Protein-3b (BMP-3b), a New Member of BMP-3, *Biochemical and Biophysical Research Communications 219*, 656-662.

2. Wozney, J. M., Rosen, V., Celeste, A. J., Mitsock, L. M., Whitters, M. J., Kriz, R. W., Hewick, R. M., and Wang, E. A. (1988) Novel regulators of bone formation: molecular clones and activities, *Science 242*, 1528-1534.

3. Bahamonde, M. E., and Lyons, K. M. (2001) BMP3: To Be or Not To Be a BMP, *J. Bone Joint Surg. Am. 83*, S56-62.

4. Hino, J., Nishimatsu, S.-i., Nagai, T., Matsuo, H., Kangawa, K., and Nohno, T. (2003) Coordination of BMP-3b and cerberus is required for head formation of Xenopus embryos, *Developmental Biology 260*, 138-157.

5. Daluiski, A., Engstrand, T., Bahamonde, M. E., Gamer, L. W., Agius, E., Stevenson, S. L., Cox, K., Rosen, V., and Lyons, K. M. (2001) Bone morphogenetic protein-3 is a negative regulator of bone density, *Nat. Genet. 27*, 84-88.

6. Gamer, L. W., Nove, J., Levin, M., and Rosen, V. (2005) BMP-3 is a novel inhibitor of both activin and BMP-4 signaling in Xenopus embryos, *Developmental Biology 285*, 156-168.

7. Yamashita, H., Ten Dijke, P., Heldin, C. H., and Miyazono, K. (1996) Bone morphogenetic protein receptors, *Bone 19*, 569-574.

8. Kugimiya, F., Kawaguchi, H., Kamekura, S., Chikuda, H., Ohba, S., Yano, F., Ogata, N., Katagiri, T., Harada, Y., Azuma, Y., Nakamura, K., and Chung, U.-i. (2005) Involvement of Endogenous Bone Morphogenetic Protein (BMP) 2 and BMP6 in Bone Formation, *J. Biol. Chem. 280*, 35704-35712.

9. Haudenschild, D. R., Palmer, S. M., Moseley, T. A., You, Z., and Reddi, A. H. (2004) Bone Morphogenetic Protein (BMP)-6 Signaling and BMP Antagonist Noggin in Prostate Cancer, *Cancer Res. 64*, 8276-8284.

10. Ebisawa, T., Tada, K., Kitajima, I., Tojo, K., Sampath, T. K., Kawabata, M., Miyazono, K., and Imamura, T. (1999) Characterization of bone morphogenetic protein-6 signaling pathways in osteoblast differentiation, *J. Cell. Sci. 112*, 3519-3527.

11. Greenwald, J., Groppe, J., Gray, P., Wiater, E., Kwiatkowski, W., Vale, W., and Choe, S. (2003) The BMP7/ActRII Extracellular Domain Complex Provides New Insights into the Cooperative Nature of Receptor Assembly, *Molecular Cell 11*, 605-617.

12. Kirsch, T., Sebald, W., and Dreyer, M. K. (2000) Crystal structure of the BMP-2-BRIA ectodomain complex, *Nat. Struct. Mol. Biol. 7*, 492-496.

13. Matthews, B. W. (1968) Solvent content of protein crystals, *J. Mol. Bio. 33*, 491-497.

14. Allendorph, G. P., Vale, W. W., and Choe, S. (2006) Structure of the ternary signaling complex of a TGF-beta superfamily member, *Proc. Natl. Acad. Sci. 103*, 7643-7648.

15. Keller, S., Nickel, J., Zhang, J.-L., Sebald, W., and Mueller, T. D. (2004) Molecular recognition of BMP-2 and BMP receptor IA, *Nat. Struct. Mol. Biol. 11*, 481-488.

16. Nickel, J., Kotzsch, A., Sebald, W., and Mueller, T. D. (2005) A Single Residue of GDF-5 Defines Binding Specificity to BMP Receptor IB, *J. Mol. Bio. 349*, 933-947.

17. Greenwald, J., Vega, M. E., Allendorph, G. P., Fischer, W. H., Vale, W., and Choe, S. (2004) A Flexible Activin Explains the Membrane-Dependent Cooperative Assembly of TGF-[beta] Family Receptors, *Molecular Cell 15*, 485-489.

18. Thompson, T. B., Lerch, T. F., Cook, R. W., Woodruff, T. K., and Jardetzky, T. S. (2005) The Structure of the Follistatin:Activin Complex Reveals Antagonism of Both Type I and Type II Receptor Binding, *Developmental Cell 9*, 535-543.

19. Hart, P. J., Deep, S., Taylor, A. B., Shu, Z., Hinck, C. S., and Hinck, A. P. (2002) Crystal structure of the human TβR2 ectodomain-TGF-β3 complex, *Nat. Struct. Mol. Biol. 9*, 203-208.

20. Macias-Silva, M., Hoodless, P. A., Tang, S. J., Buchwald, M., and Wrana, J. L. (1998) Specific Activation of Smad1 Signaling Pathways by the BMP7 Type I Receptor, ALK2, *J. Biol. Chem. 273*, 25628-25636.

21. Gray, P. C., Greenwald, J., Blount, A. L., Kunitake, K. S., Donaldson, C. J., Choe, S., and Vale, W. (2000) Identification of a Binding Site on the Type II Activin Receptor for Activin and Inhibin, *J. Biol. Chem 275*, 3206-3212.

22. Namiki, M., Akiyama, S., Katagiri, T., Suzuki, A., Ueno, N., Yamaji, N., Rosen, V., Wozney, J. M., and Suda, T. (1997) A Kinase Domain-truncated Type I Receptor Blocks Bone Morphogenetic Protein-2-induced Signal Transduction in C2C12 Myoblasts, *J. Biol. Chem. 272*, 22046-22052.

23. Lopez-Rovira, T., Chalaux, E., Massagué, J., Rosa, J. L., and Ventura, F. (2002) Direct Binding of Smad1 and Smad4 to Two Distinct Motifs Mediates Bone Morphogenetic Protein-specific Transcriptional Activation of Id1 Gene, *J. Biol. Chem. 277*, 3176-3185.

24. Nakashima, K., Takizawa, T., Ochiai, W., Yanagisawa, M., Hisatsune, T., Nakafuku, M., Miyazono, K., Kishimoto, T., Kageyama, R., and Taga, T. (2001) BMP2-mediated alteration in the developmental pathway of fetal mouse brain cells from neurogenesis to astrocytogenesis, *Proc. Natl. Acad. Sci. 98*, 5868-5873.

25. Suzuki, A., Raya, A., Kawakami, Y., Morita, M., Matsui, T., Nakashima, K., Gage, F. H., Rodriguez-Esteban, C., and Izpisua Belmonte, J. C. (2006) Nanog binds to Smad1 and blocks bone morphogenetic protein-induced differentiation of embryonic stem cells, *Proc. Natl. Acad. Sci. 103*, 10294-10299.

26. Feng, X.-H., and Derynck, R. (2005) Specificity and Versatility in TGF-beta signaling through Smads *Annual Review of Cell and Developmental Biology 21*, 659-693.

27. Daluiski, A., Engstrand, T., Bahamonde, M. E., Gamer, L. W., Agius, E., Stevenson, S. L., Cox, K., Rosen, V., and Lyons, K. M. (2001) Bone morphogenetic protein-3 is a negative regulator of bone density, *Nat Genet 27*, 84-88.

28. Constam, D. B., and Robertson, E. J. (1999) Regulation of Bone Morphogenetic Protein Activity by Pro Domains and Proprotein Convertases, *J.Biol. Chem. 144*, 139-149.

29. Le Good, J. A., Joubin, K., Giraldez, A. J., Ben-Haim, N., Beck, S., Chen, Y., Schier, A. F., and Constam, D. B. (2005) Nodal Stability Determines Signaling Range, *Current Biology 15*, 31-36.

30. Brown, M. A., Zhao, Q., Baker, K. A., Naik, C., Chen, C., Pukac, L., Singh, M., Tsareva, T., Parice, Y., Mahoney, A., Roschke, V., Sanyal, I., and Choe, S. (2005) Crystal Structure of BMP-9 and Functional Interactions with Pro-region and Receptors, *J. Biol. Chem 280*, 25111-25118.

31. Sopory, S., Nelsen, S. M., Degnin, C., Wong, C., and Christian, J. L. (2006) Regulation of Bone Morphogenetic Protein-4 Activity by Sequence Elements within the Prodomain, *J. Biol. Chem 281*, 34021-34031.

32. Jasuja, R., Ge, G., Voss, N. G., Lyman-Gingerich, J., Branam, A. M., Pelegri, F. J., and Greenspan, D. S. (2007) Bone Morphogenetic Protein 1 Prodomain Specifically Binds and Regulates Signaling by Bone Morphogenetic Proteins 2 and 4, *J. Biol. Chem 282*, 9053-9062.

33. Harrison, C. A., Wiater, E., Gray, P. C., Greenwald, J., Choe, S., and Vale, W. (2004) Modulation of activin and BMP signaling, *Molecular and Cellular Endocrinology 225*, 19-24.

Chapter 5. Discussion

5.1. Discussion

Members of the TGF-β superfamily are found throughout many cell and tissues types in the human body. Due to their ubiquitous nature, a great interest has been shown in using regulation of the TGF-β signaling pathway as a therapeutic device. Currently, a diverse range of clinical applications are being considered or tested from fracture repair (*1, 2*) and asthma treatments (*3*) to stem cell regulation (*4*) and cancer therapy (*5*). A basic step toward effectively utilizing TGF-β molecules as medicinal tools is fully understanding the interactions between ligands and their receptors. The studies reported in this manuscript will help advance the overall knowledge surrounding TGF-β ligand-receptor complex formation and how receptor binding and affinity are regulated.

Preceding research yielded x-ray crystal structures of TGF-β ligands bound to only one receptor type (*6-8*). In order to determine if the homology models based off these structures are accurate, a complete, 6-member signaling complex was required. Therefore, the x-ray crystal structure of BMP-2/BMPRIa-ECD/ActRII-ECD was solved to high resolution. The ternary structure reveals the spatial arrangement of the receptors in the complex generates no contacts between any of the receptors. The formation of a signaling complex without receptor-receptor contacts confirms the receptor binding predicted by the BMP-7/BMPRIa-ECD/ActRII-ECD homology model (*6*). Recently, a second ternary structure of BMP-2/BMPRIa-ECD/ActRIIb-ECD was solved and shows an identical receptor arrangement to the BMP-2/BMPRIa-ECD/ActRII-ECD structure (*9*). The existence of a second BMP ternary structure

firmly solidifies the receptor binding pattern throughout the BMP family. Interestingly, this binding pattern may not be conserved throughout the entire TGF-β superfamily. A ternary homology model for TGF-βIII/BMPRIa-ECD/ TGF-βRII-ECD predicted a receptor arrangement in which the different receptor types contacted each other (*7*). Very recently, the x-ray crystal structure of TGF-βIII/TGF-βRI/TGF-βRII was solved and, while showing contacts between the receptor types, the position of the receptors was different than homology model predicted (personal communication). This third ternary structure confirms at least two different receptor binding models in the TGF-β superfamily. This makes solving additional ligand-receptor structures, activin/ActRIb-ECD/ActRIIb-ECD e.g., even more important. The x-ray structures solved so far suggest while the conserved architecture of the superfamily creates a general pattern of complex formation, each TGF-β subfamily has subtle differences in their receptor binding arrangements. These differences may play crucial roles in regulating proper signaling *in vivo* and understanding them is critical for designing therapeutic molecules based on the TGF-β superfamily signaling pathway.

Not only did the ternary structure of BMP-2/BMPRIa-ECD/ActRII-ECD clarify the exact binding arrangement of the receptors, but yielded insight into a new TGF-β ligand-receptor interface. All the previous TGF-β ligand-receptor complexes were of a ligand bound to its high affinity receptor (*6-8, 10*) The BMP-2:ActRII-ECD interface is the first lower affinity receptor interface. BMP-2 binds ActRII ~50-fold weaker than BMP-7 and ~500-fold weaker than activin. Comparison of this lower

affinity receptor interface with the high affinity receptor interfaces of BMP-7/ActRII-ECD and activin/ActRIIb-ECD should reveal the structural basis for the varying affinities reported. Unexpectedly, all three interfaces share a high degree of similarity. There is an identical hydrophobic core region in all three interfaces, surrounded by additional, highly conserved residues. The presence of this core region, while not directly involved in determining receptor affinity, is required for receptor binding (*11*). With minimal differences between the interfaces, the residues responsible for receptor affinity should be easily identifiable. However, most of the mutations inserted into BMP-2 to make its interface more similar to BMP-7 or activin had little effect on receptor affinity. The largest increase in receptor affinity, ~10-fold, came from the L100K mutation based off of activin. This mutant was predicted to add an additional hydrogen bond to the BMP-2:ActRII-ECD interface. However, this 10-fold increase does not approach the 50 to 500-fold higher affinity exhibited by BMP-7 or activin.

A similar phenomenon is seen when trying to alter the BMP-2 type I interface. BMP-2 binds BMPRIa with ~500-fold higher affinity than BMP-7. The largest difference between BMP-2 and BMP-7 in the type I interface is a three residue segment in the H3 pre-helix loop. However, the insertion of this segment into BMP-2 only decreases BMP-2's affinity to BMPRIa by ~30-fold, instead of the recorded 500-fold difference. One explanation for this failure to significantly alter BMP-2 receptor affinity with small residue changes is that the interface residues are coupled. The coupling of residues at ligand-receptor binding interfaces has been shown to be a trend in many protein families (*12*). If this method is how BMP receptor affinity is

regulated, then mutating one residue of the pair would not be sufficient to generate the complete contacts necessary for significantly altering binding. The existence of more BMP/TGF-β ligand structures with in depth mutagenesis is necessary to further explore how ligand-receptor affinity is determinedt.

The x-ray crystal structure of the ternary complex and the subsequent mutagenesis and biochemical studies on ligand-receptor affinity did not determine the source of the known cooperative binding between receptor types. It is known that once the high affinity receptors are bound, the ligand's affinity for their lower affinity receptors is greatly increased (*6, 13*). The structural basis for this effect was tested by comparing the affinities of activin and Inhibin, a natural homodimer/heterodimer system. In a simulated membrane system (BIAcore chip surface), when activin was flowed over ActRIIb-ECD surfaces with varying receptor densities, the observed affinity increased 10-fold from the low to high density surface. This affinity increase was confirmed as being imparted by activin's bidentate receptor binding since Inhibin, which can only bind receptors in a monodentate fashion, did not show a similar trend in binding affinities. When activin binds to one high affinity receptor, this event increases the local concentration of the ligand as well as reducing the ligand's rotational freedom. The binding of the second high affinity receptor does not have constrain the ligand to the surface nor overcome entropy of the flexible ligand, making it easier to bind. The reduced barriers to binding leads to the observed increase in affinity. The same trend would hold true for the binding of the lower affinity receptors. The high affinity receptors lock the TGF-β ligand to the cell membrane in a

fixed, signaling ready conformation reducing the energy of binding for the lower affinity receptors. This ease in binding would be reflected as an increase in observed binding affinity.

To address lack of BMP/TGF-β ligand data, the x-ray crystal structures of unbound BMP-3 and BMP-6 were solved to high resolution. While the inability to crystallize these ligands bound to receptors bound is unfortunate, their absence does not render the ligand structures useless. With the highly conserved architecture of the TGF-β family, ternary homology models of BMP-3 and BMP-6 were created based on the already solved BMP-2/BMPRIa-ECD/ActRII-ECD structure. When superimposed, both the BMP-3 and BMP-6 ligand aligned very well with BMP-2. The good overlay created well fit interfaces between the ligands and receptors of the models. Both of the predicted type II interfaces of ActRII-ECD with BMP-3 or BMP-6 share the previously mentioned hydrophobic core motif. However, when type II receptor affinities were measured, BMP-3 showed some unexpected properties. BMP-3 displayed a unique 30-fold specificity preference of ActRIIb over ActRII. Further, the affinities for both these receptors was low, especially for ActRII. This was interesting considering ActRIIb was suggested to be a high affinity receptor for BMP-3 (*14*). Looking specifically at the BMP-3:ActRII interface, two residues were identified as the possible reason for this low affinity. When these residues, Ser-28 and Asp-33, were mutated to alanine the affinity increased greatly for both ActRII and ActRIIb. However, the specificity preference of BMP-3 for ActRIIb was unchanged. The focus was then shifted to the receptors to locate the specificity determinant. A single residue

difference between the receptors, Lys-76 of ActRII and Glu-76 of ActRIIb, was found. These residues interact with Lys-30 of BMP-3 and generate an unfavorable or favorable interaction, respectively. When the lysine was inserted into ActRIIb, the observed specificity difference between the receptors was eliminated. These results suggest that while receptor affinity may not be determined by a single residue, the specificity preference a ligand can be modulated by only a single residue. If a similar trend can be found in other TGF-β ligands, it may be possible to engineer ligands which will only interact with a chosen receptor. A ligand which can only activate a specific signaling pathway would be useful as a drug candidate.

5.2. Continuing Research and Future Directions

With only a half dozen different TGF-β ligand x-ray crystal structures and over 40 TGF-β superfamily members, there is a continued push for additional ligand and ligand-receptor complexes. The immediate aim is to discover if the other TGF-β ligand subfamilies have their own distinct mode of receptor complex assembly. This goal has been hampered by the inability to obtain large enough quantities of ligands for crystallization. The ligands are heavily disulfide bonded, making their expression in *E. coli* as soluble proteins difficult. Some ligands have been able to be refolded from inclusion bodies following a published protocol (*15*), but this method's success has been limited. TGF-β ligands have been expressed in mammalian expression systems, CHO cells e.g., but the yield from these cells is extremely low (*16*).

Hopefully, the implementation of emerging protein expression methods, cell free expression systems is one possibility, will help overcome this barrier.

Shifting away from a purely structural analysis of TGF-β signaling, a focus on the signaling properties of these ligands is equally important. While mostly homodimers, TGF-β heterodimers have been shown to exist in nature. Further, these heterodimers have been shown to be critical for signaling in axonal nerve development (*17*) or dorsal patterning (*18*). The exact reason for heterodimers playing the key role in signaling is unclear. However, it may have to do with the unique signaling characteristics of the heterodimers compared to the homodimers. Heterodimers, BMP-2/BMP-7 e.g., have been shown to have greater activity than either homodimer alone (*19*). Preliminary studies in our lab have indicated that the heterodimers are at least 10-fold more active than their respective homodimers.

The reason for this increased activity is not overtly clear. One possibility is the multiple high affinity binding sites. A typical TGF-β homodimer has lower and high affinity receptor types. With a heterodimer, the ligand could have high affinity receptor binding sites for both receptor types. This multiple high affinity binding could lead to the observed hyper-activity. To address this question, the redundant nature of the TGF-β signaling pathway must first be determined. The TGF-β ligands exist as dimers and they bind two each of two different receptor sets. But are all four receptors necessary for proper signaling? While a previous study suggests all receptors must be bound to insure correct signaling (*20*), a more detailed analysis is needed to confirm these findings. By introducing mutations into TGF-β ligand

monomers to knockout type I and type II receptor binding sites, these monomers can be combined into various different heterodimers. Each heterodimer will have a unique receptor stoichiometry and the position of the receptors in the complex will be known relative to each other. By comparing the signaling activity of these ligands, the basic receptor requirements for signaling can be determined.

The most interesting finding will revolve around the Trans or Cis phosphorylation of the type I receptors. Trans phopsphorylation is defined as phosporylation across the ligand dimer, while Cis phopsphorylation is defined as on the same ligand monomer. In a complete 6-member complex, it is difficult to determine which type II receptor phosphorylates which type I receptor. The ability to control the number and position of the receptors will eliminate this problem. These signaling experiments will allow for discovering the direction of phosphorylation. By incorporating BIAcore affinity data with the signaling information from the heterodimers, it will be possible to ascertain how heterodimers achieve their signaling properties. By combining the structural knowledge for determining receptor affinity with the ability to tailor recombinant TGF-β ligands to activate specific signaling pathways, the use of TGF-β ligands as therapeutic agents will broaden into new and exciting areas.

5.3. References

1. Biase, and Capanna. (2005) Clinical applications of BMPs, *Injury 36*, S43-S46.

2. Wozney, J. M., and Seeherman, H. J. (2004) Protein-based tissue engineering in bone and cartilage repair, *Current Opinion in Biotechnology 15*, 392-398.

3. Howell, J. E., and McAnulty, R. J. (2006) TGF-β: Its Role in Asthma and Therapeutic Potential, *Current Drug Targets 7*, 547-565.

4. Koay, E. J., Hoben, G. M. B., and Athanasiou, K. A. (2007) Tissue Engineering with Chondrogenically-differentiated Human Embryonic Stem Cells, *Stem Cells.*, 2007-0105.

5. Mishra, L., Shetty, K., Tang, Y., Stuart, A., and Byers, S. W. (2005) The role of TGF-β and Wnt signaling in gastrointestinal stem cells and cancer, *Oncogene 24*, 5775-5789.

6. Greenwald, J., Groppe, J., Gray, P., Wiater, E., Kwiatkowski, W., Vale, W., and Choe, S. (2003) The BMP7/ActRII Extracellular Domain Complex Provides New Insights into the Cooperative Nature of Receptor Assembly, *Molecular Cell 11*, 605-617.

7. Hart, P. J., Deep, S., Taylor, A. B., Shu, Z., Hinck, C. S., and Hinck, A. P. (2002) Crystal structure of the human TβR2 ectodomain-TGF-β3 complex, *Nat. Struct. Mol. Biol. 9*, 203-208.

8. Kirsch, T., Sebald, W., and Dreyer, M. K. (2000) Crystal structure of the BMP-2-BRIA ectodomain complex, *Nat. Struct. Mol. Biol. 7*, 492-496.

9. Weber, D., Kotzsch, A., Nickel, J., Harth, S., Seher, A., Mueller, U., Sebald, W., and Mueller, T. D. (2007) A silent H-bond can be mutationally activated for high-affinity interaction of BMP-2 and activin type IIB receptor, *BMC Structural Biology 7*, 6.

10. Thompson, T. B., Woodruff, T. K., and Jardetzky, T. S. (2003) Structures of an ActRIIB:activin A complex reveal a novel binding mode for TGF-β ligand:receptor interactions, *EMBO J. Apr 1*, 1555-1566.

11. Gray, P. C., Greenwald, J., Blount, A. L., Kunitake, K. S., Donaldson, C. J., Choe, S., and Vale, W. (2000) Identification of a Binding Site on the Type II Activin Receptor for Activin and Inhibin, *J. Biol. Chem 275*, 3206-3212.

12. Halperin, I., Wolfson, H., and Nussinov, R. (2004) Protein-Protein Interactions: Coupling of Structurally Conserved Residues and of Hot Spots across Interfaces. Implications for Docking, *Structure 12*, 1027-1038.

13. Rodriguez, C., Chen, F., Weinberg, R. A., and Lodish, H. F. (1995) Cooperative Binding of Transforming Growth Factor (TGF)-β2 to the Types I and II TGF-β Receptors, *J. Biol. Chem. 270*, 15919-15922.

14. Daluiski, A., Engstrand, T., Bahamonde, M. E., Gamer, L. W., Agius, E., Stevenson, S. L., Cox, K., Rosen, V., and Lyons, K. M. (2001) Bone morphogenetic protein-3 is a negative regulator of bone density, *Nat. Genet. 27*, 84-88.

15. Groppe, J., Rumpel, K., Economides, A. N., Stahl, N., Sebald, W., and Affolter, M. (1998) Biochemical and Biophysical Characterization of Refolded Drosophila DPP, a Homolog of Bone Morphogenetic Proteins 2 and 4, *J. Biol. Chem. 273*, 29052-29065.

16. Israel DI, Nove J, Kerns KM, Moutsatsos IK, and RJ., K. (1992) Expression and characterization of bone morphogenetic protein-2 in Chinese hamster ovary cells., *Growth Factors 7(2)*, 139-150.

17. Butler, S. J., and Dodd, J. (2003) A Role for BMP Heterodimers in Roof Plate-Mediated Repulsion of Commissural Axons, *Neuron 38*, 389-401.

18. Shimmi, O., Umulis, D., Othmer, H., and O'Connor, M. B. (2005) Facilitated Transport of a Dpp/Scw Heterodimer by Sog/Tsg Leads to Robust Patterning of the Drosophila Blastoderm Embryo, *Cell 120*, 873-886.

19. Israel DI, Nove J, Kerns KM, Kaufman RJ, Rosen V, Cox KA, and JM., W. (1996) Heterodimeric bone morphogenetic proteins show enhanced activity in vitro and in vivo., *Growth Factors 13*, 291-300.

20. Knaus, P., and Walter, S. (2001) Cooperativity of Binding Epitopes and Receptor Chains in the BMP/TGFß Superfamily, *Biological Chemistry 382*, 1189-1195.

Chapter 6. Materials and Methods

6.1. Protein Expression and Purification

The extracellular domain (ECD) of human BMPR-Ia, residues 1-129, and mouse ActRIIb, residues 1-98, were expressed in *E. coli* as a thioredoxin fusion proteins and purified using a modification of previously published strategies (*1*). The ECD of mouse ActRII, residues 1-102, was expressed and purified using a *P. pastoris* expression system as previously described (*2*). The mature, wild type domains of human BMP-2, (residues 1-114), human BMP-3 (residues 1-110), and human BMP-6 (residues 1-132) were expressed in *E. coli* as inclusion bodies. All three ligands were purified and refolded from inclusion bodies using a modified protocol (*3*). In brief, the purified inclusion body pellet was allowed to completely denature in a solution of 6 M Guanidinium HCl, 50 mM Tris, pH 7.9, and 2 mM DTT for two hours at room temperature. The denatured ligands were then rapidly diluted into a pre-chilled refolding buffer of 50 mM Tris, pH 7.9, 1.25 M NaCl, 1.8% (w/v) 3-[(3-Cholamidopropyl)dimethylammonio]-1-propanesulfonate (CHAPS), 1 mM oxidized, and 2 mM reduced glutathione at a final concentration ranging from 25 to 100 mg/L. The proteins were allowed to refold for a minimum of 72 hours at 15° C.

To purify the refolded ligands, the refolding buffer was concentrated and buffer exchanged into 6 M urea, 50 mM Tris-HCl, pH 7.9, 100 mM NaCl using an Ultracette tangential flow concentrator (Pall). The samples were then loaded onto a HiTrap Heparin column (GE Healthcare) and eluted with a linear gradient of 0.1-1.0 M NaCl. The fraction corresponding to the dimer was then loaded onto a C4 reverse phase column (Vydac) and eluted with a linear gradient of 20-40% Acteonitrile.

Human activin and inhibin were purified from the medium of stably transfected CHO cells. For the generation of all BMP-2, BMP-3, and BMP-6 mutants, site directed mutagenesis, generated by Quik Change (Invitrogen), was used. The BMP ligand mutants were expressed and purified the same manner as the wild type ligands. The samples were lyophilized following purification on the reverse phase columns and, prior to use in all experiments, resuspended in 10 mM Na acetate, pH 4.

6.2. Protein Crystallization

To form the BMP-2/BMPRIa-ECD/ActRII-ECD complex, BMP-2 was first diluted 1:1 into a 4x high salt, Tris/CHAPS buffer (4x HSTC: 200 mM Tris, pH 7.9, 2.8 M NaCl, and 7.2% CHAPS). The binary complex of BMP-2 and BMPR-Ia-ECD was formed using a 1:2 molar ratio in a final buffer of 1x HSTC. This complex was purified over a Superdex-75 (Pharmacia) column and then concentrated using a Vivaspin 6 concentrator with a 5 kD cutoff (Sartorius). The ternary complex was generated by adding 2.2 molar equivalents of ActRII-ECD to the purified binary complex. The final concentration for the ternary complex was adjusted to 10 mg/mL total protein. The complex was crystallized by the hanging drop vapor diffusion method in 4 M Na Formate, 0.1 M HEPES, pH 7.5, and 3% dioxane. After one week at 4° C, hexagonal crystals grew to an average size of 100 x 100 x 40 μm in the space group $P6_522$ with a=b= 104.8 Å, and c=363.3 Å.

A similar method was used to crystallize the BMP-3 and BMP-6 ligands. Both BMP-3 and BMP-6 were reconstituted in 10 mM Na acetate, pH 4.0 at a concentration of 10 mg/mL prior to crystallization. BMP-3 was crystallized using the hanging drop

vapor diffusion method in 26% tert-butanol and 0.1 M sodium citrate, pH 5.6. The hexagonal crystals grew to an average size of 200 x 200 x 50 μm in three days at ambient temperature in space group H3 with a=b= 96.8 Å and c = 101.5 Å. BMP-6 was also crystallized using the hanging drop technique in 15% MPD (2-methyl-2,4-pentanediol), 0.2 M tri-sodium citrate, and 0.1 M HEPES, pH 7.5. These crystals were triangular in shape and grew to 200 x 100 x 50 μm after a week at ambient temperature in space group $P3_121$ with a=b= 97.4 Å and c=87.4 Å.

6.3. X-ray Data Collection

The BMP-2/BMPRIa-ECD/ActRII-ECD crystals were soaked in mother liquor with 15% xylitol (used as a cryoprotectant) for less than 5 minutes before being flash frozen in liquid nitrogen. Diffraction data were collected for two separate crystals. Data for crystal number one was collected at the Advanced Light Source (ALS) on beamline 5-2. Data for crystal number two were collected at Stanford Synchrotron Radiation Laboratory (SSRL) on beamline 9-2. The data from both crystals were scaled and integrated using HKL2000 (*4*). The BMP-3 crystals were soaked in mother liquor with 15% glycerol (used as a cryoprotectant) for <5 min before being flash frozen in liquid nitrogen. Diffraction data from a single crystal were collected at ALS beamline 8.3.1. The BMP-6 crystals were flash frozen in liquid nitrogen as above with no additional cryoprotectant added. Data from a single BMP-6 crystal were collected at SSRL on beamline 9-2. Both BMP-3 and BMP-6 data sets were integrated and scaled using HKL2000 (*4*).

6.4. Structure Solution and Data Refinement

To solve the initial phases for crystal one of the BMP-2/BMPRIa-ECD/ActRII-ECD structure, molecular replacement was performed using Phaser (*5*). The best solution was found by searching with two independent halves (one BMP-2 monomer with one BMPRIa receptor) of the previously solved BMP-2/BMPRIa-ECD structure (*6*). The asymmetric unit consists of two complete, independent ternary monomers related by a two-fold non-crystallographic symmetry (NCS). The model was refined using REFMAC5 (*5*) interspersed with rounds of manual building in O (*7*). The initial model was refined to 2.5 Å using data from crystal number one and then further extended to 2.15 Å using data from crystal number two. The final BMP-2/BMPRIa-ECD/ActRII-ECD structure yielded an R factor of 19.8%, with a free R factor of 24.0%. The overall geometry of the structure was good as determined by PROCHECK (*8*) with 87.4% of the residues in the most favorable regions and none in the disallowed regions.

Molecular replacement, using PHASER (*5*), was used to solve for the initial phases of the BMP-3 diffraction data. The best model was achieved by searching for two, independent monomers using a BMP-2 monomer as the search model for BMP-3. Similar to the BMP-2 ternary complex, two BMP-3 monomers are found in the asymmetric unit and they are related by a 2-fold NCS. The model was then refined using REFMAC5 (*5*) interspersed with rounds of manual building in COOT (*5*) and O (*7*). A single translation, liberation, and screw rotation (TLS) group was used for each monomer of BMP-3 during the refinement. BMP-3 was refined to a final resolution of 2.20 Å with an *R* factor of 22.8% and a free *R* factor of 25.7%. The overall geometry

of the structure was good with 89.1% of the residues in the most favored regions and none in the disallowed region, as evaluated by Ramachadran plot.

The initial phases for the BMP-6 diffraction data was also solved for by using molecular replacement, PHASER (*5*), with a BMP-7 monomer (*9*) as the search model for BMP-6. The best solution found was by searching for two BMP-6 monomers in the asymmetric unit and these monomers are related by a 2-fold NCS. As with the previous structures, the BMP-6 model was refined using REFMAC5 (*5*) interspersed with rounds of manual building in COOT (*5*) and O (*7*). A single translation, liberation, and screw rotation (TLS) group was used for each monomer of BMP-6 during the refinement. The final BMP-6 structure was refined to a resolution of 2.49 Å with an *R* factor of 23.3% and a free *R* factor of 27.6%. The BMP-6 structure showed good overall geometry as determined by PROCHECK (*8*), with 86.4% positioned in the most favored regions and none in the disallowed regions, as determined by Ramachandran plot.

6.5. Surface Plasmon Resonance (BIAcore) Affinity Studies

To test the affinity of BMP-2 and the BMP-2 mutants for the type I receptor BMPRIa and the type II receptor ActRII was monitored using a BIAcore 3000 and the data were analyzed using BIAevalution Software ver. 4.1 (GE Healthcare). Using primary amine coupling, ActRII-ECD was immobilized on a CM5 chip in flow cell 3. BMPRIa-ECD was immobilized to Flow cell 4 and Flow cell 1 was left blank as a negative control. At a flow rate of 5 µL/min, both receptors were immobilized for 5 minutes at 50 µg/mL in 10 mM sodium acetate, pH 4.0. The experiments were

performed at 40 μL/min in 20 mM Tris-HCl, pH 7.9, 200 mM NaCl, 0.36% CHAPS, and 0.005% P20. At least four concentrations, plus a zero concentration, were run per sample for kinetic analysis and the data were fit using a 1:1 Langmuir binding with no bulk refractive shift.

To test the affinity of wild type BMP-3, wild type BMP-6, and the BMP-3 and BMP-6 mutants for BMPRIa, ActRII, and ACTRIIb, a Biacore 3000 was also used (GE Healthcare) and the data were analyzed by using BIAevaluation software ver. 4.1 (GE Healthcare). Using primary amine coupling, receptor ECDs were immobilized on a CM5 chip. The receptors were immobilized independently on flow cells 2-4 for 10 minutes at a flow rate of 5 μL/min and a concentration of 20 μM in 10 mM sodium acetate, pH 4.0. Flow cell 1 was left blank with no immobilized protein as a negative control. The experiments were performed at a flow rate of 50 μL/min in 20 mM Tris-HCl pH 7.9, 250 mM NaCl, 0.36% CHAPS, and 0.005% P20. At least five concentrations, plus a zero concentration, were run per sample for kinetic analysis and the data were fit by using a global 1:1 Langmuir binding with mass transfer.

To monitor the co-operative receptor binding differences between activin and inhibin, the BIAcore 3000 and data evaluated as previously described. For these experiments, ActRIIb-ECD was immobilized on a CM5 chip surfaces at different densities via primary amine coupling. The immobilizations were performed in 10 mM Na acetate, pH 4.0 at a protein concentration of ~50 μg/mL. Flow cell 2 had a final response unit (RU) of 600, while flow cell 3 had a 20 RU response and flow cell 4 had a response of 100 RU. As with the BMP experiments, flow cell 1 was left blank to be used as a control surface. All measurements were done in duplicate at 10 μL/min in

20 mM Tris-HCl, pH 7.4, 500 mM NaCl, 0.36% CHAPS, and 0.005% P20. Kinetic data from at least four concentrations were globally fit to a 1:1 Langmuir binding model.

6.6. Luciferase reporter assays

Smad-1 dependent luciferase assays were performed as previously described (*10*). In brief, C2C12 myoblast cells are cultured in Dulbecco's minimum essential medium (DMEM) + 5% FBS supplemented with L-Glutamine and antibiotics. For the luciferase reporter assays, cells were trypsinized, washed twice with PBS, and plated into 48-well plates with DMEM + 0.1% FBS. Twenty four hours later, cells were transfected with –1147Id1-luciferase construct containing the Smad binding sites (Id1-Luc) (*10, 11*), a Smad1 expression construct, and a CAGGS-LacZ plasmid by using Fugene6 (Roche) according to the manufacturer's instruction. Luciferase activity was measured 24 hours after stimulation with ligands and the values were normalized for transfection efficiency by using beta-galactosidase activity. The activity of the luciferase reporter is expressed in fold-induction relative to control values that are obtained by using –927Id1-luciferase that lacks Smad binding domains (Id1-Luc mut).

6.7. References

1. Kirsch, T., Nickel, J., and Sebald, W. (2000) Isolation of recombinant BMP receptor IA ectodomain and its 2:1 complex with BMP-2, *FEBS Letters 468*, 215-219.

2. Greenwald, J., Le, V., Corrigan, A., Fischer, W., Komives, E., Vale, W., and Choe, S. (1998) Characterization of the Extracellular Ligand-Binding Domain of the Type II Activin Receptor, *Biochemistry 37*, 16711-16718.

3. Groppe, J., Rumpel, K., Economides, A. N., Stahl, N., Sebald, W., and Affolter, M. (1998) Biochemical and Biophysical Characterization of Refolded Drosophila DPP, a Homolog of Bone Morphogenetic Proteins 2 and 4, *J. Biol. Chem. 273*, 29052-29065.

4. Otwinowski, Z. a. M., W. . (1997) Processing of X-ray Diffraction Data Collected in Oscillation Mode, in *Methods in Enzymology* (C.W. Carter, J. a. R. M. S., Eds.,, Ed.), pp 307-326, Academic Press.

5. Collaborative, C. P., Number 4. (1994) The CCP4 suite: programs for protein crystallography, in *Acta Crystallographica Section D*, pp 760-763.

6. Kirsch, T., Sebald, W., and Dreyer, M. K. (2000) Crystal structure of the BMP-2-BRIA ectodomain complex, *Nat. Struct. Mol. Biol. 7*, 492-496.

7. Jones, T. A., Zou, J. Y., Cowan, S. W., and Kjeldgaard, M. (1991) Improved methods for building protein models in electron density maps and the location of errors in these models, in *Acta Crystallographica Section A*, pp 110-119.

8. Laskowski, R. A., MacArthur, M. W., Moss, D. S., and Thornton, J. M. (1993) PROCHECK: a program to check the stereochemical quality of protein structures, in *Journal of Applied Crystallography*, pp 283-291.

9. Greenwald, J., Groppe, J., Gray, P., Wiater, E., Kwiatkowski, W., Vale, W., and Choe, S. (2003) The BMP7/ActRII Extracellular Domain Complex Provides New Insights into the Cooperative Nature of Receptor Assembly, *Molecular Cell 11*, 605-617.

10. Nakashima, K., Takizawa, T., Ochiai, W., Yanagisawa, M., Hisatsune, T., Nakafuku, M., Miyazono, K., Kishimoto, T., Kageyama, R., and Taga, T. (2001) BMP2-mediated alteration in the developmental pathway of fetal mouse brain cells from neurogenesis to astrocytogenesis, *Proc. Natl. Acad. Sci. 98*, 5868-5873.

11. Suzuki, A., Raya, A., Kawakami, Y., Morita, M., Matsui, T., Nakashima, K., Gage, F. H., Rodriguez-Esteban, C., and Izpisua Belmonte, J. C. (2006) Nanog

binds to Smad1 and blocks bone morphogenetic protein-induced differentiation of embryonic stem cells, *Proc. Natl. Acad. Sci. 103*, 10294-10299.